Multiscale study of the intermittency of plastic deformation by acoustic emission method

Ivan Shashkov

Ecole Doctorale Energie Mécanique et Matériaux

LABORATOIRE D'ÉTUDE DES MICROSTRUCTURES ET DE MÉCANIQUE DES MATÉRIAUX

UNIVERSITÉ DE LORRAINE

Multiscale study of the intermittency of plastic deformation by acoustic emission method

DISSERTATION

submitted to obtain the degree of

Docteur de l'Université de Lorraine

Discipline: Materials Science
Speciality : Mechanics of materials

was presented for defence on 11 December 2012

By

Ivan Shashkov

Doctoral Committee

Joel COURBON	Professor, INSA-Lyon	Reviewer
Benoit DEVINCRE	DR CNRS, CNRS / ONERA	Reviewer
Claude FRESSENGEAS	Professor, Université de Lorraine	President
Nikolay KOBELEV	Senior Researcher, ISSP RAS, Russia	Examiner
Mikhail LEBEDKIN	DR CNRS, LEM3-Metz	Director of Research
Vladimir GORNAKOV	Principal Researcher, ISSP RAS, Russia	Director of Research

---

LEM3, UMR CNRS 7239
Université de Lorraine, Ile du Saulcy, 57045. Metz Cedex01

Acknowledgments

The work reported in present dissertation has been carried out in the Laboratoire d'Etude des Microstructures et de Mécanique des Matériaux at the Université de Lorraine and in the Institute of Solid State Physics Russian Academy of Sciences during the years 2009-2012.

First of all I wish to thank my advisors Mikhail Lebedkin and Vladimir Gornakov for their inspiring and active guidance during these years, without which completing this thesis would not have been possible.

I would also like to thank Tatiana Lebedkina, she has repeatedly expressed her encouragement and moral support.

The work presented in this thesis has been done in fruitful collaboration with Prof. František Chmelík and his collegues who I wish to thank: for kind hospitality and interesting discussions during my two visits to Charles University of Prague.

My sincere thanks also goes to Prof. Joel Courbon and Dr. Benoit Devincre, who has accepted the heavy task of review of my work.

I would like to thank the rest of my doctoral committee: Prof. Claude Fressengeas and Dr. Nikolay Kobelev for their encouragement, insightful comments, and hard questions.

I also want to thank all the members of the LEM3 for interesting conversations and good atmospher.

Finaly, I am grateful to my family and especially to my wife Alena for encouraging and supporting me during this project.

Résumé

Les études récentes de la déformation plastique à l'aide de techniques expérimentales à haute résolution témoignent que les processus de déformation sont souvent caractérisés par des effets collectifs qui émergent à une échelle mésoscopique, intermédiaire entre celle de défauts cristallins et celle d'une éprouvette macroscopique. Notamment, la méthode de l'émission acoustique (EA) révèle, dans divers conditions expérimentales, l'intermittence de la déformation plastique, qui se manifeste par une propriété de l'invariance d'échelle, caractéristique de phénomènes d'auto-organisation.

L'objectif de la thèse a été d'étudier la structure inhérente de l'EA pour différents mécanismes de déformation plastique, d'examiner sa dépendance à la vitesse de déformation et à l'écrouissage du matériau, et d'appréhender les liens entre les petites échelles de temps, liées à l'organisation des défauts, et celles qui relèvent de l'approche continue de la plasticité. L'étude a été réalisée sur des alliages AlMg et des alliages base Mg, dont la déformation plastique est accompagnée d'une forte activité acoustique et contrôlée par differénts mécanismes physiaues : l'effet Portevin-Le Chatelier (PLC) dans les premiers et une combinaison du maclage et du glissement des dislocations dans les deuxièmes.

L'utilisation de la technique d'enregistrement continue de l'EA ("data streaming") a permis de montrer que le comportement apparent - discrète ou continue - de l'EA accompagnant l'effet PLC dépend de l'échelle de temps d'observation et du paramètre physique étudié. Cependant, contrairement à une vision traditionnelle, il se trouve que l'EA a un caractère intermittent pendant l'écoulement macroscopiquement lisse tant que pendant l'instabilité macroscopique de la déformation plastique. Grace aux méthodes d'analyse issues de la théorie des systèmes dynamiques non linéaires, telles que l'analyse multifractale, une tendance à la transition entre la dynamique invariante d'échelle et les comportements caractérisés par des échelles intrinsèques a été trouvée lors de l'écrouissage des matériaux. Enfin, nous avons prouvé que les distributions statistiques en loi puissance persistent dans des larges intervalles de variation des paramètres, conventionnellement utilisés pour individualiser les événements acoustiques. Ce résultat est d'une importance générale car il s'applique à tous les processus avalancheux émergeant dans différents systèmes dynamiques.

Mots clés : déformation plastique, dynamique des dislocations, effet Portevin - Le Chatelier, maclage, émission acoustique, systèmes dynamiques, auto-organisation, analyse statistique, analyse multifractale.

Abstract

Recent studies of plastic deformation using high-resolution experimental techniques testify that deformation processes are often characterized by collective effects that emerge on a mesoscopic scale, intermediate between the scale of individual crystal defects and that of the macroscopic sample. In particular, the acoustic emission (AE) method reveals intermittency of plastic deformation in various experimental conditions, which is manifested by the property of scale invariance, a characteristic feature of self-organized phenomena.

The objective of the dissertation was to study the inherent structure of AE for different mechanisms of plastic deformation, to examine its dependence on the strain

rate and strain hardening of the material, and to understand the relationships between short time scales related to organization of defects and those relevant to the continuous approach of plasticity. The study was performed on AlMg and Mg-based alloys, the plastic deformation of which is accompanied by a strong acoustic activity and controlled by different physical mechanisms: the Portevin-Le Chatelier (PLC) effect in the first case and a combination of twinning and dislocation glide in the second case.

Application of a technique of continuous AE recording ("data streaming") allowed proving that the apparent behavior, discrete or continuous, of AE accompanying the PLC effect depends on the time scale of observation and the physical parameters surveyed. However, unlike the traditional view, it appears that AE has an intermittent character during both stress serrations and macroscopically smooth flow. Using methods of the theory of nonlinear dynamical systems, such as the multifractal analysis, a tendency to a transition between the scale-invariant dynamics and the behaviors characterized by intrinsic scales was detected during work hardening. Finally, we proved that the power-law statistical distributions persist in wide ranges of variation of parameters conventionally used to individualize acoustic events. This result is of general importance because it applies to all avalanche-like processes emerging in dynamical systems.

Contents

Introduction

The plasticity of crystalline materials results from the motion of defects of crystal structure – dislocations, twins, point defects, and so on. Until recently, the research in plasticity was divided into two major parts, that of the microscopic motions of defects and that of the macroscopic behavior of the material. The latter was considered as resulting from averaging over local random fluctuations of the distribution and mobility of defects, dislocations *par excellence*, which statistically compensate each other and give rise to spatially uniform and continuous plastic flow. Since the 1980th, however, many studies showed that the ensemble of crystal defects represents an example of nonlinear dissipative dynamical systems in which the interaction between various constituents may lead to self-organization phenomena. The properties of the collective dynamics appear to be common for dynamical systems of different origin, coming from various fields, such as physics, mechanics, chemistry, biology,....[1, 2]. Each example of collective effects, interesting by itself, is also interesting as a representative of a class of phenomena characterized by universal behavior. The complex dynamics of such systems is often associated with the property of scale invariance, or self-similarity, which manifests itself through power-law relationships.

It was found that self-organization of dislocations concerns both spatial and temporal behavior and results in formation of dislocation structures and/or intermittency of plastic deformation, characterized by non Gaussian statistics and invalidating the averaging operations. These phenomena give rise to a very complex problem because depending on the material and deformation conditions, the collective dynamics of defects may show up at different scales and lead to various collective effects, displaying both

universal and unique properties. The main challenges for investigations of this problem are to determine the limits of the continuous approach to the description of plasticity and to find a link between the elementary mechanisms of plastic deformation and the macroscopic behavior of deforming materials. Understanding such multiscale behavior is especially important nowadays because the technological developments are turning towards micro- and nanosystems with dimensions comparable to the scales imposed by collective processes in the dislocation system.

In this framework, the present doctoral research will mostly concern the problem of the intermittency of plastic deformation of crystals. The intermittent collective motion of defects generates jumps in the plastic strain rate, which are characterized by nonrandom statistics and in particular, by power-law statistical distributions. Such properties were first identified for different mechanisms giving rise to macroscopic plastic instabilities, mostly the Portevin-Le Chatelier effect (PLC) – jerky flow in dilute alloys caused by interaction between dislocations and impurities[3, 4]. In tensile tests with constant strain rate, this effect displays a complex spatiotemporal behavior, associated with repetitive strain localization in deformation bands and concomitant abrupt variations of the deforming stress. Various approaches to the analysis of serrated deformation curves were proposed [5, 6, 7, 8, 9, 10, 11]. They all showed that spatiotemporal patterning corresponds to nontrivial dynamical regimes. In particular, the dynamical [12] and statistical [5] analyses testified to the existence of a deterministic chaos [13] in some range of strain rates, and a transition, at higher strain rates, to self-organized criticality (SOC) [14] which is generally considered as a paradigm of avalanche-like processes. These two modes demonstrate different statistics of amplitudes and durations of serrations: distributions with characteristic peaks in the case of chaos and power-law distributions in the case of SOC. It should be noted, however, that chaos is also associated with scale invariance reflected in the geometry of the phase trajectory of the corresponding dynamical system. Moreover, application of the multifractal analysis [15] revealed scale-invariant behaviors in the entire strain-rate range in which the PLC effect is observed. Recently, acoustic emission (AE) technique was applied to study the PLC

effect in an AlMg alloy [16, 17, 18]. AE stems from transient elastic waves generated within a material due to localized changes of microstructure, therefore, it reflects the motion of group of defects. Surprisingly, power-law distributions were found for amplitudes of AE events in all experimental conditions. This result indicates, on the one hand, that plastic deformation is an inherently intermittent, avalanche-like process at mesocopic scales relevant to AE, and, on the other hand, that scale invariance may not spread out to the macroscopic scale.

Furthermore, another group of investigations showed that "regular" plastic flow is also intermittent although the jumps in the strain rate are smaller than those leading to macroscopic stress serrations. These jumps can however be evaluated using high-resolution extensometry or the AE technique. The AE statistics was studied rather in detail during macroscopically homogeneous deformation of some pure crystalline solids, such as ice single and polycrystals and copper single crystals, and displayed a persistent power-law character [19, 20]. This conclusion was later confirmed in experiments on local extensometry during plastic flow of Cu single crystals [21, 22]. Power-law statistics were also found for the AE accompanying twinning of single crystals of Zn and Cd [23], as well as for stress serrations observed during compression of microscopic pillars of pure metals [24].

All the above-described results led to the growing recognition of a ubiquitous character of self-organization phenomena in dislocation ensembles. Moreover, various data on small-scale intermittency in pure single crystals provided approximately the same value for the power-law exponent, thus giving rise to a "universality" conjecture [25]. However, different exponent values were reported for AE in ice polycrystals [26]. Besides, the exponents obtained for AE accompanying the PLC effect were found to depend on strain rate and microstructure [27, 17, 18]. These differences raise a question on the relationship between the general laws governing the collective dislocation dynamics at relevant mesoscopic scales and the role of specific mechanisms of plasticity. Furthermore, as can be seen from the above-said, the range of scale invariance is limited from above. However, the transition to the macroscopic scale is not well understood because

the macroscopic behaviors include not only smooth deformation curves but also jerky flow, with statistics depending on the experimental conditions. On the other hand, the scale invariance must also break at small scales because of the limited experimental resolution. So, the classical analysis of EA considers as elementary the acoustic events at the time scale inferior to 1 ms. However, a recent study under conditions of the PLC effect showed that these "elementary" events may possess a fine structure detected by the multifractal analysis [28]. It can be supposed that such temporal structures characterize short-time correlations between the motions of defects, which have not been studied up to date.

With these questions in view, the objective of the present doctoral research was to study the intrinsic structure of AE at different time scales and for different mechanisms of plasticity; to characterize the relationships between the correlations of deformation processes at very short time scales, corresponding to "elementary" acoustic events, and the long-time correlations, up to the macroscopic scale of the deformation curve; and to examine the influence of strain and/or strain rate on the observed statistical behavior. Mg and Al based alloys were chosen as the main objects of this study. Both these alloys exhibit a highly cooperative character of plastic deformation, leading to strong acoustic activity which is governed by distinct microscopic mechanisms, – respectively, mechanical twinning and the PLC effect. In order to get a comprehensive description of complex behavior the data treatment combined various methods, including the statistical, spectral, and multifractal analyses.

The thesis contains six chapters. The first chapter reviews literature data concerning the problem of intermittency of plasticity, gives examples of similar behaviors in solid state physics, introduces notions of nonlinear dynamical systems, and describes the mechanisms of the PLC effect and twinning. Experimental details on the materials, testing, and data recording are given in Chapter 2. Chapter 3 introduces the relevant types of data analyses. The results of investigations are presented in Chapters 4 to 6. Chapter 4 dwells on the effect of the parameters of individualization of acoustic events on their apparent statistics. This study treats a general question arising in experimen-

tal investigations of avalanche processes of different nature: are the results of statistical analysis not affected by the superposition of the analyzed events? Indeed, the superposition might occur for various reasons, for example, because of an almost instantaneous emergence of avalanches or because of insufficient resolution of individual events. Understanding this influence is an indispensable basis for the quantitative evaluation of the critical exponents characterizing scale invariance. However, there are virtually no pertinent studies in the literature, or at least this question is only considered theoretically. Chapter 5 utilizes a technique of continuous AE recording to compare the nature of AE during jerky and smooth flow in an AlMg alloy. As a matter of fact, the AE accompanying unstable plastic deformation is usually considered to be composed of discrete bursts associated with the motion of large dislocation ensembles, giving rise to stress serrations, and a continuous emission generated during macroscopically smooth plastic flow. This traditional viewpoint however contradicts the observation of intermittency of plastic flow in smoothly deforming pure materials. A minute examination of AE records reported in Chapter 5 allows overcoming this contradiction and provides a basis for the subsequent analysis of AE statistics. The chapter is completed with first results of similar investigations on Mg alloys. The last chapter describes the results of the statistical and multifractal analysis of AE in Al and Mg alloys. The general conclusions and discussion of the perspectives for future investigations complete the dissertation.

Chapter 1

BACKGROUND

The current research into self-organization of crystal defects and collective deformation processes explores various directions and is developing into a large field of investigation. Without trying to give an exhaustive overview of related problems, this chapter will treat some aspects which concern the above-formulated objectives of the doctoral study and are necessary for understanding its results. We first outline observations of scale-invariant behavior, associated with power laws, during plastic flow of crystalline solids. In order to position the plasticity phenomena within a more general problem of avalanche-like processes in physics and mechanics, we further present examples of power-law statistical behavior in solid state physics and introduce some general concepts of nonlinear dynamical systems and theoretical frameworks for explanation of power-law statistics. This general representation is followed by a more detailed description of the Portevin-Le Chatelier effect, which will be one of the main focuses of investigation. After briefly introducing the macroscopic manifestations and the microscopic mechanism of the effect, we present experimental observations and computer modeling of the complexity of its spatiotemporal behavior, with an accent put on statistical properties and application of AE method to experimental investigation of jerky flow. The chapter ends with the description of the phenomenon of twinning – another mechanism of plastic deformation studied in this dissertation and characterized by strong AE displaying features qualitatively different from those observed for the PLC effect.

1.1 Intermittency and power-law scaling in plastic flow

Plastic deformation of crystalline solids is governed by the multiplication and motion of crystal defects – dislocations, twins, point defects, and so on. Consequently, it is intrinsically heterogeneous and discontinuous at the microscopic scale. By contrast, the macroscopically smooth plastic deformation of crystals is conventionally viewed as homogeneous and continuous plastic "flow." This is understood as a result of averaging over independent motions of a very large number of defects contained in the material. Indeed, the typical densities of dislocations in deformed samples are of the order of magnitude of 10^{10} per cm^2. The approximate sense of this viewpoint which supposes that the interaction between defects can be neglected has been recognized for a long time. On the one hand, application of the electron microscopy to investigation of dislocations revealed formation of complex spatial structures (e.g., [29, 30]). However, the development of this spatial heterogeneity was observed during macroscopically smooth deformation and investigated regardless of the problem of discontinuity of plastic flow, although the numerical models proposed for explanation of the spatial aspect of self-organization of dislocations are also promising as to understanding its temporal aspect [31, 32, 33]. On the other hand, due to utilization of elaborated experimental techniques, several observations of sporadic bursts in plastic strain rate were reported very early, even before the occurrence of the concepts of plastic deformation through motion of defects (e.g., [34, 35]). These bursts were however considered as resulting from large stochastic fluctuations in the system of defects. Finally, in some cases the continuous plastic flow becomes unstable at macroscopic scale and serrated deformation curves are observed. The jerky flow may be caused by various microscopic mechanisms which have been extensively studied, e.g., the Portevin-Le Chatelier (PLC) effect controlled by interaction of dislocations with solutes [3, 4, 36, 37], thermomechanical instability caused by insufficient heat evacuation from samples deformed at very low temperatures [38, 39], twinning [40, 41], martensitic transformations [42, 43], and so on.

The observation of jerky flow testifies that at least in certain conditions, interaction

between defects may lead to intermittent plastic flow caused by short-time cooperative motion of large groups of defects. The creation of the theory of nonlinear dissipative systems which are characterized by self-organization [2, 1] made it possible to analyze discontinuous plastic deformation from the viewpoint of collective processes. Such investigations started in 1980th, mostly using the example of the PLC effect, which displays complex spatiotemporal behavior associated with strain localization within deformation bands and stress serrations of various kinds. A detailed description of this phenomenon will be given in § 1.5. Essentially, various approaches to the analysis of stress drops showed that spatiotemporal patterning corresponds to nontrivial dynamical regimes [5, 6, 7, 8, 9, 10, 11]. In particular, power-law Fourier spectra of series of stress serrations and power-law statistical distributions of their amplitudes and durations were found in a range of high strain rates [5, 6, 7, 8]. The power-law dependences are equivalent to scale-free behavior, as can be easily seen from the relationship $p(kx) \propto (kx)^{\beta} \propto k^{\beta}x^{\beta} \propto k^{\beta}p(x)$ which displays self-similarity upon scaling. This scale-free behavior bears witness to possible manifestation of self-organized criticality. The concept of SOC was introduced by *P. Bak et al.* [44] as a general framework for explaining the avalanche-like phenomena in spatially extended dynamical systems and, more specifically, the flicker noise characterized by $1/f$ power density spectrum. Although some authors contest the application of SOC to explain the $1/f$-noise [45], it is widely used to model earthquakes and dry friction – the phenomena presenting certain similarities with jerky flow. It should be noted that such a hypothesis is consistent with the infinite number of degrees of freedom of the dislocation ensembles. At lower strain rates histograms with characteristic peaks were observed. They were shown (e.g., [4, 7, 8]) to neither be associated with stochastic behavior, but with the so-called deterministic chaos [46]. Interestingly, this observation means a drastic reduction in the number of degrees of freedom because chaos occurs in low-dimensional systems. It is also characterized by scale invariance which is reflected in the so-called fractal geometry (see § 3.3 and Appendix) of the attractor of phase trajectories of the dynamical system.

Observing scale invariance in the distributions of stress serrations at the macroscopic

level, suggests extending the analysis to finer event scales by using more sensitive techniques. Recently, acoustic emission (AE) technique was used to investigate statistics of the PLC effect [16, 17, 18]. Surprisingly, it was found that acoustic emission is characterized by power-law statistics of event size for all strain rates. Moreover, a similar statistical behavior of AE was found for both jerky flow and macroscopically smooth plastic flow in the same tests. Such persistence of statistical behavior testifies to the invariant nature of deformation processes during both stable and unstable deformation, and implies an inherently intermittent scale-invariant character of plastic activity at a mesoscopic scale relevant to AE. It is noteworthy that this conjecture is conform with the earlier observations of power-law statistics of series of electric signals accompanying stress serrations during low-temperature catastrophic dislocation glide or twinning in pure metals [47, 48].

Although the above research testifies to an important role of self-organization of dislocations, the PLC effect is often considered as a particular, exotic case. Nevertheless, application of AE technique to pure materials, either displaying serrations caused by twinning (Cd, Zn) or deforming by smooth dislocation glide (ice, Cu), showed that the intermittency of plastic deformation is rather the rule than the exception and results from an avalanche-like collective dislocation motion [19, 49, 21, 25, 23]. An example of power-law statistical distributions of acoustic energy bursts in ice single crystals deformed by creep is illustrated in Fig. 1.1. The results of AE studies were recently confirmed using another sensitive method based on high-resolution extensometry[21, 22]. In this case, power-law distributions were found for local strain-rate bursts detected during plastic flow of Cu single crystals. All these results bear evidence to the intermittent scale-invariant character of macroscopically uniform plastic activity, albeit at sizes of the local strain-rate bursts much smaller than in jerky flow.

Finally, serrated deformation curves and power-law distributions of serration amplitudes were recently observed in the compression of microscopic pillars of various pure

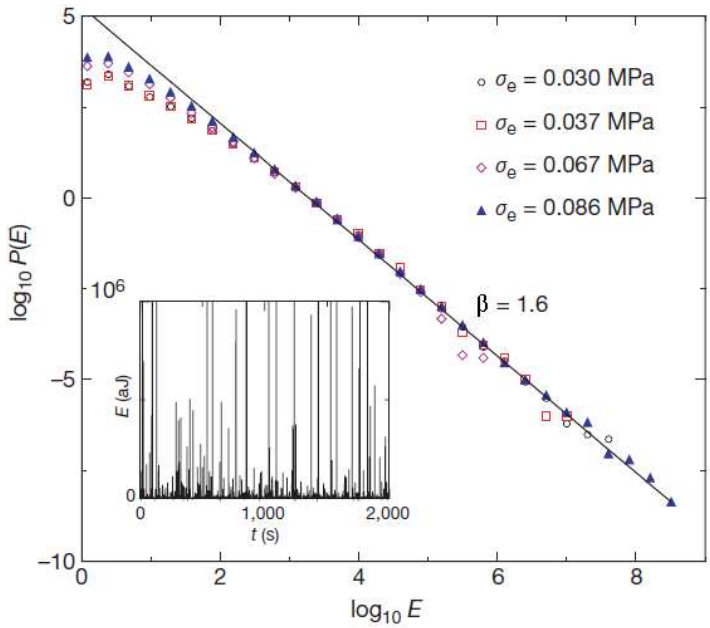

Figure 1.1: Statistical distributions of acoustic energy bursts recorded in ice single crystals under constant stress. [49]

metals (Fig. 1.2)[24, 50, 51]. These works provide a direct proof of collective dislocation dynamics, which shows up on the deformation curves when the size of the deformed specimens is small enough, so that their plastic deformation cannot be considered anymore as a result of averaging over many independent plasticity events.

The collection of all the above-described results led to the growing recognition of a ubiquitous character of self-organization phenomena in dislocation ensembles.[1] The various data on small-scale intermittency in pure single crystals provided approximately the same value for the power-law exponent. Namely, distributions $p(E) \propto E^{\beta}$ with $\beta \approx -(1.5 \div 1.8)$ were reported for the energy E of AE events recorded during deformation of single crystals of various materials with hexagonal and cubic crystal structure [19, 20, 23]. A similar β-range was found for jerky displacements in the tests on micropillars. As the abrupt displacement takes place at approximately the same force level, it determines the produced mechanical work and, therefore, also characterizes the energy dissipated in the process of plastic deformation. The entirety of these data gave

[1]It is noteworthy that recent investigations using optical methods bear evidence to another generic behavior observed in various materials [22, 52, 53]. Namely, it is shown that the intermittent strain localization may self-organize in space so that to give rise to a kind of excitation waves. However, this aspect goes beyond the scope of the present thesis.

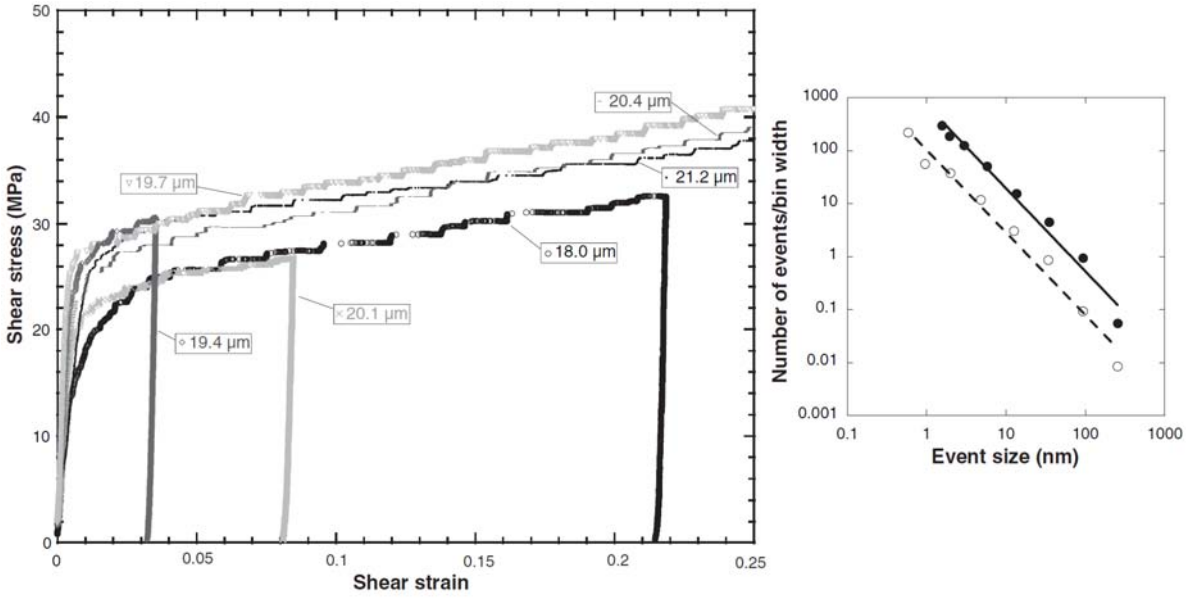

Figure 1.2: Left: intermittency of the shear-stress vs. shear-strain curve for Ni sample with [$\bar{2}69$] orientation; the numbers designate the pillar diameter. Right: distribution of slip events plotted in logarithmic coordinates. Open circles - data for a single sample with diameter ~ 20 μm, solid circles - aggregate data from several samples.[24]

rise to a "universality" conjecture [25]. Concurrently, the value $\beta^* \approx -1.35$ was found for the amplitude distribution of AE in ice polycrystals [26]. This value corresponds to an even higher estimate of the exponent β for the energy distribution, as can be illustrated with the aid of the approximation suggested in [20], that the energy dissipated during an acoustic event is proportional to the square of its peak amplitude. Using this simplification, the relationship $\beta = (\beta^* - 1)/2$ can be easily deduced (see, e.g., [22]) and gives an estimate $\beta \approx -1.2$. Much lower values, $\beta \approx -(2 \div 3)$, which in addition depend on strain rate and evolve with work hardening, were reported for AE accompanying the PLC effect[16, 17, 18]. Taking into account that at the macroscopic scale of stress serrations the power-law distributions were only found at high strain rates, with exponents varying in rather large intervals for various samples $\{\beta \approx -(1 \div 1.7)$ was typically reported for amplitude distributions of stress serrations$\}$, the questions on the relationship between the general laws governing the collective dislocation dynamics and on the role of specific mechanisms of plasticity remain open.

1.2 Analogues in physics

The observations of power-law statistics in plasticity are reminiscent of similar features in nonlinear phenomena of various natures, often referred to as "crackling noise". Numerous investigations following the development of the theory of dynamical dissipative systems proved that the emergence of scale invariant behavior is one of the fundamental properties of self-organization phenomena in systems consisting of a large number of interacting elements. Their behavior is expressed by a jerky response to smoothly changing external conditions. Well known examples in physics and material science include the Barkhausen noise in magnetic materials [54], vortex avalanches in type II superconductors [55], charge density waves [56], fracture [57, 58], martensitic transformations[59], dry friction [60], earthquakes [61], and so on. All these phenomena are characterized by avalanche-like relaxation processes alternating with periods of slow loading, and are characterized by power-law distributions of sizes and durations of the avalanches. Several examples of such behavior are presented below in some detail.

The Barkhausen effect is an instability responsible for the jerky character of magnetization of ferromagnets [62]. Discovered in 1919, it provided direct experimental evidence for the existence of magnetic domains. Let us consider a ferromagnet below the Curie temperature. In a zero magnetic field it is divided into domains whose magnetic moments tend to disorder, in order to compensate each other and to minimize the internal energy which is the lowest in the unmagnetized state. When an external magnetic field is applied to the material, its magnetization takes place through displacement of the domain boundary walls. If the crystal structure were free of defects, the domain walls would move in infinitesimal magnetic fields. In reality they interact with various pinning centers, such as dislocations, polycrystalline grains, stacking faults, surface roughness, etc. In particular, this explains the existence of permanent magnets, i.e., materials having a spontaneous magnetic moment in the absence of external magnetic field, because their full demagnetization is impeded by pinning of the domain walls. The other consequence of pinning is the Barkhausen effect which is caused by jump-like displacements

of domain walls. The corresponding jumps in magnetization can be observed, e.g., with the help of inductive techniques. Recently, the development of magneto-optical methods allowed direct (*in situ*) observations of the intermittent motion of domains walls [63]. However, the most reliable experiments in terms of signal statistics are still based on inductive measurements. A typical example of such measurements is presented in Fig. 1.3. The left figure displays a burst-like voltage signal induced in a coil of wire wound on a ferromagnet and the magnetization curve obtained by integration of this signal over time. The almost horizontal portions of the magnetization curve correspond to smooth motion of domain walls and their pinning on obstacles. The upward jumps reflect the moments when the domains configuration becomes unstable and suddenly change to a new state. The statistical analysis of the voltage bursts reveals power-law distributions of event sizes and durations (right figure).

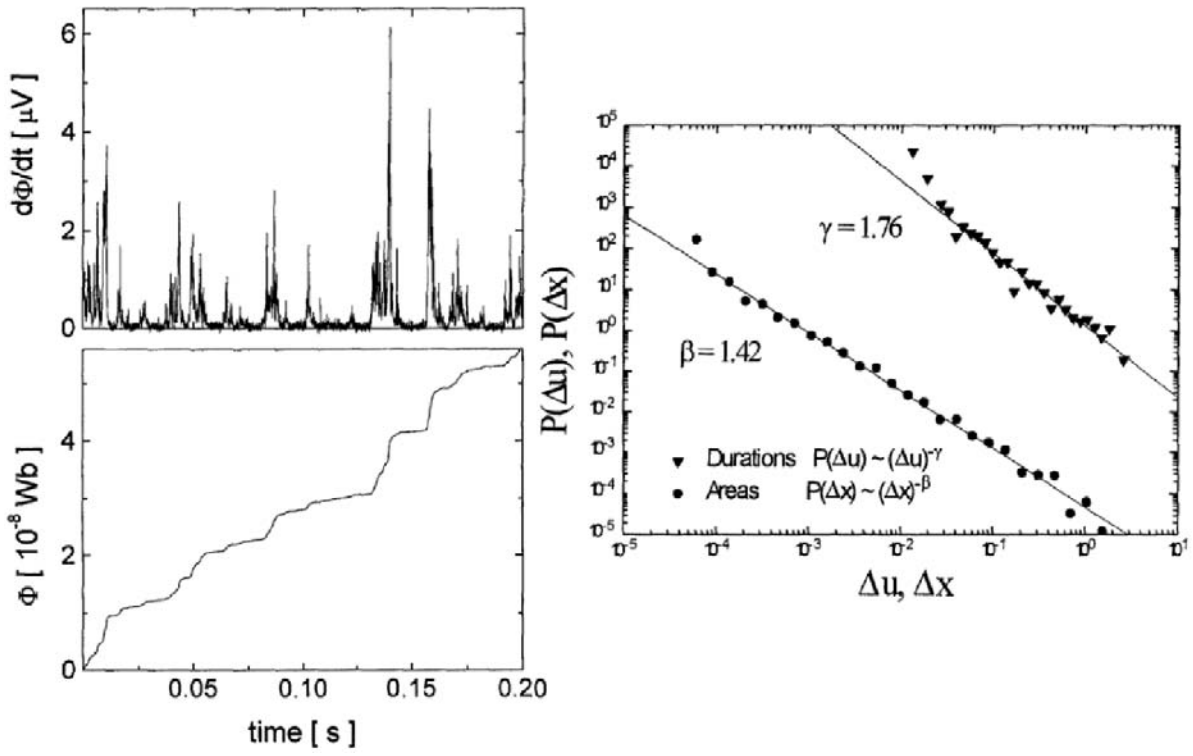

Figure 1.3: Barkhausen effect. Left: Voltage signal measured in annealed $Fe_{73}Co_{12}B_{15}$ amorphous ribbon and its time integral showing a staircase magnetization curve. Right: Distribution of Barkhausen jump duration and amplitude for Si-Fe[64].

Figure 1.3 shows a striking similarity with jerky deformation curves and acoustic signals in Figs.1.1 and 1.2. This analogy is rather profound as both phenomena are

related to the problem of collective pinning. It is not surprising that the same authors who studied the phenomenon of plastic instability also suggested a model of unstable magnetization processes [65]. However, most of works treating in some way the analogy between plasticity and magnetization problems mostly considered the motion of individual domain walls through pinning centers (e.g., [66]).

An avalanche dynamics of magnetic flux, characterized by power-law statistics, was also observed in type II superconductors [55, 67] and in discrete superconductors - Josephson junction arrays [68, 69]. Magnetization of these materials is determined by the dynamics of a system of vortices (called, respectively, Abrikosov or Josephson vortices) carrying magnetic flux. There are evident qualitative similarities between the magnetic flux flow in such materials and the plastic flow. Indeed, both vortices and dislocations are linear "defects" which are subjected to external forces (Lorentz force [70] and Peach-Koehler force [71], respectively), pinning forces, and mutual interaction forces. It should be noted, however, that the case of dislocations presents more complexity. In particular, the magnetic vortices are oriented in the direction of the applied magnetic field and their interactions are mostly reduced to repulsion, whereas the interactions between dislocations depend on their type, Burgers vector, mutual orientations, bounding to certain slip systems, and so on, and include annihilation and multiplication [71].

Perhaps, the most famous example of avalanche-like behavior is rock fracture. Whereas the above examples are typically characterized by self-similar statistics over only 1-3 orders of magnitude of the measured variable, because of strong limitations of the sample size in the laboratory conditions, in geology the avalanches can reach the size of giant earthquakes. Consequently, the distribution of sizes of seismic events obeys a power law, known as the Gutenberg-Richter law, over more than eight orders of magnitude[61]. The dynamics of earthquakes is generally related to a stick-slip mechanism, which involves sliding of a plate of the earth crust along another plate [60]. Their key feature is that the friction force, which acts along the fault line between the plates, decreases with increasing the slip velocity. As argued in [72], the mechanism responsible for such behavior is similar to that responsible for the property of negative strain-rate sensitivity of stress

under conditions of the PLC effect.

1.3 Application of AE technique to statistics of deformation processes

The sudden changes in the internal structure of materials (cracking, motion of dislocation pile-ups, phase transitions, twinning, etc.) under action of external forces lead to emission of sound waves. This phenomenon has been known since long ago because the sound is sometimes audible, as in the well-known case of mechanical twinning during bending of a tin bar ("tin cry"). The recording of the acoustic signal provides information about these processes, taking place on various spatial and temporal scales. The regular application of the AE technique as an *in situ* method of investigation has started since a comprehensive study by *Kaiser* [73, 74]. It has proven to be a powerful tool to study the mechanisms of plastic deformation and failure in wide time and space ranges, from microscopic scales corresponding to the motion of groups of defects to the macroscopic scale of the deforming sample (see, e.g., reviews [75, 76] and references therein). In particular, simple estimations show that a measurable stress drop of a few hundredth of MPa requires cooperative motion of the order of 10^5 dislocations through the sample cross-section, whereas the motion of a few hundred dislocations through a polycrystalline grain can provoke a measurable acoustic event [77]. Indeed, significant AE accompanies even macroscopically smooth deformation curves of pure materials [21]. Consequently, this technique is particularly useful for the study of the collective motion of dislocations.

In spite of a wide application of AE to monitoring microstructural changes in deforming materials, its interpretation is not direct because the signal is affected by the transfer function of the AE sensor, the sound reflections, the modulations by the propagating medium, etc... In some cases, comparison of AE data with microstructural studies may provide information on the possible sources of elastic waves. In other cases, the interpretation depends on the physical assumptions. Dislocations-based models of AE usually consider three mechanisms: (i) relaxation of stress fields caused by dislocation motion;

(ii) annihilation of dislocations; (iii) "bremsstrahlung" radiation from accelerated dislocation [76]. The estimates of the energy released by these sources prove a preponderant role of the first type of AE sources (see, e.g., [75]). A model of such source was proposed by *Rouby et al.* [78], who considered the motion of a straight dislocation line at a constant velocity. Pursuing this approach, *Richeton et al.* [79] deduced the following relationship for the amplitude of the acoustic wave generated by a dislocation avalanche with a total dislocation length L and the average velocity v:

$$A(t) = \frac{3C_T^2}{4\pi C_L^2} \frac{\rho b}{D^2} Lv \tag{1.1}$$

where C_T and C_L are, respectively, the transverse and longitudinal wave velocities, ρ is the density of the material, b is the Burgers vector, and D is the distance between the AE source and the sensor. The term Lv corresponds to the rate of area sweeping by dislocations: $Lv = dS/dt$. Normalized by volume and combined with the Orowan equation [80] for plastic strain rate,

$$\frac{d\varepsilon}{dt} = k\rho_m bv,$$

where ρ_m is the density of mobile dislocations and k is a geometrical factor, this relationship shows that $A(t) \sim d\varepsilon/dt$. In statistical investigations the maximum amplitudes A of acoustic events are usually examined. Integration of Eq. 1.1 under assumption that the avalanche velocity v exponentially decays with time leads to a proportionality relationship between A and the strain increment caused by the dislocation avalanche: $A \sim \varepsilon$. Its feasibility is confirmed, e.g., by experiments on ice single crystals, which showed proportionality between the global AE activity and plastic deformation [19]. *Weiss et al.* [21] provide arguments that this relationship should be valid in a more general case, e.g., for a decay following a power-law, as could be expected for avalanche-like behavior.

It is often supposed that the radiated acoustic energy is a more relevant characteristic of deformation processes, also applicable to non dislocation sources, e.g., twinning or

cracking [81, 20, 82]. This characteristic is considered to scale with A^2, as follows from the estimate of the energy dissipated at the source by a single screw dislocation [83]:

$$E = KL^2b^2v^2 \tag{1.2}$$

where K is given by a combination of material constants, and its comparison with Eq 1.1. As specified in § 3.1, this approach is used for the statistical analysis in the present study.

1.4 Theoretical approaches to power-law statistics

The theory of nonlinear dynamical systems can be found in many books and journal reviews, starting from the classical ones [1, 2]. The most striking feature of such systems is that they self-organize. The result of self-organization may be a very complex behavior which cannot be understood in terms of summation of random or periodic motions. Three aspects of complexity, i.e., fractals, deterministic chaos, and self-organized criticality, have already been mentioned above. Since SOC is characteristic of infinite dimensional systems and leads to power-law statistics, it seems to be relevant to the studied problem and will be described below in some detail. Alternative interpretations of power laws will be also presented. At the same time, the correlation between the system elements may drastically reduce the effective number of degrees of freedom controlling its dynamics. It was shown in the case of the PLC effect that this reduction may lead to a transition from SOC to low-dimensional chaos [7, 84]. Moreover, it is known that a system composed of many oscillators may reach perfect synchronization leading to simple periodic behavior, when all oscillators move in phase [85]. Another realization of synchronization can occur through propagation of a kind of switching waves [86], giving rise to the so-called "relaxation oscillations" which are characterized by alternation of fast and slow kinetics [87]. Relationships between SOC and these dynamical modes will be shortly discussed.

Finally, another remarkable feature of dynamical systems is universality, i.e., similar

behavior of systems governed by distinct mechanisms and even coming from different fields of science, which allows classifying various systems into classes of universality. Thanks to this feature, simple models, like the ones presented below, often prove usefulness for understanding and modeling real behaviors.

1.4.1 Self-organized criticality

Despite a vast literature on self-organized criticality there is no clear definition of this concept, which is usually explained using examples of specific dynamical systems. The SOC concept was proposed by *Bak et al.* to explain the behavior of a simple cellular automaton model of a "sandpile" [44]. It was shown that the sandpile reaches a kind of critical state, characterized by power-law correlations, similar to second-order phase transitions. The salient feature of the behavior is that in contrast to phase transitions, the sandpile reaches the critical state spontaneously, without fine tuning of an order parameter.

A simple sandpile model can be demonstrated using a square grid, each element of which is assigned an integer variable $z(x, y)$ representing the number of sand grains accumulated on this site. At each time step a grain is placed on a randomly selected site. If $z(x, y)$ reaches a critical value (equal to 4 in $2D$ case) on a given site, the grains are redistributed among its nearest neighbors or, eventually, leave the system through the grid boundaries. This redistribution may trigger chain processes leading to formation of an avalanche, with size s defined as the total number of "toppling" sites and duration T given by the number of time steps during which the chain process is developed. It can be said that the system performs avalanche-like transitions between different metastable states. The avalanche behavior is characterized by several power laws which describe the fractal structure of avalanche patterns, the probability densities $P(s)$ and $P(T)$, the relationship $s(T)$ between the variables, and the Fourier spectra of time series representing the time evolution of system variables. The last feature explains why SOC is often considered as a possible mechanism of $1/f$-noise. More specifically, the dependencies demonstrate a cut-off at large scale because of the finite dimensions

of the system. For example, $P(s)$ is generally described by a relationship:

$$P(s) = s^{\beta_s} f_c(s/s_0), \tag{1.3}$$

where β_s usually varies between *-1* and *-2*, and the cut-off scale s_0 is associated with the linear system size.

The cellular automata present stochastic models of SOC. Another kind of models is based on a deterministic approach. The so-called spring-block models were proposed to explain the Gutenberg-Richter statistical law for earthquakes [88, 89, 60]. Such models usually consider an array of blocks connected to their neighbors by springs. The blocks are pulled across an immobile plate by a driving plate to which they are also connected with the aid of springs. In this case the role of the parameter z is played by the local force acting on a given block. Moving the driving plate leads to adding a small force to each block. As mentioned in §1.2, the nonlinear friction law between the blocks and the immobile plate (see Fig.1.4) results in a stick-slip behavior. If the local force exceeds the friction threshold, the corresponding block slips and the resulting rearrangement of local forces may trigger a chain process. Again, it was found that the dynamics of the system is described by power laws, providing that the driving rate is low. This simple scheme demonstrates three basic ingredients controlling the dynamics of such models: the threshold friction, separation of a slow time scale (loading) and a fast time scale (avalanche-like relaxation), and spatial coupling between blocks. Using $2D$ and $3D$ block-spring models, a good agreement was found between the simulated power-law exponents and the values following from earthquakes catalogues. As the earthquakes are related to accumulation of stresses in the earth crust, there is a direct analogy between this natural phenomenon and the plastic deformation of solids [5, 72]. Consequently, the block-spring schemes are of special interest for modeling the intermittent plastic flow. In particular, they were successfully used to simulate the PLC behavior, as will be discussed in § 1.5.4.

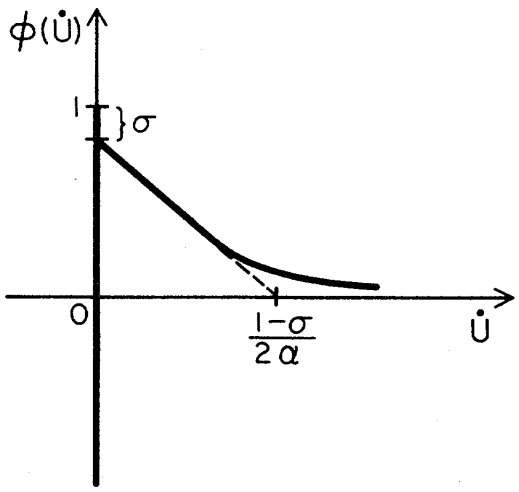

Figure 1.4: The velocity-weakening slip-stick friction law[60].

1.4.2 Alternative explanations of power-law behavior

Although SOC was proposed as a general framework for explanation of numerous observations of power-law statistics, the systems for which it has been clearly established are rare. Various alternative models were proposed in the literature to explain such critical-like behavior within the concept of "plain old criticality", by adding some uncertainty. For example, *Sethna et al.* [90] studied a random field Ising model to explain the Barkhausen effect [90]. The Ising model considers a lattice of magnetic spins and represents a classical model for a first-order transition in a ferromagnet below Curie temperature: when the magnetic field passes through zero, the equilibrium magnetization reverses abruptly. By adding disorder in the form of a random magnetic field the authors did not only reproduce magnetic hysteresis, instead of a sharp transition, but also found scale-free fluctuations of magnetization for certain values of disorder.

Another model giving power laws without parameter tuning was proposed by *Sornette* [91]. It is based on the slow sweeping of a control parameter [91]. The idea of this approach can be illustrated using a fiber bundle made of N independent parallel fibers with identically distributed independent random failure thresholds. The bundle is subjected to a force F. The ratio F/N plays the role of the control parameter whose value changes because when the applied force F is increased, more and more fibers break down. Again, the numerical simulation reveals power-law distributions of rupture sizes

for a low loading rate.

These models are conform with a general consideration by *Weissman* [45], who examined various mechanisms of $1/f$-noise and concluded that it can occur because of smeared kinetics features. In particular, a system described by characteristic rates which are determined by a large number of independent factors should have a log-normal distribution. If this distribution is wide enough, its flat top might provide many octaves of power-law dependence. The author suggests that the $1/f$-noise may be viewed as an extreme limiting case of many types of broadened kinetics.

1.4.3 Role of finite loading rate and overlapping

The models presented above bear evidence that the scale-invariant statistics may be due to various mechanisms. Therefore, determination of the underlying mechanism necessitates a detailed statistical analysis and a careful measurement of various critical exponents and relationships between them. This requirement raises above all the question of reliability of experimental determination of power-law exponents. As a matter of fact, the above models suggest either a very slow driving rate or, in the ideal case, halting the loading during the propagation of an avalanche. Consequently, no two avalanches will propagate simultaneously. The experiment cannot always approach this ideal situation, so that avalanches can overlap in time and in space and be recorded as a single event. Few works concerned a possible effect of the avalanche superposition on the critical exponents. *Durin and Zapperi* [92] experimentally measured the Barkhausen noise in soft ferromagnetic materials and distinguished two cases: when the exponent β_T describing the avalanche duration probability tends to -2 for zero rate of the external magnetic field, such material shows a linear increase in β_s and β_T with an increase in the field rate; in the case when $\beta_T(0) > -2$, the slopes are independent of the field rate. *White and Dahmen* [93] proposed a theoretical explanation of this behavior by considering a linear superposition of avalanches. According to their model, the decrease in the slopes of the power-law dependencies in the former case occurs because small events are absorbed into larger ones. In the latter case the superposition is strong starting from very low

field rates, so that no changes are observed when the rate is varied. The authors also analyzed theoretically the case $\beta_T < -2$ and found that the exponents must be rate independent for small enough rates, but a crossover to one-dimensional percolation on the time axis should occur when the rate is increased.

To our knowledge, the effect of overlapping on the statistics has not been explored in the case of AE investigations of plasticity. Recent data on the distributions of AE amplitudes during the PLC effect [18] showed similar β_s values for low and intermediate strain rates and somewhat flatter dependences for higher strain rates, in qualitative agreement with the above predictions. However, even at small strain rates the PLC instability results in merging of AE events during stress serrations, the latter being short on the macroscopic time scale but quite long in comparison with the individual AE events. This merging causes distinct bursts in the duration of AE events, so that a clear power-law behavior is actually observed only for AE amplitudes. Moreover, any investigation of plasticity represents a fundamental problem: the behavior is never statistically stationary because of the microstructural changes which are at the origin of the work hardening of the material. As a result, the values of the critical exponents evolve during deformation. Since there exist no two samples with identical microstructure, and besides, the microstructure evolution depends on various factors including the strain rate, a rigourous comparison of the results obtained at different strain rates is hardly possible. To study the effect of overlapping, another strategy was adopted in the present study (see Chapter 4). Namely, the criteria used to extract events from a signal were varied, so that various sets of events were extracted from each of the recorded signals and analyzed.

1.4.4 Relation to other dynamical regimes

As mentioned above, the analysis of stress serrations has led to a conjecture that the PLC effect presents a rare example of a transition from an infinite (SOC) to low (chaos) dimensional behavior when the driving rate is decreased. Another known example of a transition from a scale-free to a chaotic state concerns the hydrodynamic turbulence [94].

It can be conjectured that spatially extended dynamical systems may find themselves in various regimes which present different manifestations of complexity. The complexity associated with the deterministic chaos is related to the sensitivity to initial conditions, which can be quantified using the so called Lyapunov exponents. To illustrate it, one can take an infinitesimal initial distance between two phase trajectories and consider the evolution of its projections on the principal directions. In the limit of small time, it is expressed in terms of $e^{\lambda_i t}$, where λ_i is the Lyapunov exponent in the ith direction. Chaos occurs when one λ_i becomes positive, which reflects instability in the sense of the exponential divergence of trajectories, while the dynamics remains stable in other directions. Although the language of phase trajectories is impractical for the description of infinite dimensional systems, SOC is often associated with almost zero Lyapunov exponents which reflect a slower, power-law divergence.

Another nontrivial dynamical regime is associated with the phenomenon of collective synchronization in a system of coupled oscillators, which spontaneously lock to a common phase, despite initially different phases of individual oscillators [85]. In fact, this phenomenon is modeled using the same lattice models as those proposed for SOC, i.e., characterized by a threshold dynamics, the separation of slow and fast time scales, and spatial coupling. *Perez et al.* [86] showed that such models allow for a transition between the scale-free and synchronized behaviors. Their dynamics is governed by the strength of the spatial coupling and the degree of nonlinearity of the driving force. More specifically, when the nonlinearity of the driving force is strong and the coupling strength is weak, large avalanches repetitively sweep the whole system, giving rise to relaxation oscillations. Moving away from these conditions leads to a gradual transition to a discrete distribution of a few avalanche sizes, coexistence of a discrete and a continuous distribution, and finally, power-law behavior.

It seems natural to suggest from these two examples that the dynamical chaos is related to synchronization of various elements of the dynamical system. However, since chaos is commonly studied in low dimensional systems, such a relationship has not been examined so far.

1.5 Portevin-Le Chatelier effect

1.5.1 General behavior

The PLC effect is a plastic instability observed in dilute alloys and caused by interaction between dislocations and solute atoms. It was discovered in the early part of the 20th century [95, 96] but continues attracting great attention of researchers up to now. One of the fundamental reasons for this interest is that the PLC effect offers a striking example of complex spatiotemporal dynamics of dislocations [4]. Indeed, as will be seen below, it is one of the cases when the heterogeneity of plastic flow shows up at the macroscopic scale, which requires collective behavior of large numbers of dislocations. Besides, understanding of this behavior presents high practical interest because of undesirable detrimental effects on the formability of materials widely used in industry, e.g., steels and aluminum alloys [97].

Most of research into the PLC effect has been realized in the geometry of uniaxial tensile tests. In this case, the effect consists in repetitive localization of plastic strain rate within transversal deformation bands, which may either propagate along the tensile axis or be immobile. The static bands have a life time about milliseconds [98]). The traces of the deformation bands which usually have width from fractions to several millimeters can be observed on the side surface of specimens using an optical microscope or even with the naked eye [99]. In the tests with a constant velocity of the mobile grip, i.e., constant imposed overall strain rate $\dot{\varepsilon}_a$, the elastic reaction of the "deformation machine-specimen" system on the unstable plastic flow of the specimen gives rise to abrupt stress variations on stress-time or stress-strain curves (see Fig. 1.5).[2]

As can be recognized in Fig. 1.5, the serrations usually onset after macroscopically uniform deformation to a certain critical strain ε_{cr} [102, 103]. Figure 1.6 represents a typical dependence of the critical strain on the imposed strain rate. It can be seen that when $\dot{\varepsilon}$ is increased ε_{cr} increases in the region of high strain rates (the so-called "normal

[2]It is noteworthy that the unstable plastic flow under conditions of a constant loading rate has been discovered by F. Savart et A. Masson as early as in 1830th [100, 101]. However, this experimental scheme is out of the scope of the present work because it leads to specimen fracture after several strain jumps only.

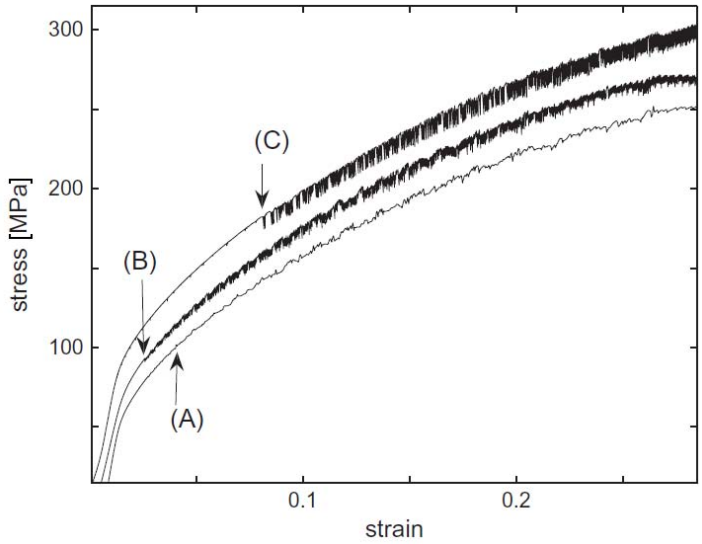

Figure 1.5: Examples of deformation curves for $Al-3at.\%Mg$ samples, recorded at room temperature for three different $\dot{\varepsilon}_a$-values and corresponding to three commonly distinguished types of the PLC effect [18]: type C ($\dot{\varepsilon}_a = 2\times10^{-5}s^{-1}$), type B ($\dot{\varepsilon}_a = 2\times10^{-4}s^{-1}$), and type A ($\dot{\varepsilon}_a = 6\times10^{-3}s^{-1}$). The respective arrows indicate the critical strain ε_{cr} for the onset of plastic instability.

behavior") but decreases at low strain rates ("inverse behavior").

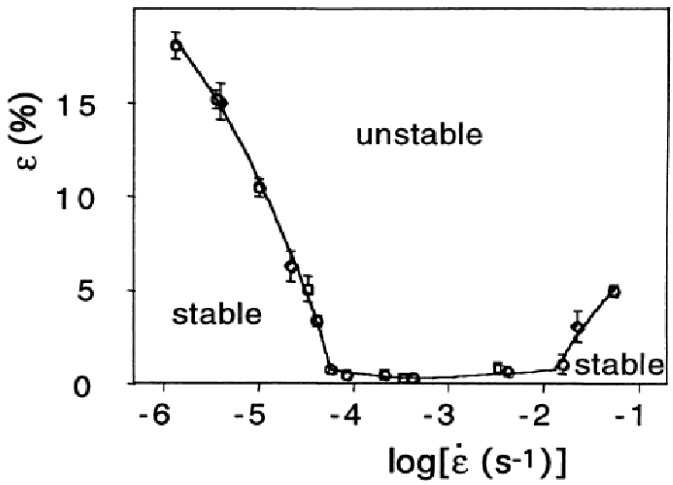

Figure 1.6: Variation of critical strain as a function of strain rate for $Al-4.8\%Mg$ alloy [104].

Figure 1.6 also indicates a strain-rate range of observation of instability. As a matter of fact, the PLC effect occurs in limited domains of temperature and strain rate. The morphology of stress variations strongly depends on the experimental conditions, as illustrated in Fig. 1.5 for variation of $\dot{\varepsilon}_a$ at room temperature. In general, the shape

of the deformation curves also depends on the material composition, microstructure, and sample dimensions. Nevertheless, several generic types of behavior have been found (e.g., [105]).

Usually three persistent types called A, B, and C are distinguished, depending on the shape of the deformation curve and the spatial pattern of deformation bands [4]. A salient feature is the gradual transition between different behaviors, which takes place when either T or $\dot{\varepsilon}_a$ is varied from one to another boundary of the respective range of instability. At a given temperature, type A behavior occurs close to the upper bound of the strain-rate interval of existence of the PLC effect, typically above $10^{-3}s^{-1}$ for AlMg alloys. It is characterized by irregular stress fluctuations without visible characteristic amplitude, which are associated with deformation bands usually nucleating near one specimen end and propagating quasi-continuously along the tensile axis. Some stress fluctuations are likely to result from fluctuations of the width and velocity of a propagating band. Besides, the band propagation through the sample is followed by a phase when the stress increases until a new band is nucleated, upon which the stress falls towards the envelope deformation curve – the imaginary prolongation of the smooth curve prior to ε_{cr}. Such a pattern of stress drops preceded by stress rises gave rise to a name of "locking serrations" for type A behavior.

Type B instability is observed around $\dot{\varepsilon}_a = 10^{-4}s^{-1}$ and is characterized by rather regular stress drops, such that the stress oscillates around the envelope curve. Each stress drop results from a static deformation band nucleated ahead of the previous band, for which reason this regime is often referred to as "hopping propagation" of a band. As the localized plastic deformation results in the material work hardening within the band, the serrations often form groups corresponding to the hopping band propagation along the entire specimen and separated by periods of smoother deformation, during which the stress is increased to finally trigger a new band.

When the strain rate is further decreased, the transition to type C instability occurs upon approaching $\dot{\varepsilon}_a = 10^{-5}s^{-1}$. This behavior is associated with "unlocking serrations" – sharp stress drops below the envelope curve. Like type B serrations such stress drops

display a characteristic size. They are usually attributed to randomly nucleated bands, although the analysis of serrations bears evidence to existence of some correlation [106]. Finally, mixed behaviors are observed at intermediate strain rates.

1.5.2 Microscopic mechanism

Since the dislocation mechanism of plasticity is governed by thermally activated motion of dislocations through obstacles [71], it is characterized, like any other activated process, by a positive dependence of the driving force on the rate of the process: a higher force is necessary to sustain a higher rate. The occurrence of the PLC instability is generally associated with a negative value of the strain-rate sensitivity (SRS) of the applied stress σ: $S = \frac{\partial \sigma}{\partial ln\dot{\varepsilon}} < 0$. The inversion of the sign of S is attributed to dynamic strain aging (DSA) of dislocations [107, 108], engendering a recurrent process of pinning-unpinning of dislocations from solute atoms. The DSA mechanism can be schematically described as follows. On microscopic scale the motion of dislocations is discontinuous: their free motion lasts very short duration and alternates with long arrest on local obstacles, such as forest dislocations, during the waiting time for thermal activation. The impurity atoms diffuse to dislocations during t_w and additionally anchor them. This additionnal pinning stress is thus determined by the competition between two time scales, the waiting time t_w and the solute diffusion time t_a, which depend on the strain rate and temperature. The PLC effect occurs when the two time scales are comparable. This is illustrated in Fig. 1.7(a) which schematically represents the $\sigma(\dot{\varepsilon})$-dependence for a given temperature. If the strain rate is very high, t_w is much smaller than t_a and the dislocations move as if there were no impurity atoms. In the opposite limit ($t_w \gg t_a$) the dislocations are constantly saturated with solute atoms and move together with solute clouds. In both cases a normal positive-slope $\sigma(\dot{\varepsilon})$-dependence is observed for thermally activated process, as shown in the figure for the intervals $\dot{\varepsilon} < \dot{\varepsilon}_1$ and $\dot{\varepsilon} > \dot{\varepsilon}_2$. However, the left-hand side of the curve corresponds to a higher stress level. Consequently, a negative slope occurs in the interval $\dot{\varepsilon}_1$ and $\dot{\varepsilon}_2$, where the concentration C of solutes on dislocations diminishes with an increase in $\dot{\varepsilon}$. The overall behavior is thus represented

by a N-shaped $\sigma(\dot{\varepsilon})$-dependence. The interval of instability covers several orders of magnitude of $\dot{\varepsilon}$ (the scheme in Fig. 1.7(a) would look realistic if the $\dot{\varepsilon}$-axis was supposed to be logarithmic).

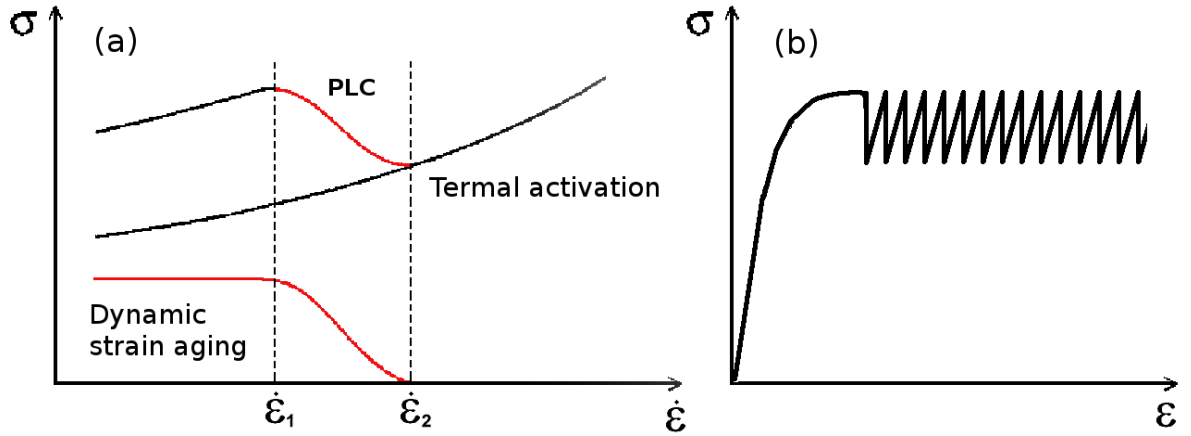

Figure 1.7: (a) A scheme explaining the occurrence of an N-shaped SRS as a result of competition between two microscopic mechanisms; (b) The resulting instability in the form of a saw-toothed deformation curve.

Such a stress-rate dependence leads to an instability in the form of relaxation oscillations [87], providing that the imposed strain rate value finds itself in the range between $\dot{\varepsilon}_1$ and $\dot{\varepsilon}_2$. Indeed, as demonstrated by *Penning* [109], when the loading brings the system to the threshold stress, $\dot{\varepsilon}$ undergoes a jump from the "slow" to the "fast" positive-slope branch of the characteristic N-curve. In velocity-driven experiments (constant $\dot{\varepsilon}_a$) the elastic reaction of the deformation machine converts the strain rate jump into drastic unloading, which terminates with a backward $\dot{\varepsilon}$ jump to the slow branch. The alternation of the slow loading and abrupt stress drops gives rise to a saw-toothed deformation curve, as illustrated in Fig. 1.7(b). Such a cyclic behavior is similar, for example, to the Gann effect in a medium with a negative differential resistance [110].

Different mathematical descriptions of this behavior use variants of the following constitutive equation composed of three additive terms:

$$\sigma = \sigma_h(\varepsilon) + S_0 \ln(\frac{\dot{\varepsilon}}{\dot{\varepsilon}_0}) + \sigma_{DSA}\{1 - exp(-\left(\frac{\Omega(\varepsilon)}{\dot{\varepsilon}\tau}\right)^p)\}, \tag{1.4}$$

where the first term reflects the strain hardening, S_0 is the positive SRS in the absence of DSA, and the third term is due to DSA [111, 112]. In the last term, σ_{DSA} is the

maximum pinning stress corresponding to saturation of dislocations with solutes, τ is the characteristic diffusion time of solutes, p is equal to 2/3 for the bulk diffusion [113] or 1/3 for the diffusion in dilocation cores [114], $\Omega(\varepsilon) = b\rho_m\rho_f^{-1/2}$ is the quantity introduced in [112] to describe the "elementary plastic strain", i.e., the strain produced when all mobile dislocations are activated and move to the next pinned configuration (b and ρ_m are the Burgers vector and density of mobile dislocations, ρ_f is the density of forest dislocations).

This equation allows explaining the existence of a critical strain for the onset of the PLC effect. *Kubin and Estrin* [112] considered the evolution of Ω with deformation to find the conditions when the SRS becomes negative. Alternatively, the evolution of τ due to generation of vacancies during deformation was examined [115]. These analyses provided qualitative explanations of the normal and inverse behaviors of ε_{cr} but the quantitative predictions were quite loose, especially for the inverse behavior. Recently, several attempts were made to improve the quantitative predictions. Some of these approaches are based on taking into account the strain dependencies of either σ_{DSA} or the solute concentration on dislocations, the latter leading to a modification of the argument of the exponential function in Eq. 1.4 [116, 117]. *Mazière and Dierke* [118] showed that the agreement with experimental results can be improved by replacing the condition $S < 0$ by a stronger condition leading to an exponential growth of instability. This question remains a matter of debate.

1.5.3 Observations of complex behavior

Complexity on the macroscopic scale of stress serrations The qualitative prediction of plastic instability associated with propagating PLC bands and saw-toothed deformation curves was one of the important successes of the microscopic models. However, the experimental observations display more diverse and complex patterns. Some aspects of this complexity were mentioned above (see also Introduction). Various observations are shortly summarized below.

During the last few decades quite a number of different approaches were proposed

to quantify the complexity of serrated deformation curves, e.g., dynamical analysis [12], statistical analysis [5], wavelet analysis [119], multifractal analysis [120], and so on, each method highlighting one or another aspect of behavior. The entirety of results proved a correlated nature of stress serrations, with correlations strongly depending on the material and experimental conditions (temperature, strain rate, microstructure). In particular, power-law statistical distributions of the stress drop size and duration, as well as power-law Fourier spectra of deformation curves were found for type A instability [5, 7, 84]. The analysis of critical exponents allowed for a conjecture of SOC-type behavior. However, this hypothesis remains a matter of debate. For example, *Annathakrishna and Bharathi* [121] pointed out that SOC models require a slow driving rate, while the behavior of the PLC effect is peculiar in this sense: whereas power-law statistics are observed at high $\dot{\varepsilon}_a$-values, the decrease in $\dot{\varepsilon}_a$ leads to peaked histograms. These authors suggested that the critical behavior at high $\dot{\varepsilon}_a$ is similar to that in the hydrodynamic turbulence [94]. For type B serrations the emergence of deterministic chaos was proved [12, 7, 84]. In this case the statistical distributions of stress drops acquire an asymmetrical peaked shape. Finally, type C serrations are characterized by near Gaussian distributions. However, even these serrations are not completely uncorrelated, as revealed by the multifractal analysis [106]. As a matter of fact, multifractal scaling was found for stress-time curves in the entire strain-rate range of instability [84, 122, 120].

Recent studies revealed that power-law distributions may appear even under conditions of type C behavior [18]. Unexpected in such conditions, this conclusion concerns stress fluctuations that occur on a smaller scale than the deep type C serrations. Indeed, amplifying the deformation curves, one can distinguish two distinct scales of stress drops at low strain rates. The mechanism responsible for the occurrence of small drops attracted little attention so far. Usually, they are considered as "noise" caused by the material heterogeneity. This point of view is confirmed, e.g., by their dependence on the surface treatment [123]. Nevertheless, such fluctuations show a nontrivial statistical behavior. When they are not disregarded, the statistical analysis results in bimodal histograms with two distinct peaks [11, 16]. Application of the analysis separately to the

two groups of events shows that whereas the large stress drops follow rather symmetrical peaked distributions, power-law behavior with an exponent between -1 and -1.5 is found for small serrations (Fig. 1.8) [16, 18]. This observation proves their non-random nature. Therefore, it reveals the multiscale character of deformation processes and adds interest to investigations with a higher resolution, e.g., with the aid of the AE technique.

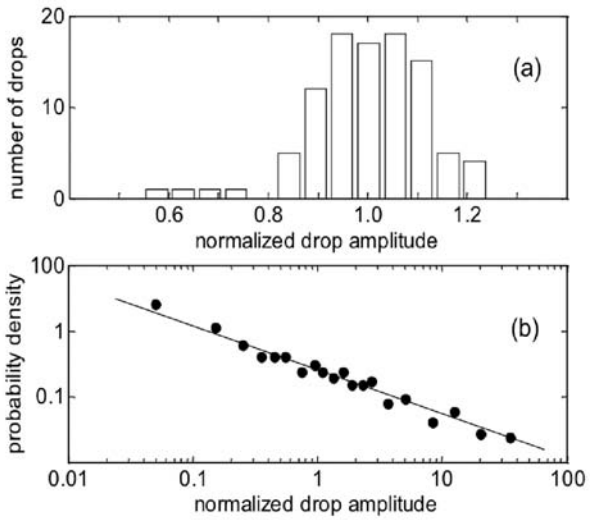

Figure 1.8: Distribution of the amplitudes of (a) large stress drops and (b) low-amplitude serrations observed in an AlMg alloy at $\dot{\varepsilon}_a = 2 \times 10^{-5} s^{-1}$ [18].

Complexity on a mesoscopic scale of AE Until recently, the AE study of the PLC effect was mostly concentrated on the analysis of average characteristics, such as the AE count rate [124, 125, 126]. Here, a count is recorded each time when the amplitude of an acoustic oscillation exceeds a given threshold value, usually set at the level of the background noise, as described in § 2.4. Figure 1.9 illustrates typical results for an AlMg alloy. Similar to other materials, including those deforming smoothly, the AE occurs very early during the nearly elastic deformation. The count rate quickly increases and passes a maximum in the region of the elastoplastic transition which sometimes displays a Lüders plateau, as shown in Fig. 1.9(a). The latter phenomenon is often observed in the same alloys which show the PLC effect. It is generally interpreted as due to propagation of a deformation band through the gauge length of the specimen, a process associated with unpinning of dislocations from their solute atmosphere in a

statically aged material, whereas the PLC effect is governed by dynamical strain aging of dislocations [71].

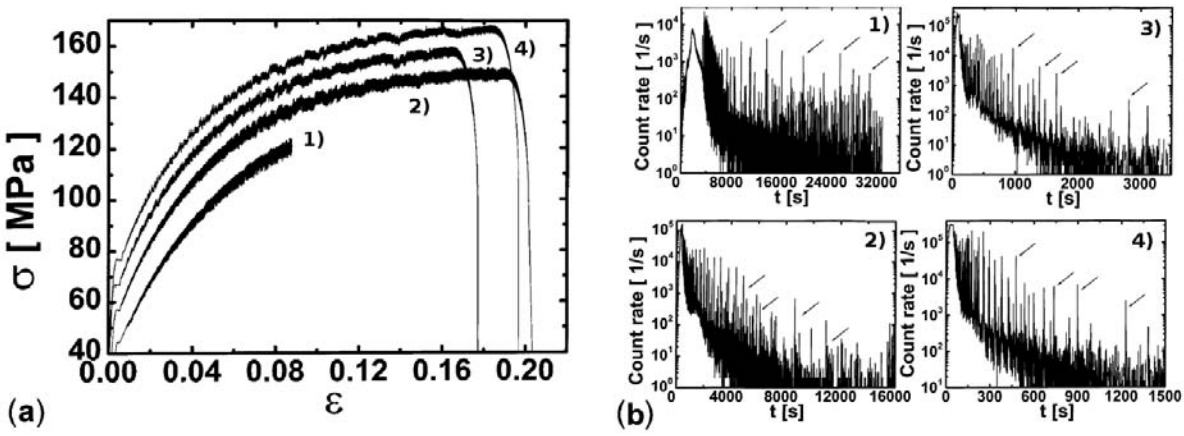

Figure 1.9: (a) Stress-strain curves and (b) the corresponding time dependencies of AE count rate for Al-1.5%Mg alloys deformed at room temperature and various strain rates: (1) $\dot{\varepsilon}_a = 2.67 \times 10^{-6} s^{-1}$; (2) $\dot{\varepsilon}_a = 1.33 \times 10^{-5} s^{-1}$; (3) $\dot{\varepsilon}_a = 5.33 \times 10^{-5} s^{-1}$; (4) $\dot{\varepsilon}_a = 1.33 \times 10^{-4} s^{-1}$[124].

Figure 1.9(b) illustrates that the abrupt stress drops of type C are accompanied with bursts of AE count rate. When $\dot{\varepsilon}_a$ is increased, such a correlation disappears progressively. So, only a part of type B serrations is accompanied with such bursts. Moreover, the strongest AE is observed during the phase of nucleation of a new relay race of deformation bands, although this region is characterized by less abrupt stress fluctuations. In the case of type A behavior the AE bursts are rare and they seemingly correlate with stress humps associated with nucleation of new deformation bands. The observation of the correlation between the AE count rate and the distinct stress drops, particularly for type C serrations, led to a suggestion that the PLC instability gives rise to discrete burst-like AE events produced by large-size dislocation ensembles, in consistence with the macroscopic size of stress serrations, whereas smaller-size dislocation avalanches occur randomly during the macroscopically smooth plastic flow, and generate virtually continuous AE. This hypothesis was also corroborated by the observation of discrete acoustic events during serrated deformation, whereas continuous AE signals superimposed with discrete events were found to accompany the propagation of Lüders bands [124] (see Fig. 1.10). It should be noted, however, that the acoustic equipment

available at this time did not allow accurate correlation of stress drops with the observed AE events.

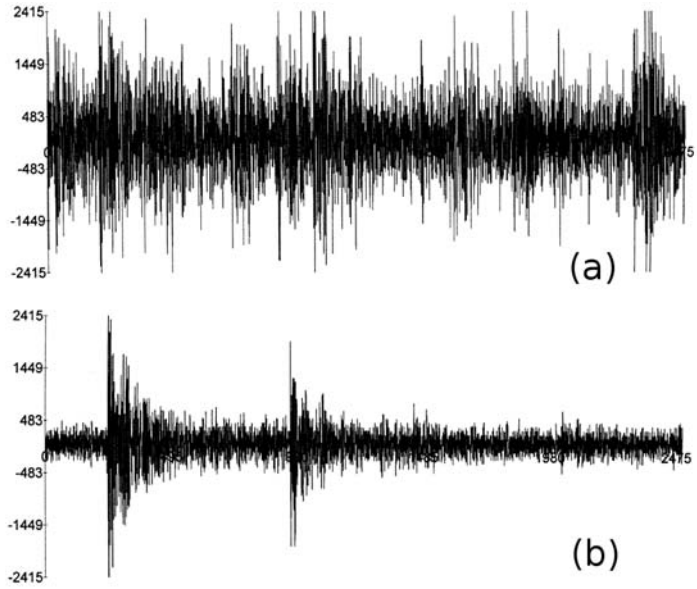

Figure 1.10: AE signal waveforms observed during (a) Lüders phenomenon and (b) PLC effect[124]. The total time interval length is 2.5 ms.

This confrontation of the discrete and continuous AE under conditions of the PLC effect has been questioned recently. First, the amplitudes of acoustic events were found to vary in the same range during smooth and jerky flow in an AlMg alloy, whereas bursts were observed for their durations and related characteristics such as the count rate or energy [16]. It was supposed that the PLC band is formed through a process of synchronization of glide events in a similar amplitude range, due to propagation of elastic waves, which leads to merging of the corresponding acoustic events. This conjecture is consistent with the optical observations of the complex evolution of the forming deformation bands [127, 128], although it should be remarked that the optical methods applied were limited by millisecond time scale. It is also conform to the results of the multifractal analysis of individual waveforms recorded during jerky flow in an AlCu alloy [28], which proved that the single AE events may not be elementary but possess a fine structure. On the other hand, in *Vinogradov and Lazarev* [129] application of the data streaming technique, which allows recording the entire AE signal (see § 2.3), proved a continuous character of AE accompanying the PLC effect in α-brass. However,

only type A behavior has been examined in this work.

The statistical analysis of AE during the PLC effect started several years ago [27, 16, 17, 18]. As already mentioned above in this Chapter, one of the major results of these works is that AE is characterized by power-law statistics of event size in all experimental conditions. Moreover, the AE events extracted separately during stress serrations and during smooth intervals revealed very close distributions. These results led to a conjecture that the deformation processes relevant to the mesoscopic scale (uncovered through AE measurements) have a similar nature during both stress serrations and smooth plastic flow. This unexpected result was also confirmed due to application of the multifractal analysis to the series of AE events, which testified that the temporal correlations characterizing the AE show no peculiarities associated with the PLC effect [17]. At the same time, the exponents of the power-law distributions of AE amplitudes are clearly different from those observed for pure materials and are not unique. In particular, the values of the exponents depend on $\dot{\varepsilon}_a$ and evolve in the course of deformation.

1.5.4 Numerical modeling

The numerical models of the PLC effect aimed at reproducing the observed complex behavior of serrated deformation curves by allowing for strain heterogeneity and spatial coupling between differently strained regions in the deforming specimen. The general framework for phenomenological models was proposed by *Zbib and Aifantis* who suggested a spatial coupling term in the form of the second gradient of strain [130]. It appears as either an additional internal stress,

$$\sigma = \sigma_h(\varepsilon) + F(\dot{\varepsilon}) + c\frac{\partial^2 \varepsilon}{\partial^2 x} \tag{1.5}$$

or in the form proposed by *Jeanclaude and Fressengeas* [131] and describing the dislocation transport due to double cross-slip of dislocations [71],

$$\sigma = \sigma_h(\varepsilon) + F(\dot{\varepsilon} - D\frac{\partial^2 \varepsilon}{\partial^2 x}) \tag{1.6}$$

where $F(\dot{\varepsilon})$ is the above described N-shaped characteristic given by the sum of the 2nd and the 3rd terms in Eq. 1.4, c is a constant having an elastic nature, and D is a diffusion-like coefficient. Various mechanisms governing the coupling via internal stresses were examined in the literature: plastic strain incompatibility, which must by compensated by an elastic strain and thus gives rise to internal stresses [132], elastic fields of dislocations[133], nonlocal strain hardening [130], rotation of the specimen axis in the case of single crystals [134], variation of the specimen cross-section, leading to a triaxial character of stress [135]. The comparison of various mechanisms showed that long-range incompatibility stresses play a preponderant role in the most frequent case of polycrystals [134, 136], although the transport of dislocations may manifest itself on a short-range scale [137].

Several $1D$ models using these ideas and representing the deforming sample as a chain of coupled blocks were proposed. *McCormick and Ling* considered solid blocks, all obeying the same constitutive equation and coupled via triaxial stresses [138]. The model successfully reproduced certain aspects of deformation curves of type A and type B, as well as deformation band propagation. *Lebyodkin et al.* used a similar model in which solid blocks were coupled by elastic springs [5, 6]. It reproduced not only the characteristic types of behavior but also the transition from a power-law to a bell-shaped statistics. *Ananthakrishna et al.* developed a model which does not apply a phenomenological nonlinear constitutive law to each block but considers diffusion and mutual reactions of several dislocation densities, one of which corresponds to dislocations carrying solutes (see review [139] and references therein). The coupling between blocks was supposed to be due to the double cross-slip of dislocations. Although this model does not apply the same formulation of the DSA mechanism as that used in other models, it also reproduces various aspects of the PLC effect, including the transition from scale-free to chaotic behavior.

Similar ideas, based on the combination of the nonlocal approach with the above-described microscopic model of DSA, were used to implement $3D$ finite-element models (e.g. [140, 141, 142, 137]). Whereas 3D models are very expensive with regard to com-

putation time, they provide an opportunity to avoid explicit conjectures on the nature of spatial coupling. For example, *Kok et al.* suggested a model of the PLC effect in polycrystals, in which spatial coupling appears due to incompatibility of plastic strains between differently oriented adjacent grains, provided that dislocation glide is considered in various slip systems characteristic of *fcc* metals [140]. This model described salient spatiotemporal features of the PLC effect, as well as the power-law and chaotic dynamical regimes. The entirety of these results proves that the dynamics of the PLC effect is essentially determined by two factors: the negative strain rate sensitivity, stemming from DSA and leading to instability of the homogeneous plastic flow, and strain heterogeneity, which tends to disappear due to spatial coupling but is recurrently resumed because of the instability.

1.6 Twinning

1.6.1 Mechanisms and dynamics

In some cases plastic deformation may proceed by twinning. The term "twinning" describes a situation when two crystals with the same crystal lattice but different orientation adjoin each other and are separated by an interface. The crystallography of twins is described in various manuals [143, 71]. A simple scheme is presented in Fig.1.11, where the open circles denote the atomic positions in a perfect crystal lattice and the black circles show atoms in twinned positions, so that the upper half of the crystal is a mirror reflection of the original lattice. It is noteworthy that although the shear of the two parts of the crystal is macroscopic, this scheme shows that it can be realized due to shifting each atom over only a part of the interatomic distance. Such shift in one atomic plane may be produced by a displacement of a partial disclocation with a Burgers vector smaller than a translation vector of the lattice. In contrast, dislocation glide involves motion of perfect dislocations which shift the lattice by a complete translation vector and do not create an interface. As the energy of a dislocation is proportional to b^2, the partial dislocation carries less energy and seems to provide a favorable mechanism of

plasticity. However, the interfaces occurring during deformation of real crystals are not perfect and their creation needs much energy. Consequently, twinning requires high local overstresses and occurs when dislocation glide is impeded for some reason. For example, it is often observed at low temperatures, even in materials with high symmetry, e.g., face-centered cubic and body-centered cubic crystals which possess many slip systems [41]. The low-temperature twinning is usually explained by a faster increase of the flow stress for perfect dislocations than for partial dislocations. Furthermore, twinning is important in materials with a limited number of slip systems, such as hexagonal close-packed crystals [75]. It should be underlined that twinning and dislocation glide are interdependent processes. On the one hand, piling-up of dislocations provides internal stress concentration necessary for twin nucleation. On the other hand, twinning locally changes orientation of the crystal lattice and makes it more favorable for slip[144].

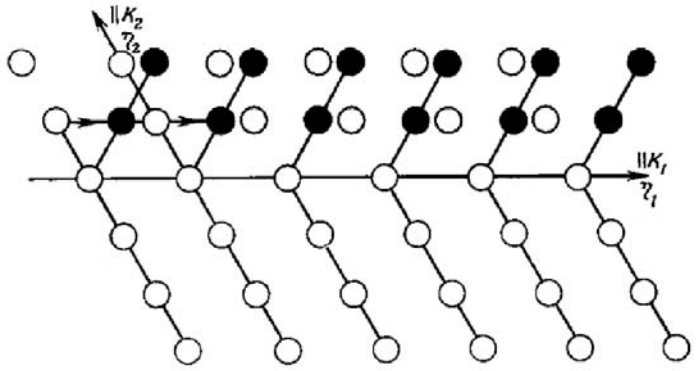

Figure 1.11: Rearrangement of the crystal lattice due to twinning. The twinning plane and the corresponding shear direction are denoted by K_1 and η_1.

The deformation (or mechanical) twins occur in the form of thin layers confined by two boundaries. In this sense, there is a similarity between twinning and unstable plastic flow, because both are associated with a localized shear. Various twinning mechanisms were suggested in the literature. Perhaps, the most known is the Cottrell-Bilby pole mechanism which considers formation of a twin layer due to rotation of a twinning dislocation around a fixed point, so that the dislocation shifts with each turn to an adjacent crystallographic plane [143]. Among other, such mechanisms were considered as the breakaway of partial dislocations from sessile dislocation configurations, nucleation

of partial dislocations due to splitting and double cross-slip of dislocations near dislocation pile-ups [143], autocatalytic mechanism of twin nucleation similar to martensite transformation [145], and so on. Even this incomplete list shows that different models often aim at describing different aspects of the process, which is likely to include several mechanisms. Indeed, numerous experimental observations proved that nucleation of twinning dislocations and their motion leading to formation of interfaces is a very fast process (the twin tip velocity can reach hundreds of meters per second) [146, 147, 41], in agreement with the need of high local overstresses for its triggering. This can hardly be explained by the pole mechanism, which can however allow for the subsequent twin widening with velocities about 10^{-3} cm/s [41].

Twinning is known to be accompanied with high-amplitude discrete AE and, therefore, it offers another model system for the present study. Moreover, as it involves fast nucleation, multiplication, and motion of dislocations, twinning possesses features of avalanche processes. In particular, it can give rise to serrations on deformation curves. The jerky flow occurs as a rule at low temperatures [40] but is also observed at room temperatures [82]. Finally, it is generally suggested that the fast twin nucleation process is responsible for the occurrence of AE during twinning, whereas the slow twin growth is virtually silent [75].

In the present thesis twinning was studied using Mg polycrystalline alloys with *hcp* crystal structure. There are three main slip planes in Mg (Fig.1.12): basal $(0\,0\,0\,1)$, prismatic $\{1\,\overline{1}\,0\,0\}$, and first-order pyramidal plane $\{1\,0\,\overline{1}\,1\}$, which provide a total of four independent slip systems. According to the von Mises criterion [148], plastic deformation of polycrystals necessitates operation of five independent slip systems. The dislocations in the second-order pyramidal plane have a very large Burgers vector and their activation was only observed above 200° C [149]. Consequently, twinning is found to be an important deformation mode of Mg alloys at room temperature. The main twinning system in a Mg crystal deformed by tension is $\{1\,0\,\overline{1}\,2\}\langle 1\,0\,\overline{1}\,1\rangle$, which provides extension along the *c*-axis of the hexagonal lattice. However, as the polycrystalline grains are differently constrained, twins were also observed in other planes, mainly in

$\{1\,0\,\overline{1}\,1\}$ and $\{1\,0\,\overline{1}\,3\}$ [150].

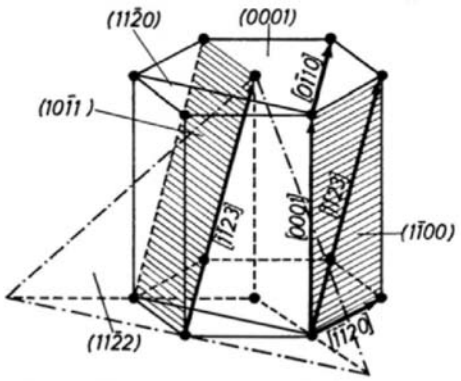

Figure 1.12: Slip systems in the hexagonal close-packed lattice. The prismatic and first-order pyramidal planes are hatched. The second-order pyramidal plane is outlined by a dash-and-dot line.

1.6.2 AE studies

Acoustic emission in single and polycrystals of magnesium and its alloys was studied in a number of works (e.g., [151, 76, 152, 153, 154]). However, all these papers were devoted to investigation of the overall AE behavior as a function of material and experimental conditions: material composition, orientation of single crystals, strain rate, and temperature. It was proven that both deformation twinning and dislocation glide contribute to the AE. To our knowledge, no statistical investigation was carried out on this material, except for a paper [155] included in this thesis.

Several works on the statistics of AE in other hexagonal metals (cadmium and zinc) appeared recently [82, 23]. Figure 1.13 displays examples of stress-strain curves for Zn-0.08%Al single crystals with different orientations with regard to the tension direction. The deep serrations observed on the deformation curves testify to intense twinning in these crystals. Usually, there are too few stress drops before fracture, so that the statistical analysis of their amplitudes is hardly possible. In contrast, such materials manifest a strong AE, the statistics of which was studied in the cited papers.

Figure 1.14 presents one of the main results of this investigation. It was shown that the statistical distributions of the energy of AE events obey a power law with an

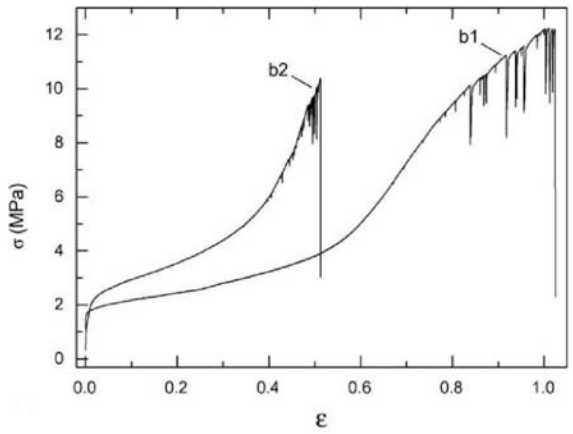

Figure 1.13: Stress–strain curves for $Zn - 0.08\%Al$ single crystals with different orientation[82].

exponent ranging from -1.4 to -1.6. This β-value is similar to the data for ice single crystals deformed by basal glide [20]. Moreover, no difference was found in [82] between the distributions obtained for the stage of easy basal glide and for the subsequent stage characterized by intense twinning, as illustrated in Fig. 1.14 for a Cd single crystal. This result testifies that from the viewpoint of complex dynamical systems, twinning and dislocation glide may belong to the same universality class.

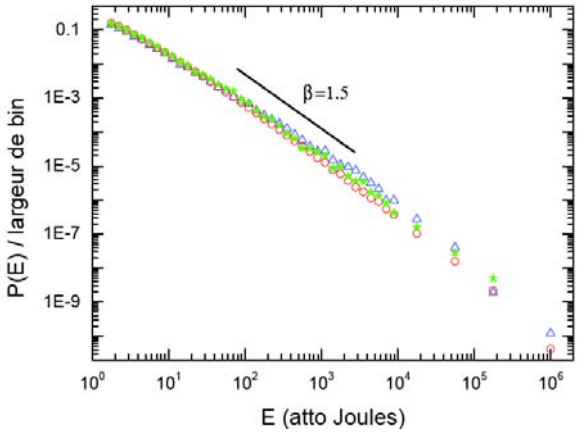

Figure 1.14: Probability density functions of AE energies for the stage of easy basal glide (stars) and the stage manifesting twinning (circles). Cd single crystal.

Another interesting result consists in the observation of two distinct AE waveforms depicted in Fig.1.15. This result will be discussed in § 5.2.3 in relation to the present study. However, some aspects are noteworthy here. Based on a similarity with the data obtained on sapphire single crystals [156], the authors supposed that the abrupt

events (upper figure) are generated by dislocation avalanches and the complex patterns (bottom figure) are indicative of twinning. In the latter case, the initial high-frequency burst is supposed to correspond to the abrupt twin nucleation and the next low-frequency behavior is associated with the twin growth. The last statement contradicts the above-mentioned opinion that the twin growth generates virtually no AE [75]. On the other hand, by analyzing the evolution of the ratio between AE peak amplitude and AE root mean square amplitude (Fig. 1.16), which takes on higher values for short events, the authors found that such events indeed dominate during the basal slip, whereas the second type of waveforms becomes preponderant when twinning occurs (see Fig. 1.16). Whatever the exact nature of each of these types of events, their separation allowed for an important observation that they mutually trigger each other. It can be concluded that twinning and dislocation glide are interdependent processes not only on the macroscopic time scale, associated with the work hardening, but also on a mesoscopic scale related to avalanche deformation processes.

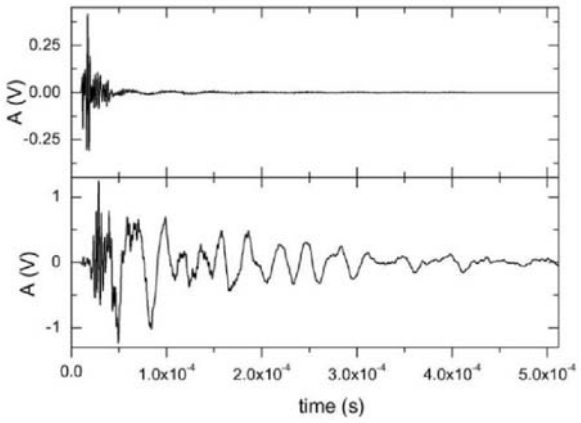

Figure 1.15: The main types of AE waveforms observed in [82].

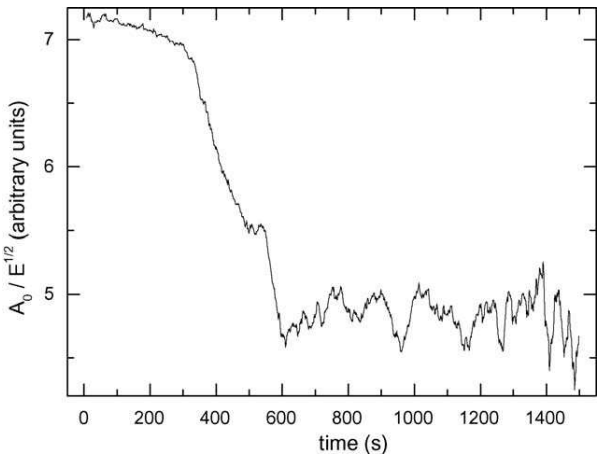

Figure 1.16: Time evolution of the averaged ratio between the peak amplitude and square root of energy of AE events recorded for Cd single crystal [82].

Chapter 2

Experimental methods

2.1 Objects of investigation and specimens preparation

As stated in the Introduction, the aim of the present study was two-fold : (1) to examine the general problem of the effect of the parameters of individualization of acoustic events on their statistics; (2) to investigate specific and generic properties of the statistics of intermittent processes of plastic deformation of solids. These goals require testing various materials whose plastic deformation is governed by different microscopic mechanisms and is accompanied with unlike AE signals. Polycrystalline AlMg and Mg alloys with various compositions were investigated. Both these kinds of alloys are known to exhibit a highly cooperative character of plastic flow, leading to strong acoustic activity [124, 75]. At the same time, having different crystal structure, they are characterized by distinct microscopic mechanisms of plastic deformation: a combination of twinning and dislocation glide in hexagonal Mg and the Portevin–Le Chatelier effect in face-centered cubic Al alloys. Furthermore, the use of polycrystalline alloys allows for varying their grain structure and defect microstructure by special heat treatments.

AlMg alloys. Tensile tests were carried out using aluminium alloys of 5000 series with 5wt.% and 3wt.% of Mg. The average grain size in these two kinds of alloys was about 4-6 μm and 30 μm, respectively (Figs. 2.1). Specimens with a dog-bone shape and gauge

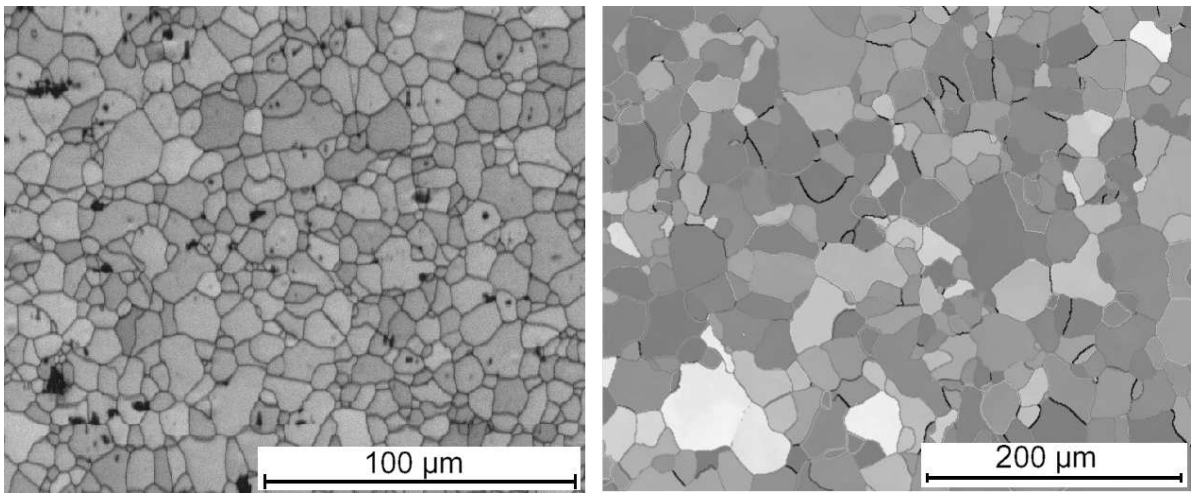

Figure 2.1: Microstructure of Al-5wt.%Mg(left) and Al-3wt.%Mg(right) before solution treatment.

parts $30 \times 7 \times 1mm^3$ (Al5Mg) or $25 \times 6.8 \times 2.5mm^3$ (Al3Mg) were cut from cold-rolled sheets in two orientations, along and across the rolling direction, and tested either in as-rolled conditions or after annealing for 2h at 400°C, followed by water quenching. Such heat treatment is well-known in literature. It is aimed at dissolution of second-phase inclusions and obtaining a virtually homogeneous solid solution with a uniform distribution of magnesium atoms [157]. For both alloys, it led to partial recrystallization and resulted in grain size about twice as large as it was initially (Figs. 2.2).

Mg alloys. A thorough study was realized using MgZr alloys which are known to be prone to twinning. Samples with different Zr content were taken as it strongly influences on the grain size. Specimens with a rectangular cross-section of $5 \times 5mm^2$ and gauge length of 25 mm were prepared from material with 0.04wt%, 0.15wt%, and 0.35 wt% of Zr, which had the average grain size of 550 μm, 360 μm, and 170 μm, respectively (cf. Fig. 2.3). All samples were obtained as cast and annealed for 1h at 250°C before deformation, in order to reduce the density of dislocations and twins formed during casting. Some tests were done on an industrial alloy AZ31 (2.9wt.% Al, 0.98 wt.% Zn, 0.29 wt.% Mn). Cylindrical samples 35 mm long and 6 mm in diameter were obtained by extrusion from melt using different regimes (extrusion speed of 8 m/min and 45 m/min,

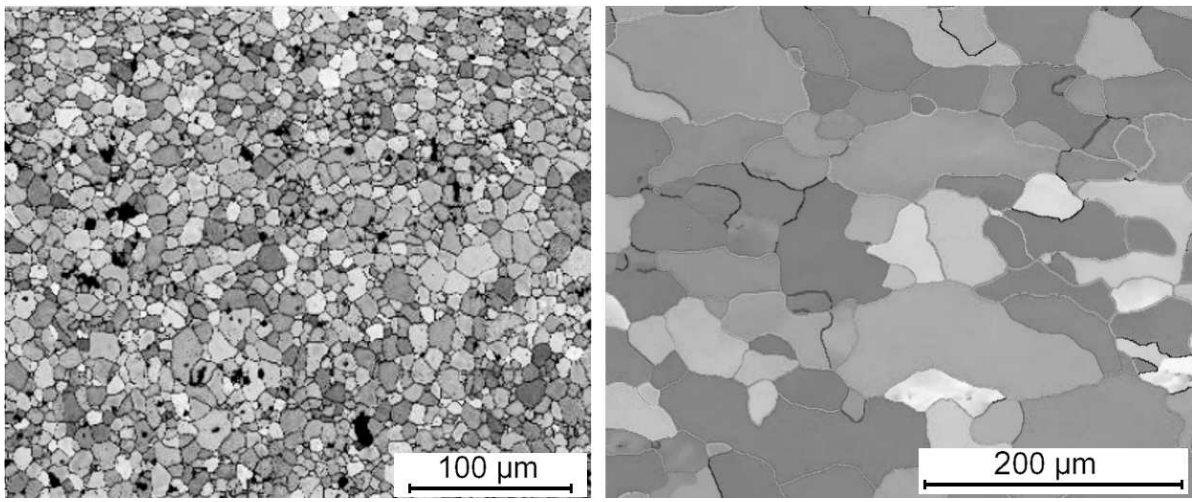

Figure 2.2: Microstructure of Al-5wt.%Mg(left) and Al-3wt.%Mg(right) after solution treatment.

extrusion ratio 1:28 and 1:30, temperature in the range from 100°C to 300°C), resulting in essentially two polycrystalline structures: one with rather coarse grains (about 15 μm) and the other containing a fraction of finer grains (about 3 μm). Examples of metallography of Mg alloys are presented in Fig. 2.4. Hereafter, we will use designation *s1* and *s2* for structures shown in Figs. 2.4(left) and 2.4(right) respectively.

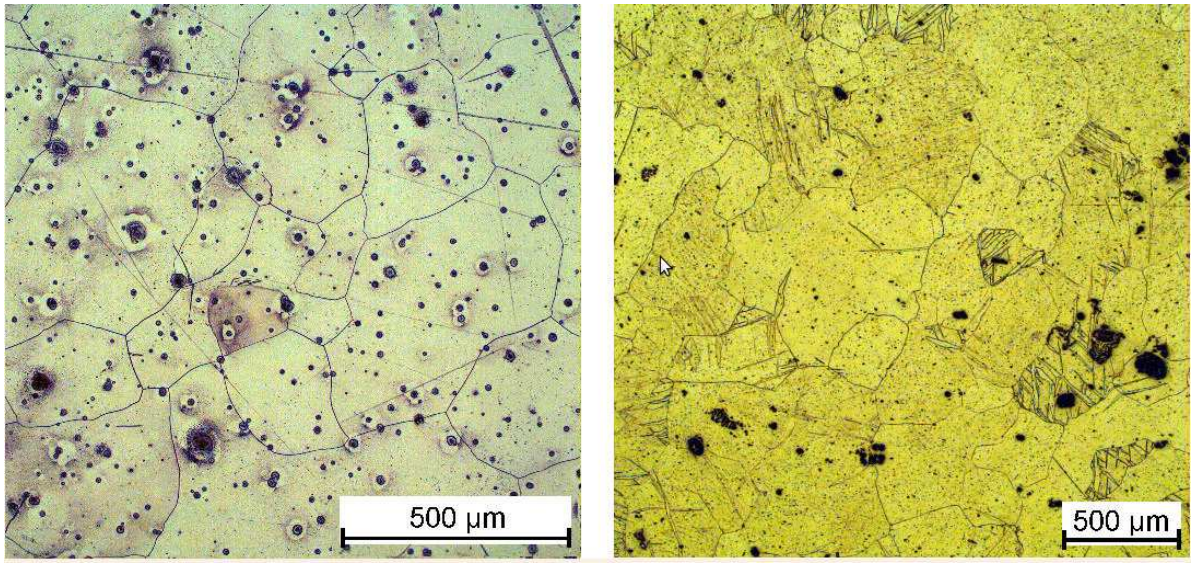

Figure 2.3: Microstructure of Mg-0.35wt.%Zr (left) Mg-0.04wt.%Zr (right) alloys.

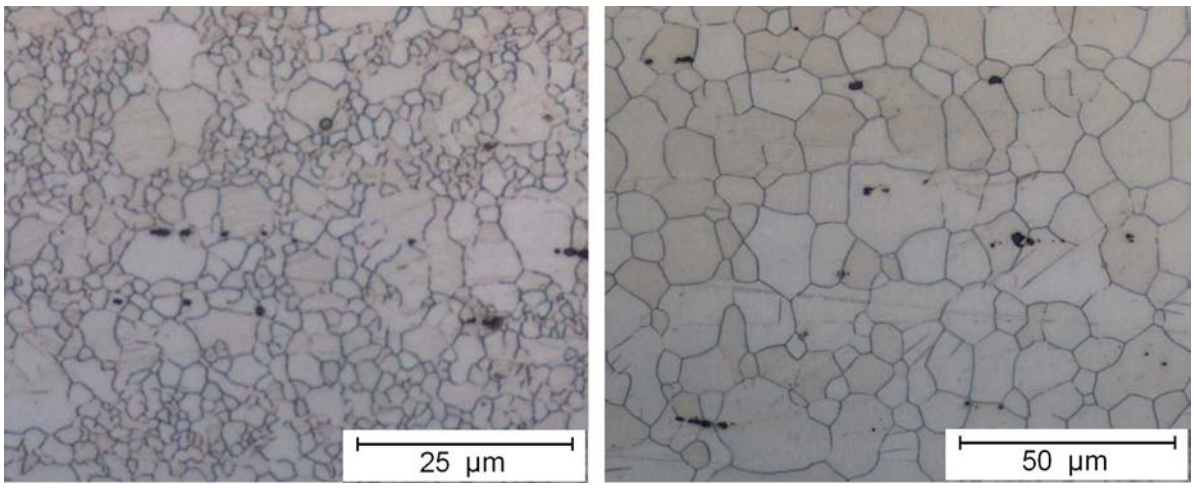

Figure 2.4: Microstructure of AZ31 alloy: structure with a fraction of finer grains (left), structure with coarse grains (right).

2.2 Mechanical testing

The present work presents data obtained in tensile tests. The AlMg samples were deformed in a highly sensitive screw-driving *Zwick/Roell 1476* machine controlled by the software package *testExper*. Either $10kN$ or $100kN$ load cell was used depending on the specimens cross-section, in order to warrant the maximum resolution. The tests were carried out at a constant crosshead speed V, i.e. in the hard-machine configuration (the machine stiffness was approximately $10^7 N/m$). This loading mode is known to be characterized by complex deformation curves and acoustic emission, for which various nontrivial dynamical regimes have been found (see Chapter 1) [12, 5, 82]. It is also worth reminding the analogy between the PLC effect in the hard machine and the dynamical "stick-slip" models of earthquakes, which was suggested in several works [5, 6] and adds interest to the analysis of AE from the general viewpoint of investigation of avalanche-like processes.

Since the PLC effect displays various types of behavior depending on the imposed strain rate and/or temperature, V was varied in a wide range corresponding to the nominal applied strain rate (referred to the initial specimen length) in the range $\dot{\varepsilon}_a = 2 \times 10^{-5} s^{-1} \div 2 \times 10^{-2} s^{-1}$. All tests were performed at room temperature. The choice of the acquisition time for recording the stress-time curves was a compromise between the

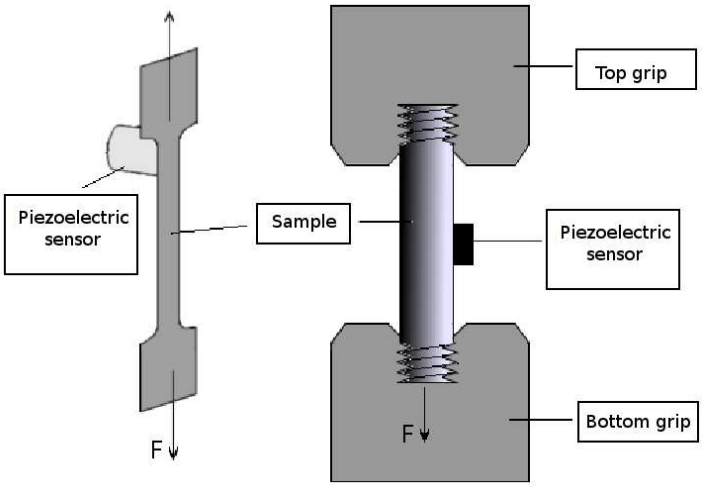

Figure 2.5: Scheme of acoustic sensor disposition for an AlMg sample (left) and an AZ31 sample (right).

limited storage capacity of the software and the requirement of sufficient resolution of stress drops caused by the PLC instability. Accordingly, the sampling time was chosen in a range from 4 ms for the fastest tests lasting tens of seconds and 0.5 s for the slowest ones lasting several hours.

The Mg alloys were tested in the framework of French-Czech Republic collaboration, using a *Zwick Z50* deformation machine with a similar stiffness, available in Charles University in Prague. The tests were carried out at room temperature with a constant nominal strain rate in the range $\dot{\varepsilon}_a = 1 \times 10^{-4} s^{-1} \div 1 \times 10^{-3} s^{-1}$ and sampling rate of 0.01 s or 0.1 s.

2.3 Acoustic emission measurements

Since the present work was aimed at investigating the intrinsic structure of the global AE signals generated in the deformed sample, this allowed using not very long specimens and a single acoustic sensor in each experiment. Spatial localization of the sources of AE events, i.e., mapping the sites where local plastic processes take place, will be a task for future work.

The AE was captured by piezoelectric transducers clamped to the specimen surface using silicon grease and a spring, to warrant a good acoustic contact. Most of experi-

ments on AlMg alloys were done using a Micro-80 sensor with the operating frequency band 200-900 kHz and sensitivity of 57 V/(m/s) (dB), fabricated by Physical Acoustic Corporation. During tension tests, it was usually clamped to the wide specimen head above its gauge length, in order to avoid direct shocks when the deformation bands emerge on the surface (Fig.2.5). The control tests with the transducer fixed in the middle of the gauge length of the specimens did not show influence of the sensor location on the AE statistics.

The same sensor location was used in all tensile tests on Mg alloys (Fig. 2.5). In these experiments, a miniaturized MST8S piezoelectric transducer (3mm diameter, frequency band from 50 to 600 kHz, sensitivity 55 dB (ref. $1V_{eff}$)) was used, which helped keeping a good acoustic contact in spite of the specimen surface distortion during deformation.

The AE recording equipment utilized in the present study was based on the systems which allow for continuous sampling of the AE signal arriving from the piezoelectric transducer. This made possible a comprehensive post-processing of both the complete stored signal and the waveforms of individual acoustic events. Since such continuous recording results in huge data files, the entire data stream was only gathered for high enough strain rates, $\dot{\varepsilon}_a > 2 \times 10^{-4} s^{-1}$. The signal was recorded piece-wise in the slower tests. In all cases, the equipment additionally used a standard procedure of picking out acoustic events ("hits") during the entire test, applying some preset criteria (without data streaming), as described below (see §2.4).

In the experiments on AlMg and MgZr alloys, the signal from the transducer was pre-amplified by 40 dB and recorded with the aid of the Euro Physical Acoustics system (PCI-2 18-bit A/D device fabricated by Physical Acoustic Corporation), with the sampling rate of 2 MHz or 1 MHz, respectively.[1]The AE measurements during deformation of AZ31 samples were carried out with the aid of DAKEL-CONTI-4 AE system developed by ZD RPETY - DAKEL Rpety (sampling frequency of 2 MHz; 4-channel data acquisition with 12-bit A/D converter for each channel), which allows for recording data in four channels with different amplification, in order to avoid overamplification

[1]In the first tests on AlMg alloys, an older Physical Acoustics LOCAN 320 system was utilized, which did not provide data stream but recorded series of acoustic events, using preset parameters.

and saturation of the measured voltage. The signals were pre-amplified by 26 dB; the total gain was varied between 26 and 80 dB.

2.4 Individualization of acoustic events

As follows from the discussion of the possible overlapping of avalanche processes in § 1.4.3, the problem of extraction of individual events from a continuous signal is very important for application of quantitative analyses to experimental data. For example, acoustic events may either closely follow each other or be generated almost simultaneously in different locations in the sample, and be recorded as a single event. It is not clear *a priori* how such overlap of individual events would affect the results of the statistical analysis. On the other hand, each AE event might give rise to several echoes due to sound reflections from interfaces and consequently, be recorded as a few separate events. Another source of errors stems from insufficient resolution of the individual events against noise. All these factors are affected by the criteria utilized to identify the events within the acoustic signal. Up to now, the sensitivity of the apparent statistics to these criteria has not been verified experimentally, although the problem is general and concerns a vast range of dynamical systems of different nature which are characterized by depinning transitions and avalanche-like behavior.

Since the data streaming leads to huge data files (many hundreds of gigabytes), some standard procedures are used in most of AE applications to extract significant acoustic events in real time, without recording the continuous signal itself. In order to ensure the continuity of the present results with literature data, as well as the conformity of the results obtained by different methods and for different datasets, we applied the same approach to the events identification in a continuously stored AE signal. Namely, the record is looked through and the procedure makes use of four preset parameters (Fig. 2.6):

- The threshold voltage U_0. This parameter is aimed at cutting off the part of the acoustic signal below the noise level. An event is considered to start when the

signal surpasses U_0.

- The hit definition time HDT. The event is considered to have come to an end if the signal remains below U_0 longer than during HDT.

- The peak definition time PDT which determines the event peak amplitude A. Namely, the software detects the local maxima of the signal and compares them to the current value of its absolute maximum. The current global maximum is recorded as the event peak amplitude A if it has not been exceeded during a period equal to the PDT. Otherwise, it is assigned the new value and the time counting is restarted. In what follows, this parameter is supposed to be equal to half HDT, if not stated explicitly otherwise.

- The hit lockout time (HLT), or dead time. After detecting the end of an event, no measurements is performed during HLT in order to filter out sound reflections. The HLT is triggered at the end of HDT. Consequently, the sum of HDT and HLT represents the minimum time between the end of one event and the start of the next one.

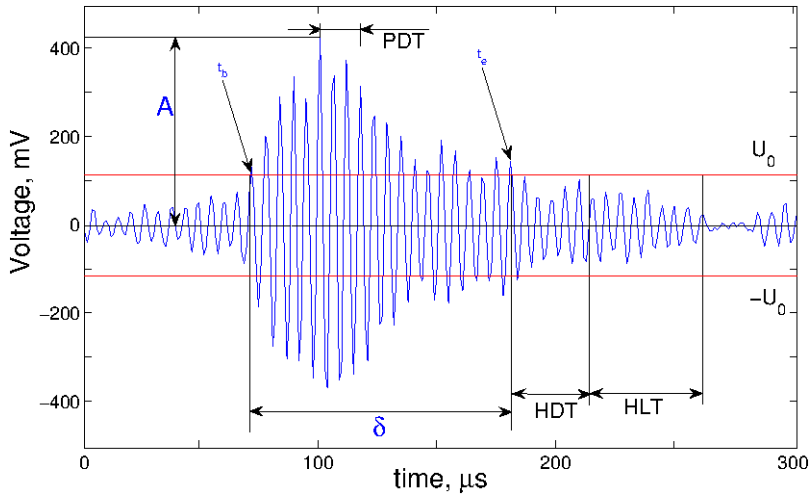

Figure 2.6: Scheme of event selection

Using these preset parameters, various characteristics can be determined for each acoustic event, among which

- The peak amplitude A (see above);

- The starting time t_b;
- The duration δ;
- The dissipated energy E computed as the integral of the squared signal amplitude over the event duration: $E = \int_{t_b}^{t_b+\delta} U^2(t)dt$;
- The count-rate defined as the number of crossings of the acoustic signal over the noise threshold.

It is obvious that the choice of U_0, HDT, and HLT may influence on the identification of the AE events and, therefore, on the apparent statistical distributions of their characteristics. The conventional AE studies apply the following rules of thumb to set the time parameters. In one approach, a high value is chosen for HDT in order to include all sound reflections into the event. HLT can then be taken small. The disadvantage of this approach is that the event duration and the related parameters, such as the AE energy, are loosely determined. In the opposite case, a small HDT is set in order to separate the hit from the sound reflections which are then cut off by choosing a large HLT. This method is not free from drawbacks either, because it results in a lost of a part of the useful signal, particularly, the "aftershocks" that may follow the initial plastic event [82]. In any case, the criteria of "smallness" or "largeness" are approximate. These difficulties justify the need for investigation of the influence of the parameters of the events individualization on their statistics, which was undertaken in the present thesis.

Chapter 3

Data analysis

3.1 Statistical analysis

The statistical analysis proved to be rather useful for studying plastic deformation because of numerous examples of intermittent deformation behavior which is associated with non-gaussien, power-law statistical distributions of plasticity processes (see Chapter 1). The statistical analysis of AE accompanying various physical processes is usually applied to the events amplitudes (e.g., [57, 82, 16]) because the duration and other allied characteristics, in particular, the dissipated energy obtained by integration over the AE event duration, do not properly reflect the properties of the source signal. Indeed, the time characteristics may be affected by the properties of the transfer function of the piezoelectric transducer, reflections and interference of sound waves, and so on. An additionnal reason for such a restriction concerning the PLC effect is the merging of acoustic events during stress serrations, which was conjectured in [16] and will be justified by explicit proofs in the present thesis. It is found that the events merging results in bursts in their apparent durations, whereas the amplitude range remains essentially unchanged. For these reasons, we will pay the most attention to the analysis of the amplitude distributions.

Two approaches to the statistical analysis of AE amplitudes are reported in the literature. The first approach is based on the qualitative analogy between plastic deformation

of solids and seismic processes. Analysis of a large number of seismic records proved that the earthquakes statistics obeys the Gutenberg-Richter relationship between their magnitude M, a characteristic roughly corresponding to the logarithmic peak amplitude of AE events, and the number N of earthquakes greater than or equal to magnitude M: $\log_{10} N = a - (b \times M)$ [61]. Here, the seismic b-value characterizes the power-law scaling. As is readily seen, a disadvantage of such a direct projection of the methods of seismology on the study of AE during plastic deformation is that power-law behavior is expected *a priori.* Another approach to the analysis of AE statistics was proposed by *Weiss et al.* who studied plastic deformation in pure materials (e.g., [20]). The authors argued that the squared value of the peak amplitude A of an acoustic wave provides a physically based measure of plastic activity, reflecting the energy E dissipated by the plastic processes in the deforming sample: $E \sim A^2$. Both approaches were used in the present thesis, and led to consistent results. In what follows, the results obtained by the latter method are presented.The following procedure was used to compute distributions of (squared) amplitudes and durations of acoustic events. For a given quantity x, its probability density function $P(x)$ is expressed as $P(x) = \frac{1}{\delta x}\frac{\delta N(x)}{N}$, where N is the total number of data in the statistical sample and $\delta N(x)$ the number of events corresponding to x-value in the interval $[x - \delta x/2, x + \delta x/2]$. To handle the statistics of rare events, e.g., events with high amplitude, the method of variable bin sizes was used. As a rule of thumb, when an initial-size bin contains less than a preset minimum number of events, it is merged with the next bins until this minimum number is reached (cf.[5, 6]). In the present work, it was chosen to be equal to 5.

In the case when the data were distributed according to a power-law in a certain interval of value, the power-law exponent was determined as the slope of the corresponding linear dependence in double logarithmic coordinates using the least-squares method. Recently, a new generalized method, based on the Monte-Carlo technique, was proposed to evaluate the closeness of experimental statistics to a power law [158]. The test calculations showed that the evaluation of the exponent and its uncertainty by these two methods provide similar results.

In order to examine the strain dependence of the power-law dependences, the time intervals where both the AE and the deformation curves look visually steady were first searched for. This partition was then refined by varying the width of the intervals and repeating the calculation of the distribution functions until finding intervals where the magnitudes of the exponents remained constant within the error determined by the least-squares method.

3.2 Fourier analysis

Another well-known fundamental tool for processing time series is Fourier transformation which allows determining the frequency spectrum by decomposing the analyzed signal $f(t)$ into the sum of harmonic functions $\{e^{ikt}\}$:

$$f(t) = \sum_{k=-\infty}^{+\infty} f_k e^{ikt}, \tag{3.1}$$

where f_k is the contribution of the frequency k, given by the following relationship:

$$f_k = \frac{1}{2\pi} \int_{-\pi}^{\pi} f(t) e^{-ikt} dt \tag{3.2}$$

For numerical analysis of discrete time series, the respective discrete form of Fourier transformation (DFT) reads:

$$F_m = \sum_{n=0}^{N-1} f_n e^{-\frac{2\pi i}{N} mn} \tag{3.3}$$

where $m = 0, 1, ..., N-1$. Equations (3.3) translate the mathematical meaning of the transform but the direct computation using this definition is often too slow. Fast Fourier transformation (FFT) is usually applied in practice[159]. In the thesis, the MATLAB realisation of this method was utilized to determine the spectra of the typical AE waveforms observed in the experiment.

This analysis is particularly efficient when the analyzed signal is composed of several harmonics. Then, the output of the computation provides their frequencies and intensi-

ties. However, the FFT applications are not limited to these cases. In fact, the Fourier transformation often provides important pieces of information on the nature of complex signals. For example, white noise possesses a continuous spectrum, where all harmonics have the same amplitude. The spectra of deterministic signals describing non-periodic motion are also continuous, however, various harmonics give different contributions. For example, the spectrum of a chaotic signal typically decreases with increasing frequency, with broad peaks or narrow lines often superposed on this background [4]. In the case of SOC, the continuous spectrum is described by a power-law $S(f) \sim 1/f^{\alpha}$, with the exponent α in the range between 1 and 2 [44]. It is worth noting that in practice, these idealized patterns are perturbed by the contribution from noise, which reduction is often a difficult task.

In addition to FFT analysis of the AE waveforms, the Fourier spectral analysis was also applied to the continuously recorded signal in order to examine the evolution of the emitted energy and the characteristic frequency of the signal. The details of the procedure can be found in the original paper by Vinogradov [160]. The data set was divided into half-overlapping windows of 4096 data points. After subtraction of the laboratory noise which was recorded before each test, the power spectral density function $P(f)$ of each subset was computed using FFT, and two characteristics were obtained from the $P(f)$: the sound "energy" E

$$E = \int_{f_{min}}^{f_{max}} P(f)df \tag{3.4}$$

and the median frequency f_{med} :

$$\int_{0}^{f_{med}} P(f)df = \int_{f_{med}}^{\infty} P(f)df \tag{3.5}$$

The so-obtained time dependences of energy and median frequency were smoothed over ten to thousand points, depending on the applied strain rate. As argued in [160], the variations in the average energy and median frequency reflect the variations in the degree of correlation in the motion of dislocations generating the AE.

3.3 Multifractal analysis

The multifractal (MF) analysis [15] has been widely used to detect self-similarity in natural systems with complex dynamics. The applications concern the treatment of both the structures emerging in such systems and the temporal signals reflecting their evolution. The well-known examples are the thin-film morphology [161], dendritic solidification [162], dielectric breakdown [163], volcano activity [164], rainfalls [165], street traffic [166], and so on. In contrast, only sparse examples of its application to plasticity problems or, somewhat more often, in the field of materials science could be cited. In particular, it was successfully used to characterize the serrated deformation curves under conditions of the PLC effect [84, 120]. The approach described in [120] is accepted in this thesis. A short outline of the method, necessary for understanding the data analysis, is given below. A more detailed description including the basic concepts of fractal dimensions is presented in Appendix 1.

The application of the MF analysis requires defining the so-called local probability measure. This quantity is constructed to characterize the intensity of the signal locally, in a time window, and allows detecting the scaling law when the window width is varied. As the papers [84, 106, 17] dealt with other kinds of time series, in particular, with stress fluctuations, one issue to be discussed here concerns the choice of the measure for the analyzed signals. In the present case, two kinds of time series have been dealt with: the raw AE signal $U(t)$ measured "continuously" with a given sampling time dt, i.e., at $t = jdt$ (j is the serial number) and the series of amplitudes of AE events, A_j. Note that in the latter case, the index j does not order the recorded data points but the extracted AE events characterized by the amplitude and time of occurrence. The same calculation procedure was utilized in both cases. In what follows, both time series will be designated as ψ_j ($j = 1...N$, where N is the total number of data points in the respective series).

The calculations were performed using the fixed-size box-counting algorithm [167]. For this purpose, the analyzed time interval T is covered by a grid with division δt (see

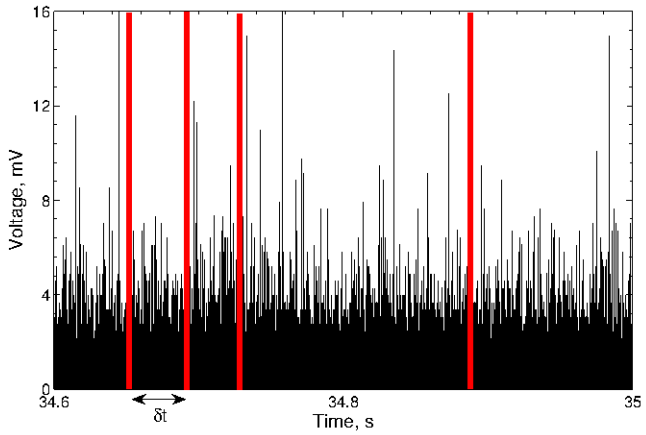

Figure 3.1: Example of AE time series. In this case, the measure is distributed on the time axis, the red line shows division into sections δt.

Fig.3.1) varied as a power of 2. The local measure $\mu_i(\delta t)$ is defined as follows:

$$\mu_i(\delta t) = \frac{\sum_{k=1}^{n} \psi_k}{\sum_{j=1}^{N} \psi_j}, \tag{3.6}$$

where n is the number of data points in the i^{th} interval.

Using this definition for the measure, the value of δt is varied and the scaling of the partition functions

$$\begin{cases} Z_q(\delta t) &= \sum_i \mu_i^q, q \neq 1 \\ Z_1(\delta t) &= \sum_i \mu_i ln \mu_i, q = 1 \end{cases} \tag{3.7}$$

is studied for several real q-values. It should be noted for clarity that the series A_j do not fill the time interval continuously. Obviously, only nonempty intervals corresponding to nonzero measure are present in these sums.

As can be easily shown (e.g., [168]), in the trivial case of self-similarity of a constant signal, Z_q is proportional to δt^{q-1} and the dependences $log(Z_q)/(q-1)$ vs $log(\delta t)$ are represented by straight lines with the same slope equal to 1 for all $q \neq 1$ ($Z_q \propto log(\delta t)$ for $q = 1$). A pure stochastic or a periodic signal on average tend to this case due to homogeneously filling the time axis above a certain characteristic scale (the magnitude of the period or the average spacing). A fractal signal would also be characterized by a unique slope. However, its value, which is called fractal dimension, differs from unity. As

insignificant as it could seem, this quantitative difference in the scaling law reflects very complex behavior. For multifractal objects, most often met in real complex systems, the slopes of the straight lines depend on q. In this case, the following relationships are fulfilled:

$$\begin{cases} Z_q(\delta t) &= \delta t^{(q-1)D(q)} \\ Z_1(\delta t) &= D(1) ln \delta t \end{cases} \tag{3.8}$$

where $D(q)$ are the generalized fractal dimensions (designation D_q will be also used when needed to facilitate reading) .

Besides the spectra of generalized dimensions, an equivalent description in terms of singularity spectra $f(\alpha)$ [169] was used as well. Here, the singularity strength α (Lipchits-Hölder index) describes one more feature of self-similar structures, namely, singular behavior of the local measure, expressed as a scaling law:

$$\mu_i \sim \delta t^{\alpha}. \tag{3.9}$$

For multifractal objects, the exponent α can take on a range of values corresponding to different regions of the heterogeneous object analyzed. The f-value gives the fractal dimension of the close-to-uniform subset corresponding to close singularity strength between α and $\alpha + d\alpha$. By representing a heterogeneous object as consisting of interpenetrating fractal subsets, this description clarifies the physical meaning of the MF analysis. At the same time, the singularity spectra are more difficult to calculate. For the sake of clariness, more details are taken to Appendix 1.

Essentially, the MF analysis allows uncovering the presence of correlations between both amplitudes and times of occurrence of events in the signal through their scaling behavior, and characterizing the heterogeneity of the scaling properties over a range of subsets of events. Focusing on a given subset is obtained through the choice of q: for example, large positive q-values tend to select large measures in the partition function, while large negative q-values allow highlighting small events. Variation of q over a set of

real numbers thus provides continuous characterization of heterogeneity, the property known as a "mathematical microscope". A wide spectrum of the values of D, f, or α indicate a substantial shift in the correlation characteristics between large events on the one hand, and small events on the other hand. Note that most natural fractals are multifractals, since (homogeneous) fractality is a more demanding property than (heterogeneous) multifractality.

In the case of real signals, the above scaling laws are satisfied in bounded ranges of δt. Indeed, experimental data always possess characteristic scales implied by the size of the system, the dimensions of its structural elements, the length of the time interval analyzed, the resolution of the equipment, the experimental noise, and so on. In order to reduce noise, two approaches were applied. First, the test calculations showed that the MF analysis of an entire AE signal leads to stochastic-type behavior. By applying a threshold U_0 and gradually increasing its height, it was found that multifractal behavior can already be detected for the data exceeding 24 dB, in spite of the incomplete suppression of the noise. This threshold level was usually applied. A complementary method of noise reduction made use of wavelet analysis described in the next section.

The MF spectra were plotted by varying q in a large interval from -20 to 40. Recently, it was shown that the estimates of the scaling exponents systematically depart from the correct values for $|q| > 10$ [170]. Still, the corresponding curves are useful as sensitive indicators of any imperfectness of the linear trend. For this reason and because the present analysis is based on the relative changes occurring when either the experimental conditions or the scale of observation are varied, such data will also be used in further illustrations.

3.4 Wavelet analysis

Wavelet transformation is a powerful tool of signal processing, whose principles and numerical implementation have been described in detail in many books and original papers (e.g., Refs. [171, 172]). Only basic concepts, which are of relevance to the

subsequent analysis, will be recapitulated in this section.

Wavelet transformation decomposes a signal into constituent parts with different frequencies and evaluates the contribution of each part on different time scales [171]. It is defined through relationship:

$$W(a,b) = \frac{1}{\sqrt{2}} \int_{-\infty}^{\infty} f(t)\psi(\frac{t-b}{a})dt, \tag{3.10}$$

where a is a scale factor, b is a time shift, and ψ is a soliton-like function, known as "mother" wavelet, which satisfies a following condition:

$$\int_{-\infty}^{\infty} \psi(t)dt = 0. \tag{3.11}$$

Note that the wavelet transformation uses a time-frequency description similar to Fourier transformation in that both are performed by taking the integral of the inner product between the signal and the analyzing function. However, in contrast to Fourier analysis, which is based on infinite trigonometric series, the wavelet transform uses a finite wavelet function. It is this property that allows revealing information on both time and frequency. The right choice of wavelet ψ makes possible examination of the local features of the signal. Computation of wavelet coefficients consists of four steps:

1. Take a wavelet and compute the coefficient from relationship 3.10.

2. Shift the wavelet to the right and repeat step 1 until the whole signal is covered.

3. Scale (stretch) the wavelet and repeat steps 1 through 2.

4. Repeat steps 1 through 3 for all scales.

In the present work, we used Matlab discrete wavelet transformation (DWT) based on dyadic scales. It is applied to series with length equal to a power of 2, and the wavelets are stretched, or dilated, by a factor of 2. In each level of analysis, the analyzed signal is decomposed into two parts: the approximation (low-frequency components) and the details (high-frequency components), as shown schematically in Fig.3.2. The

decomposition can be iterated, so that the signal becomes represented as a sum of many components with specified sets of frequencies.

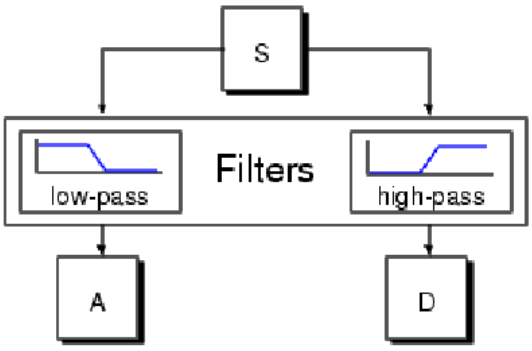

Figure 3.2: Signal decomposition scheme.

It is worth noting that for many real signals, the low-frequency content is the most essential. This remark concerns, for example, the human voice. Indeed, although the voice cleared of the high-frequency components sounds differently, the content of the speech remains recognizable. On the contrary, the removal of the low-frequency components results in a voice sounding like noise. Thus, the wavelet transformation filtering the high-frequency components may uncover the inherent elements of the signal.

Chapter 4

Role of superposition on the statistics of AE events

In this Chapter, the effect of the parameters of individualization of acoustic events on their statistics is examined using various materials the plastic deformation of which is accompanied by strong acoustic activity and controlled by different microscopic mechanisms: a combination of twinning and dislocation glide in hexagonal MgZr alloys and the PLC effect in face-centered cubic AlMg alloys. These materials present a particular interest for the analysis because on the one hand, as pointed out in Chapter 1, both the waveforms of the individual acoustic events and the overall AE behavior have different signatures in the case of twinning or dislocation glide [82, 173]. On the other hand, recent investigations reveal a persistent power-law character of the amplitude statistics of AE in different experimental conditions, although the corresponding exponent may vary with conditions. Such robustness allows analyzing the sensitivity of the experimental estimates to the event identification criteria. A detailed analysis of the AE statistics in relation with the relevant deformation processes will be the scope of the next chapters.

To study the effect of the parameters applied to individualize acoustic events on their apparent statistics, the continuous acoustic signal was recorded using "data streaming" technique. As described in Chapter 2, in order to ensure conformity of the results

obtained by different methods and for different datasets, the events identification in a continuously stored AE signal was designed to mimic the standard procedure used by the acoustic system to extract AE hits in the course of measurement. Each of the three parameters, U_0, HDT, and HLT, was varied in a wide range of magnitude while keeping the other parameters constant.

The entirety of experiments showed that for all samples, and similar to literature on various materials (e.g., [152, 174, 124]), nonstationary AE activity is observed at small strains, in the region of the elastoplastic transition. It further decreases and displays roughly stationary behavior, which allows performing the statistical analysis in a steady-state range. The conformity of the statistics for the events which are either extracted from the continuously recorded signal or detected by the equipment using preset parameters was first verified as illustrated in Fig. 4.1. Figures 4.1(a) and (b) compare the series of acoustic events detected by these two methods in tensile test performed on a specimen of the Mg0.35%Zr alloy. Intervals of approximately stationary behavior where the statistical analysis was performed for this specimen were selected for $t >$120 s. An example of comparison of the results of calculation of the statistical distributions is illustrated in Fig. 4.1(c). In this test, the threshold U_0 was chosen to be equal to 16.48 mV for the continuously measured signal, which corresponds to the logarithmic threshold of 45 dB in the case of real-time measurement. The time parameters were set at HDT = 800 μs and HLT = 100 μs. Importantly, despite the discreteness of the logarithmic measure allowed by the standard procedure, the series of events selected with the aid of two different methods coincide with high accuracy. Furthermore, it can be seen in Fig. 4.1(c) that both methods result in power-law dependences over more than three orders of magnitude of A^2 and give close values for the exponent β determined as a least-square estimate of the slope of the dependences in double-logarithmic coordinates: $\beta = -1.80 \pm 0.03$ and $\beta = -1.78 \pm 0.03$ for the "continuous" and "discrete" methods, respectively. This verification justifies the application of the continuously stored signals to the investigation of the effect of the conventional parameters of identification of AE events on their statistics. We further proceed to a detailed examination of their role for

two kinds of alloys.

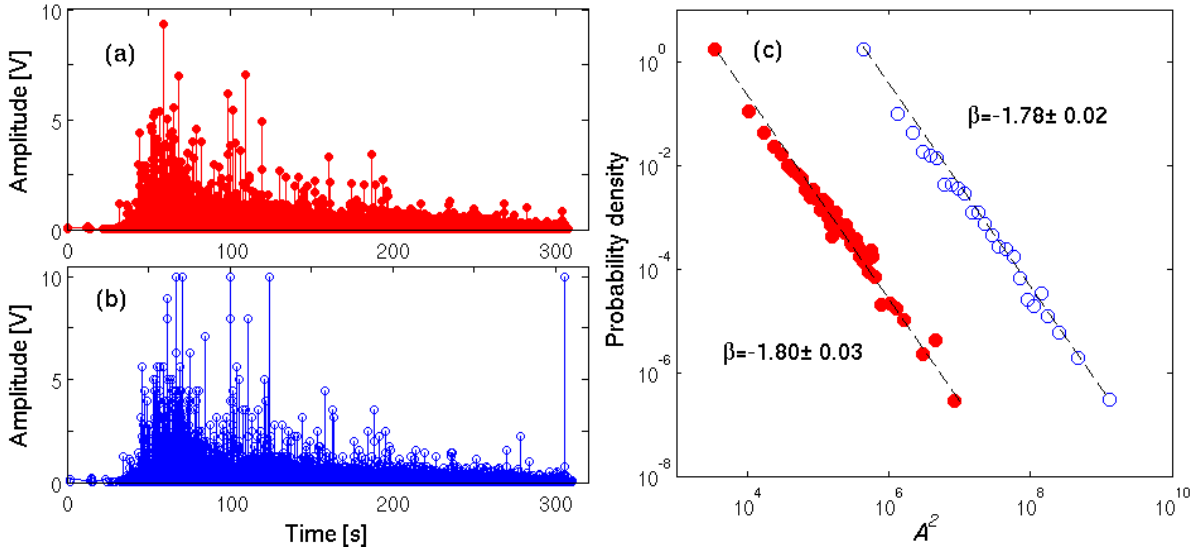

Figure 4.1: Examples of series of AE events which are either (a; red colour) extracted from the continuously recorded signal using the software developed in the present doctoral research or (b; blue colour) detected by the acoustic equipment during the test, using parameters preset before the measurement. In the latter case, the logarithmic values recorded in dB are converted to the linear scale in order to facilitate the comparison. (c) The corresponding statistical distributions. The red line is arbitrarily shifted to the left to avoid superposition of the curves. $\dot{\varepsilon}_a = 3.5 \times 10^{-4} s^{-1}$.

4.1 MgZr alloys

Figure 4.2 shows examples of the probability functions illustrating the effect of U_0 for one particular choice of time parameters, HDT = 50 μs and HLT = 100 μs, for the same Mg0.35%Zr alloy. It can be recognized that the statistics obeys power laws in a wide U_0-range and the corresponding slopes are fairly robust. The main effect of the increase in U_0 consists in the reduction of the number of events and the corresponding limitation of the interval of A^2 because of the cutoff of the low-amplitude events. Nevertheless, some decrease in β can be also detected: $\beta = -1.80 \pm 0.05$ for $U_0 = 9$ mV and $\beta = -1.87 \pm 0.02$ for $U_0 = 60.1$ mV.

Using families of such curves, the dependences of β on U_0, HDT, and HLT were traced in large ranges of variation of each parameter. Figure 4.3(a) represents $\beta(U_0)$-curves for three MgZr alloys and for two choices of the time parameters. It can be

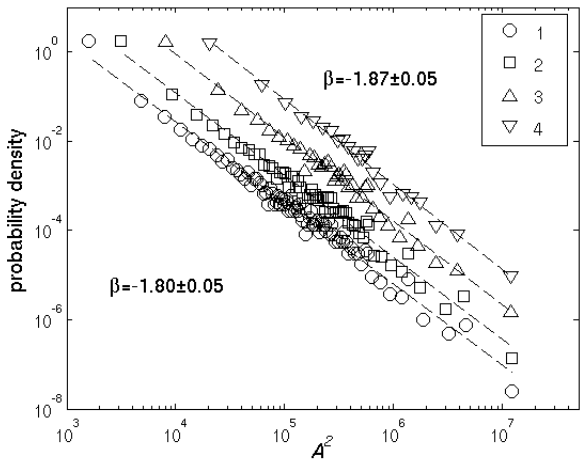

Figure 4.2: Effect of the voltage threshold on the statistics of the amplitudes of AE events for the same specimen. 1 – U_0 = 9 mV, 2 – U_0 = 15.3 mV, 3 – U_0 = 30.5 mV, 4 – U_0 = 60.1 mV.

recognized that β relatively strongly depends on U_0 only in a narrow range $U_0 < 10$ mV (even here, all changes in β do not exceed 0.2). The rate of the dependence falls with increasing U_0. A weak or no dependence (within the error bars) is observed for U_0 in the range from 10 mV to the maximum value of 90 mV, above which the amount of data becomes too small for the statistical analysis. Most probably, the initially higher β-value is explained by the merging of successive AE events when U_0 is low, so that the fraction of smaller events is decreased and the apparent power law is flatter than the true one. Indeed, such merging can take place for low U_0 values if the individual AE hits are linked to each other due to the presence of a (quasi)continuous background, e.g., noise, as illustrated in Fig. 4.4. By admitting this conjecture, the end of the fast changes in β can be explained by U_0 exceeding the continuous background level, so that the AE events become essentially isolated. The merge of such isolated hits will be weaker and will depend on the relationships between all identification parameters and the temporal arrangement (clustering) of the hits, so that some further slight (if any) evolution of β with increasing U_0 may be attributed to the diminishing merge of successive events. This suggestion is consistent with the changes observed when HDT is reduced from 800 μs to 50 μs: since less effective overlapping of successive hits is expected for the lower HDT, the initial fall in the dependence becomes sharper and β quickly saturates at an

approximately constant value. The weak dependences which can be detected in the almost saturated region may also be due to the influence of the statistics depletion. In any case, an important conclusion following from this figure is that the effect observed is weak in a wide U_0-range. Furthermore, for each HDT, a threshold value can be found above which its influence is insignificant.

Another interesting observation is that whereas two of the three kinds of samples display close β-values, the curve obtained for the material with the largest grain size goes separately. In spite of this quantitative difference, all the curves have the same shape described above. Thus, although the different power law indicates a different specific structure of the AE signal in Mg0.04%Zr, a similar effect of U_0 is found. Such robustness testifies that the quantitative difference between the materials with different microstructure is not due to artefacts of the AE method but reflects physically sound changes in the correlation of the deformation processes (see, e.g., [154]). The physical consequences of this and similar observations will be discussed in the next chapters.

The companion Fig. 4.3(b) represents the effect of HDT for the same tests and for two U_0-levels: one selected just above the range of the sharp $\beta(U_0)$-dependence (17 mV) and another taken in the far saturation region (67 mV). It can be recognized that the effect of HDT is weak in both cases and almost negligible for $U_0 = 17$ mV. Some variation of β in a narrow range of small HDT values can be detected for $U_0 = 67$ mV and is most likely due to the statistics depletion. As a whole, the analysis is quite robust against HDT variation. As far as the HLT is concerned (see Fig.4.3(c)), no significant dependence was found over the whole range studied, from 0 to 1 ms. The entirety of these results testifies that the power laws observed for MgZr alloys are robust with regard to the criteria used to select the AE events.

4.2 AlMg alloys

The case of AlMg alloys is particularly delicate for performing such analysis because the corresponding AE commonly has a low intensity and is known to be characterized

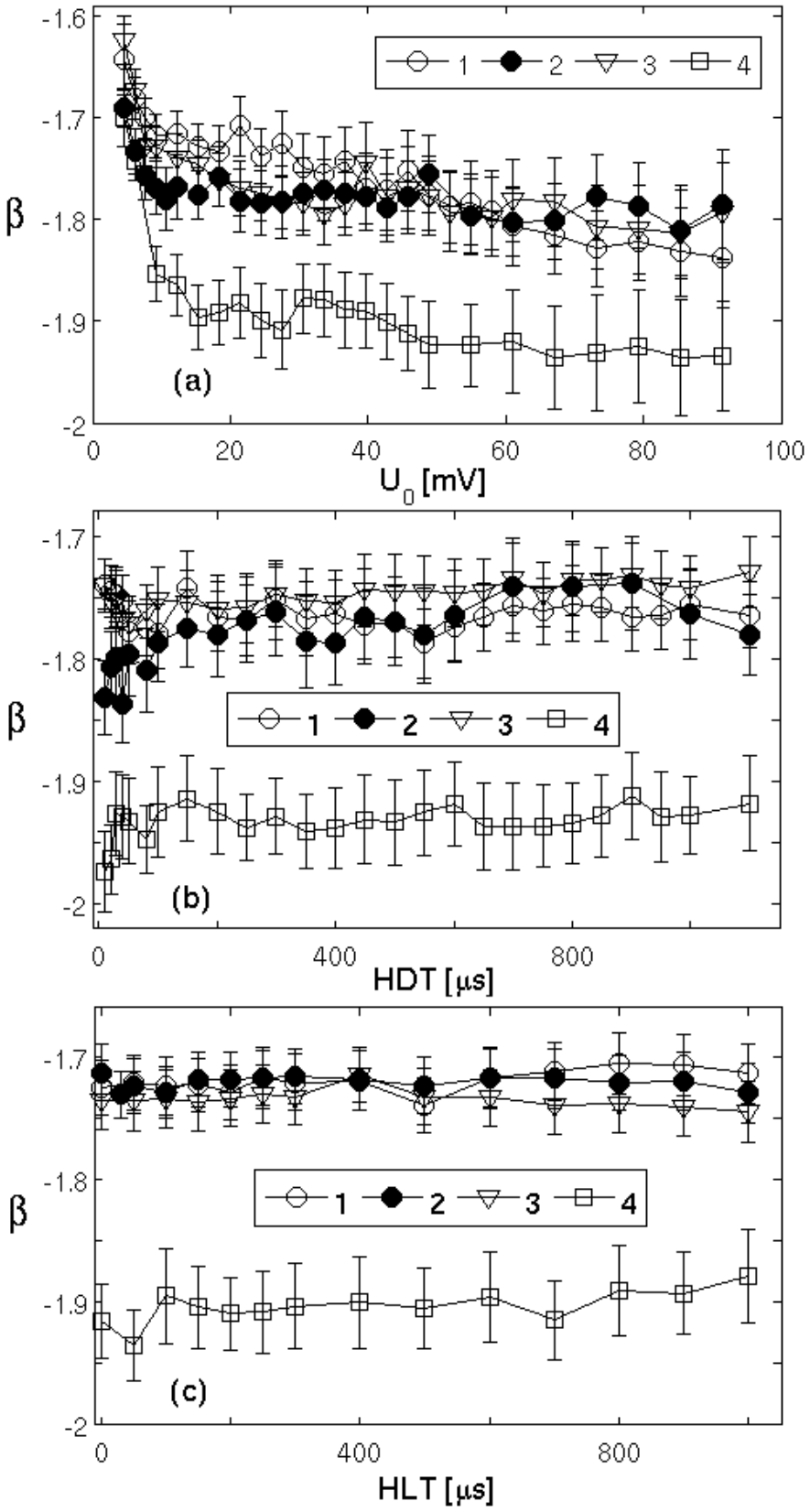

Figure 4.3: Effect of (a) U_0, (b) HDT and (c) HLT settings on the power-law index β for MgZr specimens deformed at $\dot{\varepsilon}_a = 3.5 \times 10^{-4} s^{-1}$. 1 and 2 - Mg0.35%Zr, 3 - Mg0.15%Zr, 4 - Mg0.04%Zr. HLT = 100 μs; HDT = 800 μs except for the case (2) where HDT=50 μs. (b) HLT = 0 μs; U_0 = 17 mV except for the case (2) where U_0 = 67 mV. (c) U_0 = 17 mV; HDT = 100 μs except for the case (2) where HDT = 20 μs.

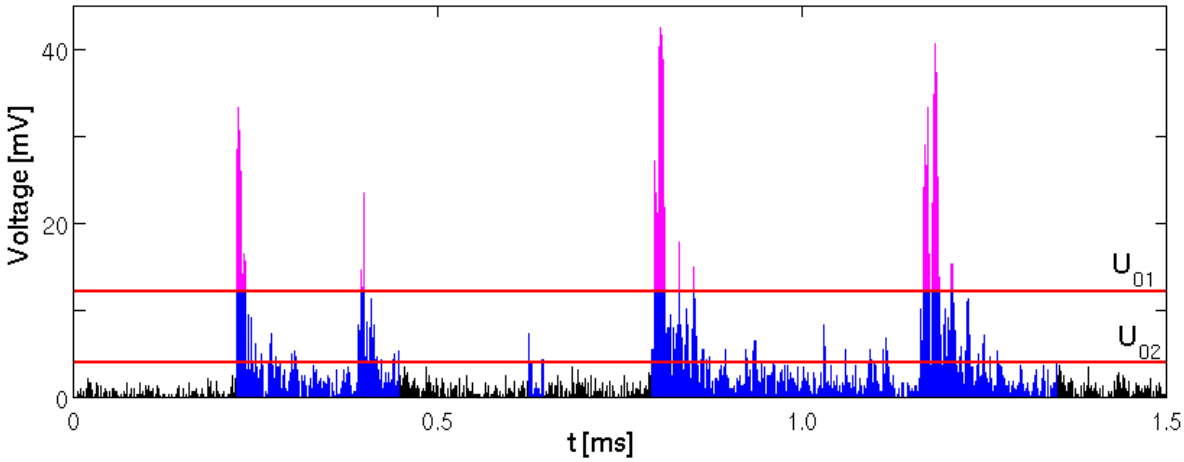

Figure 4.4: Illustration of merging of AE events. The colours show the events detected for two choices of noise thresholds, U_0, and the same choice of HDT which is deliberately taken very large. Application of a large threshold U_{01} gives four separate events (magenta colour) with relatively short duration. Decreasing U_0 leads to merging of consecutive events (blue colour). The number of detected events and the resulting stack of amplitude values do not change significantly but the apparent durations increase drastically.

by strong overlapping and merging of neighboring hits [16]. On the other hand, these features allow for attacking the investigated problem in the conditions of very noisy signals. Additional interest to this material is caused by the presence of transitions between different types of the PLC effect, which lead to different behavior of the instability at the macroscopic scale.

Figure 4.5 summarizes the results of the analysis for as-delivered and annealed Al5Mg specimens deformed at different strain rates corresponding to the three distinct types of behavior of the PLC effect[1]. It can be seen that the influence of the identification parameters is stronger than in the case of MgZr alloys and the dependences are less monotonous. It is obvious that because of the effects of merging of AE events, the results might depend on such casual factors as the specific relationships between the selected time and voltage parameters, the level of the measurement noise, and the distribution of the on-off time periods in the AE signal, which reflect the distribution of the hits durations and their occurrence times. Therefore, we will only stop on some characteristic trends.

[1]It should be reminded that the set-ups used in the tests on different materials did not have the same total gain, so that the absolute U-ranges may differ in figures for different materials.

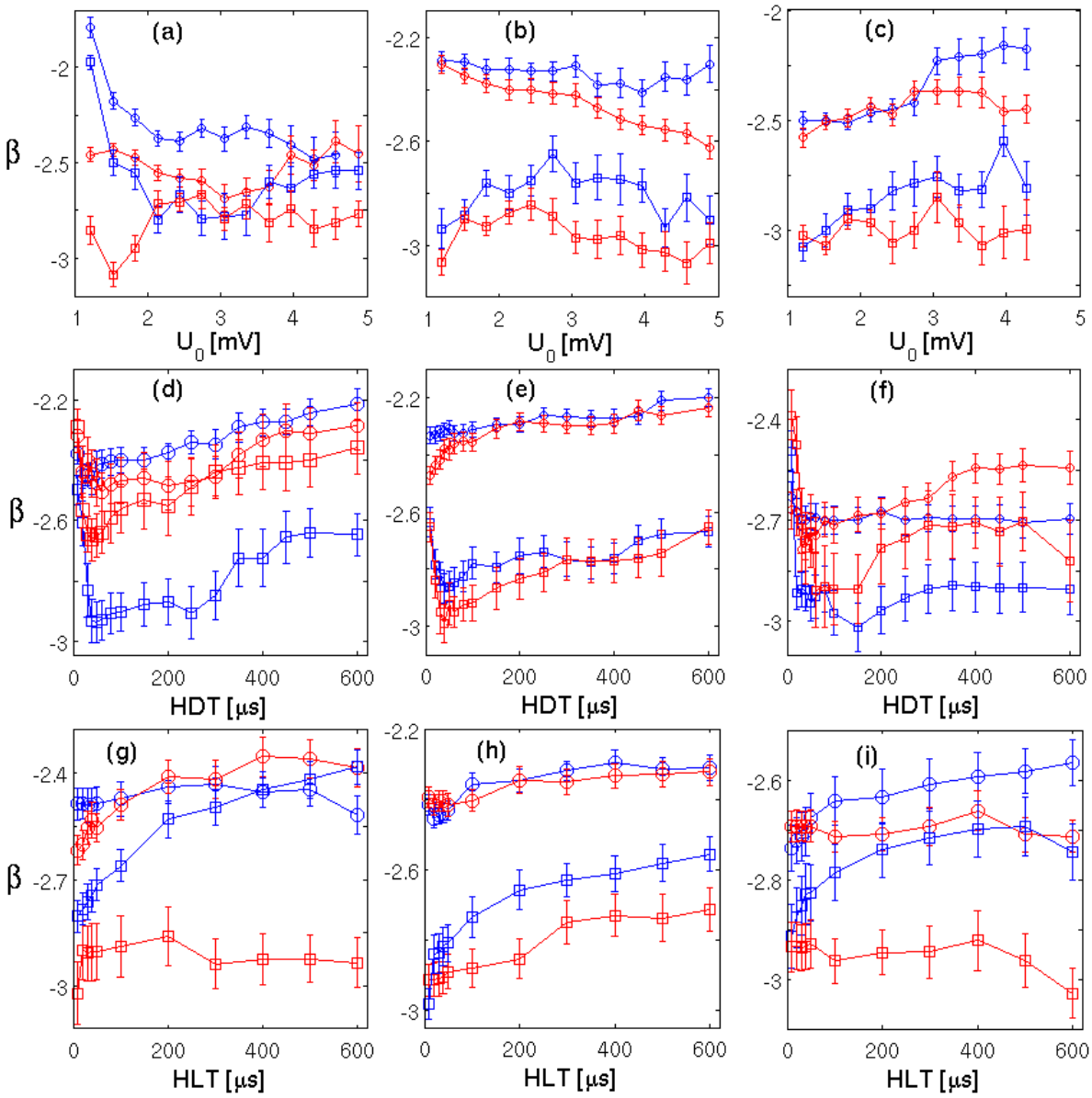

Figure 4.5: Effects of U_0, HDT and HLT parameters on the power-law index β for Al5Mg specimens deformed at (a), (d), (g): $\dot{\varepsilon}_a = 6 \times 10^{-3} s^{-1}$; (b), (d), (h): $\dot{\varepsilon}_a = 2 \times 10^{-4} s^{-1}$; (c), (e), (i): $\dot{\varepsilon}_a = 2 \times 10^{-5} s^{-1}$. Circles and squares designate results for as delivered and annealed specimens, colours designate the different choices of the parameters which are kept constant, for (a), (b) and (c): blue - HDT = 300 μs, HLT = 300 μs, red - HDT = 30 μs, HLT = 100 μs; for (d), (e) and (f): blue - U_0 = 1.85 mV, red - U_0 = 3.4 mV (HLT = 300 μs); for (g), (h) and (i): blue - HDT = 10 μs, red - HDT = 50 μs (U_0 = 1.85 mV).

First of all, it is worth noting that the β-range found for the Al5Mg alloy (typically from -2 to -3) lies remarkably below the similar range for MgZr alloys (-1.5 to -2). This difference is much more significant than any variation in β observed upon modification of the events identification criteria. Furthermore, β-values are almost always higher for

the as-delivered specimens (circles) than for the annealed ones (squares). Taking into account that annealing leads to an increase in the average grain size, this observation is consistent with the above-mentioned grain-size effect observed for MgZr alloys. Importantly, the change in β upon annealing is usually more significant than the uncertainty of β determination caused by the influence of the identification criteria.

More specifically, the first row of Fig. 4.5 represents $\beta(U_0)$-dependences. For the high strain rate (Fig. 4.5(a)) and large HDT and HLT values (blue color), β displays behavior similar to the case of Mg alloys, namely a fast initial drop followed by almost no dependence. The fast initial change, which was attributed above to linking of successive AE events by the agency of a continuous background, disappears when HDT is reduced, so that β becomes nearly constant in the entire U_0-range. It is natural to suppose that when the imposed strain rate is decreased, the measurable AE events which require motion of powerful enough dislocation ensembles become rarer and better separated (the on-off time ratio becomes larger).[2] As a result, the fast initial change does not occur for lower $\dot{\varepsilon}_a$ (Fig. 4.5(b) and (c)). The $\beta(U_0)$-dependences obtained for the lowest $\dot{\varepsilon}_a$ (Fig. 4.5(c)) using a large HDT show a somewhat opposite tendency: a slow increase with U_0. This trend is also consistent with the discussed framework. Indeed, the increase in U_0 leads to discarding small events and decaying big compound events into two or more (big) components, thus resulting in a larger fraction of big events and an apparently higher β-value. This effect is illustrated in Fig. 4.6 which demonstrates the change in the slope of the power-law for the truncated distribution. It should be noted that alongside with the left truncation, obviously stemming from scrapping small hits, some truncation from the right is also seen. It is a common effect for a limited observation time, as it is caused by the casual lost of the rare large events when they find themselves within a HLT interval. The companion curves in Fig. 4.5(c) display the behavior for a reduced value of HDT and demonstrate that the increasing trend in $\beta(U_0)$-dependences is suppressed when the AE events are better separated due to a more appropriate choice of HDT. In this case, the U_0 increase only leads to (left)

[2]The experimental observations explicitly confirming this expectation will be described in detail in Chap. 5

truncation without renormalizing the slope of the power-law dependence. It should also be noted from this point of view that in all three figures, (a)-(c), the $\beta(U_0)$-dependences corresponding to higher HDT (blue symbols) generally lie above their homologs for lower HDT (red symbols), in conformity with the discussed influence of the AE events merging on the seeming β-value.

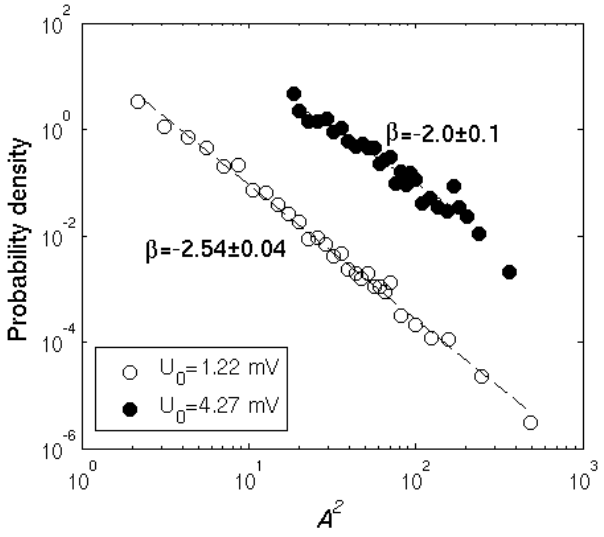

Figure 4.6: Effect of the voltage threshold on the statistics of the amplitudes of AE events for the AlMg specimen designated by blue circles in Fig. 4.5(c).

The above data prove that the choice of the time parameters may be quite important as it can entrain considerable changes in the power-low exponents. The $\beta(HDT)$-dependences are displayed in the second row of Fig. 4.5. It is noteworthy that, as illustrated in Figs. 4.5(a) and (d) for the high strain rate, choosing a small U_0-value corresponding to the range of fast changes on the $\beta(U_0)$-dependence may lead to a considerable shift of the $\beta(HDT)$-curve with regard to its counterpart for a higher U_0-value. Such a shift is observed for the annealed sample (Figs. 4.5(d), squares). The difference is inessential, though, for the as-delivered sample. It is also weak for the low strain rate and practically negligible for the intermediate strain rate which is characterized by weak $\beta(U_0)$-dependences.

In spite of these quantitative changes, similar shapes of the curves are obtained for all three strain rates: first, β rapidly decreases approximately by 0.2 with increasing HDT from 10 μs to 40 μs, then it slowly grows. The initial fast fall may be absent, as

illustrated by the two upper curves in Fig.4.5(e), which correspond to an as-delivered sample deformed at $\dot{\varepsilon}_a = 2 \times 10^{-4} s^{-1}$. This fall can be explained if one recalls that the small HDT may lead to erroneously taking one of the first local maxima of an event as its peak amplitude. This error would enhance the fraction of small events and reduce β correspondingly. Note that the strongest variations on the $\beta(HDT)$-curves obtained for MgZr alloys were observed in the same HDT-range (see Fig. 4.3(b)). Thus, the value of 40 μs determines the lower limit for selecting HDT. The following growth of the exponent, more significant for the higher strain rates, is obviously due to the above-discussed effect of AE events merging. The optimum HDT value does not seem to be the same for each strain rate. However, as the $\beta(HDT)$-dependences are rather weak above HDT=40 μs, this influence can be neglected in most cases.

The third row of Fig. 4.5 illustrates the effect of HLT for two choices of HDT. As could be expected, the power-law exponent strongly depends on HLT for small HDT values, thus confirming the above discussion of the effect of HDT. However, for HDT >= 50 μs, the influence of HLT is insignificant, similar to the data for MgZr case. Its effect mostly consists in the statistics impoverishment which should not influence on the scale-invariant distributions, provided that enough data remain in the dataset.

The effect of HDT and HLT on AE amplitude statistics was also verified in the usual (without data stream) tests on Al3%Mg samples, in which series of acoustic events were recorded using preset parameters. In these experiments, U_0 was set at 27 dB – the value corresponding to the noise level for the free-running deforming machine – and the effect of changing the HDT and HLT by a factor of ten was checked at different strain rates. Such tests are illustrated in Fig. 4.7 which presents examples of AE amplitude statistics for three AlMg samples. All samples were deformed in the same experimental conditions but the time settings used to detect the AE events were different. The analyzed data are normalized with regard to the average over the respective dataset and all three dependences fall onto one master curve, probably except for some deviations from the power law for the largest events. This and similar results obtained for different $\dot{\varepsilon}_a$ testify that the power law observed for Al3Mg alloys is quite robust against the variation of

HDT and HLT.

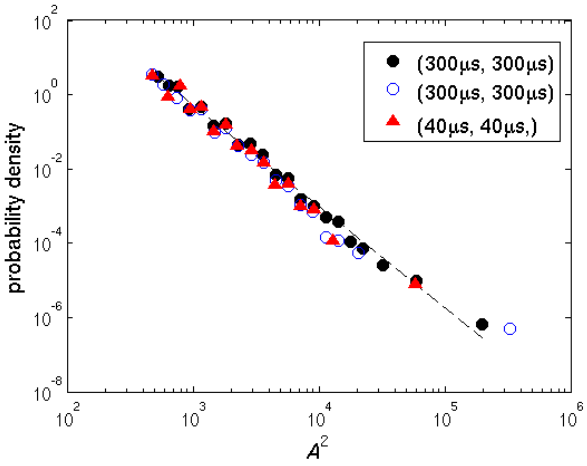

Figure 4.7: Probability density function for squared amplitude of AE events collected in the same strain range for three different samples deformed at driving strain rate $\dot{\varepsilon}_a = 2 \times 10^{-5} s^{-1}$.

4.3 Conclusion

In summary of this chapter, power-law statistics are found for the amplitudes of AE events accompanying plastic flow of various materials in different experimental conditions. The data obtained confirm the hypothesis that the plastic deformation is inherently intermittent, critical-type process at the scale relevant to AE [82, 21, 27, 26]. The major result of the above investigation is that the criteria used to identify the individual AE events weakly influence on the apparent AE statistics. This conclusion has been verified using Mg and Al alloys which are characterized by distinct deformation mechanisms and display different AE behaviors. A very week influence is detected for Mg alloys, in consistence with the literature data reporting well separated abrupt AE hits accompanying mechanical twinning. More specifically, almost no effect was discerned when HDT and HLT were varied. Somewhat stronger, albeit a weak effect is observed in a wide range of the voltage threshold U_0. The only case when a relatively strong influence on the power-law is found corresponds to a narrow range of the lowest U_0 values and is most likely due to aggregation of successive AE events.

A less favorable situation for the application of the AE method is found under con-

ditions of the PLC effect which is known to generate lasting AE events, most likely due to merge of many hits because of successive triggering of many dislocation ensembles during either repetitive formation of deformation bands at low strain rates or propagation of deformation bands at high strain rates. Nevertheless, the influence of the event identification parameters is rather weak in wide ranges of parameters even in this case. In particular, the variations in the β-value caused by the variation of the identification parameters are typically bounded in a range of several tenths, which is much narrower than the difference (about 1 to 1.5) between β-values observed for AlMg and MgZr alloys.

This robustness not only justifies the quantitative estimates of the critical indices but also provides an additional proof of the scale-invariant statistics of AE during plastic deformation. Indeed, one of the consequences of the variation of the event identification parameters is the cutoff of a part of data from the entire statistical sample. The robustness of the statistics against such cutoff is consistent with the scale invariance reflected in the power-law dependences.

Chapter 5

Multiscale study of AE during smooth and jerky flow

Since the pioneer work by Kaiser [73] in 1953, the AE technique is used as a powerful tool to study plastic deformation in various materials. However, before the occurrence of the data streaming technique these studies were based on the extraction of individual acoustic events, as illustrated in the previous chapter, followed by either an analysis of average characteristics over a series of events or, only recently, analysis of their statistics. The data streaming method has opened possibilities for an investigation of AE from a microsecond scale corresponding to individual oscillations within an acoustic event to the scale of the mechanical test. In this chapter we present first results of such investigations[175], which combine an inspection of AE patterns on different time scales with Fourier analysis of both individual waveforms and entire AE signals, as well as statistical analysis of AE events. The most detailed study was realized under conditions of the PLC effect in an Al5Mg alloy. First results are also presented for Mg based alloys. The comparison of behaviors for different materials allows formulation of further directions of these investigations.

5.1 Plastic instability in an Al5Mg alloy

As described in Chapter 1, very recent investigations [16, 17, 18, 129] questioned the conventional point of view that in the case of the PLC effect, the burst-like AE events are caused by the motion of large dislocation ensembles giving rise to stress serrations, whereas smaller-size dislocation avalanches occur randomly during the macroscopically smooth plastic flow and generate virtually continuous AE. In the present research the data streaming technique is applied to study the nature of AE accompanying the jerky flow. On the one hand, it is aimed at providing insight into the kinematics of formation of deformation bands in a wide strain-rate range corresponding to various types of behavior of the PLC effect. On the other hand, the nature of AE is compared during jerky and smooth plastic flow.

5.1.1 AE patterns

The material used for this study was the Al5Mg alloy (see Chapter 2). As shown in Fig. 5.1, it presents mechanical behavior typical of aging alloys. The plastic deformation starts with a Lüders plateau, which is generally interpreted as due to propagation of a deformation band through the gauge length of the specimen, a process associated with unpinning of dislocations from their solute atmosphere in a statically aged material. The Lüders plateau is followed by the PLC effect, governed by dynamical strain aging of dislocations. All three conventional types of deformation curves, *C*, *B*, and *A*, were found as $\dot{\varepsilon}_a$ was varied. The solution treatment led to some softening of the material, resulting in a lower yield point and enhanced ductility, but did not visibly affect the plastic instability. In the case of high and intermediate strain rate values, the plastic instability started practically immediately after the end of the Lüders plateau. At the lowest strain rate the onset of type *C* instability was observed after a significant critical strain ε_{cr} around 15%. Besides the deep type *C* serrations, the initial portions (below ε_{cr}) of deformation curves displayed stress drops described in § 1.5.1 which had much lower amplitude and frequency of occurrence (cf. [27]). The analysis of AE for the low

strain rate will be presented with most details because it responds in the best way to the purpose of comparison between AE generated before and during jerky flow.

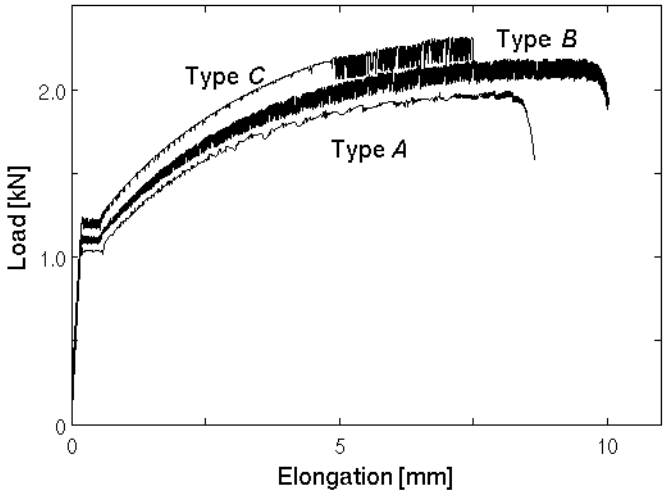

Figure 5.1: Examples of deformation curves for three values of imposed strain rate corresponding to different types of the PLC instability: $2\times10^{-5}s^{-1}$(type C); $2\times10^{-4}s^{-1}$(type B); $2\times10^{-2}s^{-1}$(type A). The two upper curves are deliberately shifted along the ordinate axis to better discern the shape of serrations.

Onset of acoustic emission Although the generation of a detectable acoustic response to plastic flow requires a collective motion of hundreds or thousands of dislocations, various authors report observation of AE signals virtually from the very beginning of loading ([176, 152, 177]). The early occurrence of AE is usually explained by a microplasticity taking place during macroscopically elastic deformation. The present results allow detecting the onset of AE more accurately. Figure 5.2 displays the initial parts of deformation curves and the accompanying acoustic events for different strain rates. The high resolution of the elongation and force makes it possible to observe the first deviation from linear elastic behavior, which begins very early with regard to the conventional yield strength. It can be recognized that AE is almost absent before this "true elastic limit". Some sporadic AE events recorded in this region may be considered as due to occasional breakthrough of dislocation pile-ups. To be precise, such events may also be due to noise pickup. However, the verification records during idling showed that

noise events with such amplitude arrive much rarer. The AE activity manifestly starts increasing after this initial period. Both the AE activity and intensity grow abruptly in the region corresponding to a slight inflection on the deformation curve, which is showed with higher resolution in the figure inset. Such inflection was characteristic of the studied Al5Mg alloy and was not observed for samples with exactly the same size and geometry made from other materials. Thus, it is likely to correspond to enhancing microplastic deformation in this material. This observation confirms that the recorded AE is generated by the (correlated) motion of dislocations. It also attests the AE as a sensitive indicator of the onset of dislocations movements.

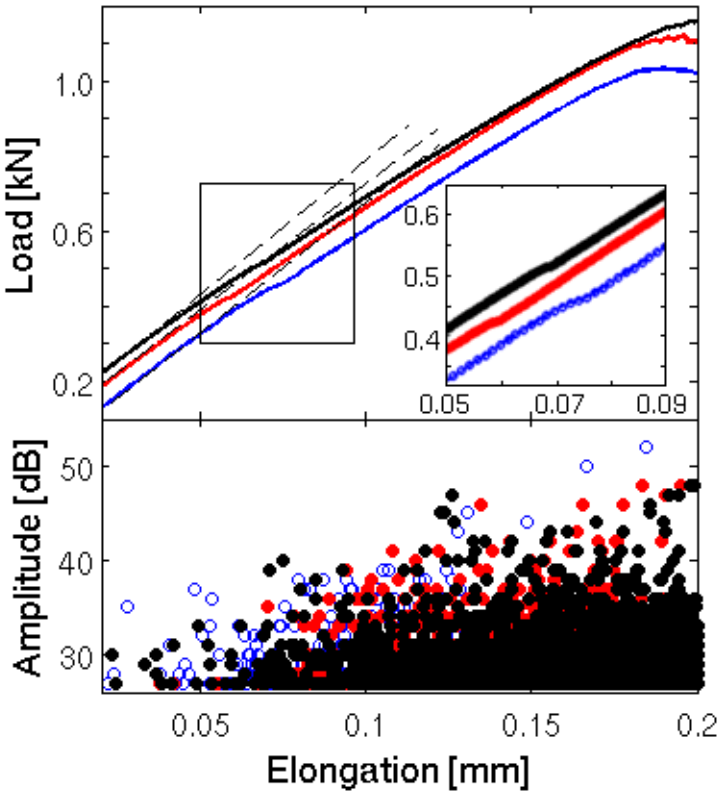

Figure 5.2: Illustration of the onset of AE in Al5Mg specimens: portions of deformation curves (top) and the accompanying acoustic events (bottom). Colors: blue - $\dot{\varepsilon}_a = 6 \times 10^{-3} s^{-1}$; red - $\dot{\varepsilon}_a = 2 \times 10^{-4} s^{-1}$; black -$\dot{\varepsilon}_a = 2 \times 10^{-5} s^{-1}$.

The data streaming reveals that already at this stage the AE appears at all strain rates in the form of discrete bursts superimposed on a continuous signal, as illustrated

in Fig. 5.3. At the lowest strain rate (Fig. 5.3(c)) short isolated bursts with a rise time of several microseconds and duration of several tens of microseconds appear above the continuous noise level. Such bursts are also detected at higher $\dot{\varepsilon}_a$. At the same time, a tendency to increasing AE is observed, as could be expected from the intensification of deformation processes required to sustain the higher imposed strain rate. Therewith, the increase is not uniform. In particular, long-duration complex events are formed due to clustering and merging of individual bursts. The merge is relatively weak at $\dot{\varepsilon}_a = 2 \times 10^{-4} s^{-1}$ (Fig. 5.3(b)), so that many of these events have a short rise time, thus allowing to distinguish the main initial shock. At the highest strain rates, the large bursts have much longer wave fronts, durations approaching a millisecond, and often a complex structure, all this indicating that such a burst reflects a developing process of deformation (Fig. 5.3(a)). Besides, the overall increase in the frequency of small pulses adds to the continuous-type signal exceeding the noise level. These patterns already contain many aspects of the signals observed at the later deformation stages. More examples presenting details of the typical waveforms will be given below.

Behavior during the Lüders plateau Figure 5.4 compares the mechanical and acoustic responses of the material for three strain rate values. At $\dot{\varepsilon}_a = 2 \times 10^{-2} s^{-1}$ (Fig. 5.4(a)) the deformation curve displays quite smooth character with low-amplitude stress fluctuations, corresponding to quasi-continuous propagation of a Lüders band, as it is usually sketched for simplicity. The overall AE grows very strongly so that the pattern of Fig. 5.3(a) develops into a continuous signal with an amplitude increased by an order of magnitude, although its pulsed nature may still be guessed. Quite different patterns are observed when the strain rate is decreased. The plateau on the deformation curve acquires a serrated shape of relaxation-oscillation type testifying to jerky propagation of the Lüders band. It can be ascertained in type *C* conditions that the amplitude of these stress drops is similar to that of the small drops preceding the onset of type *C* instability (see above).[1] As shown in Fig. 5.5, the AE recorded between the stress drops

[1]This is a rather unusual mode of propagation of the Lüders band. However, its analysis goes beyond the scope of the doctoral research.

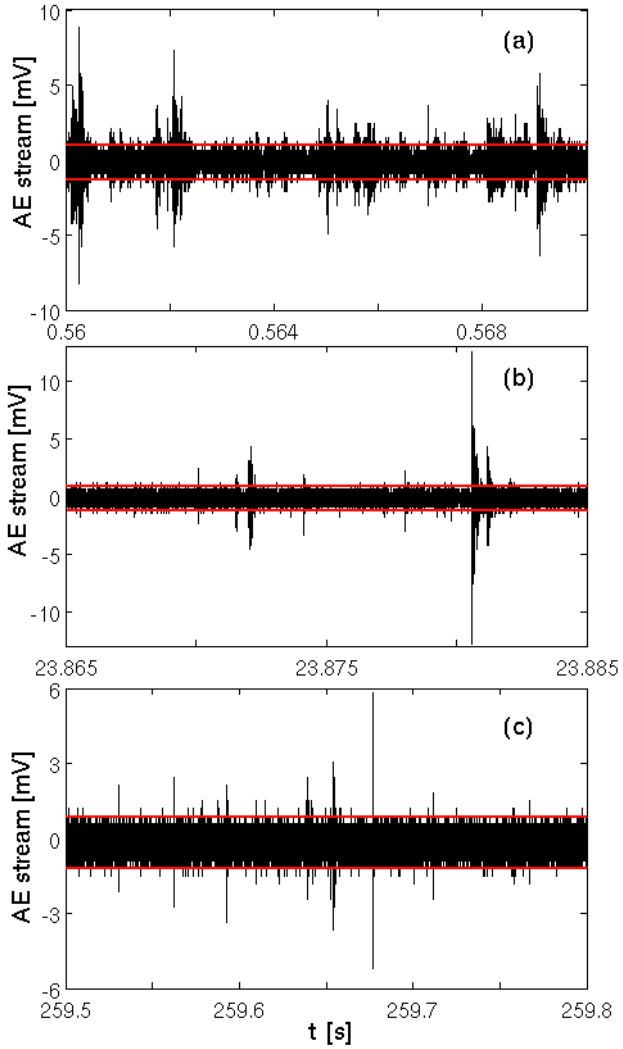

Figure 5.3: Examples of AE data streaming during macroscopically elastic parts of deformation curves. (a) $\dot{\varepsilon}_a = 6 \times 10^{-3} s^{-1}$; (b) $\dot{\varepsilon}_a = 2 \times 10^{-4} s^{-1}$; (c) $\dot{\varepsilon}_a = 2 \times 10^{-5} s^{-1}$.

is weak and similar to that observed before elasto-plastic transition, whereas very strong acoustic events with durations reaching fractions of a second accompany the serrations. Consecutive zooming of such events show that they appear as almost stationary at a millisecond scale (Fig. 5.5(b)).

Behavior in the PLC conditions Figure 5.6 illustrates the overall evolution of the AE signal recorded during deformation of an annealed specimen at $\dot{\varepsilon}_a = 2 \times 10^{-5} s^{-1}$. As can be seen in Fig. 5.6(a), both the activity and intensity of AE diminish after the end of the Lüders phenomenon. However, the qualitative features of the signal do not change: it is composed of a quasi-continuous background with amplitude varying above

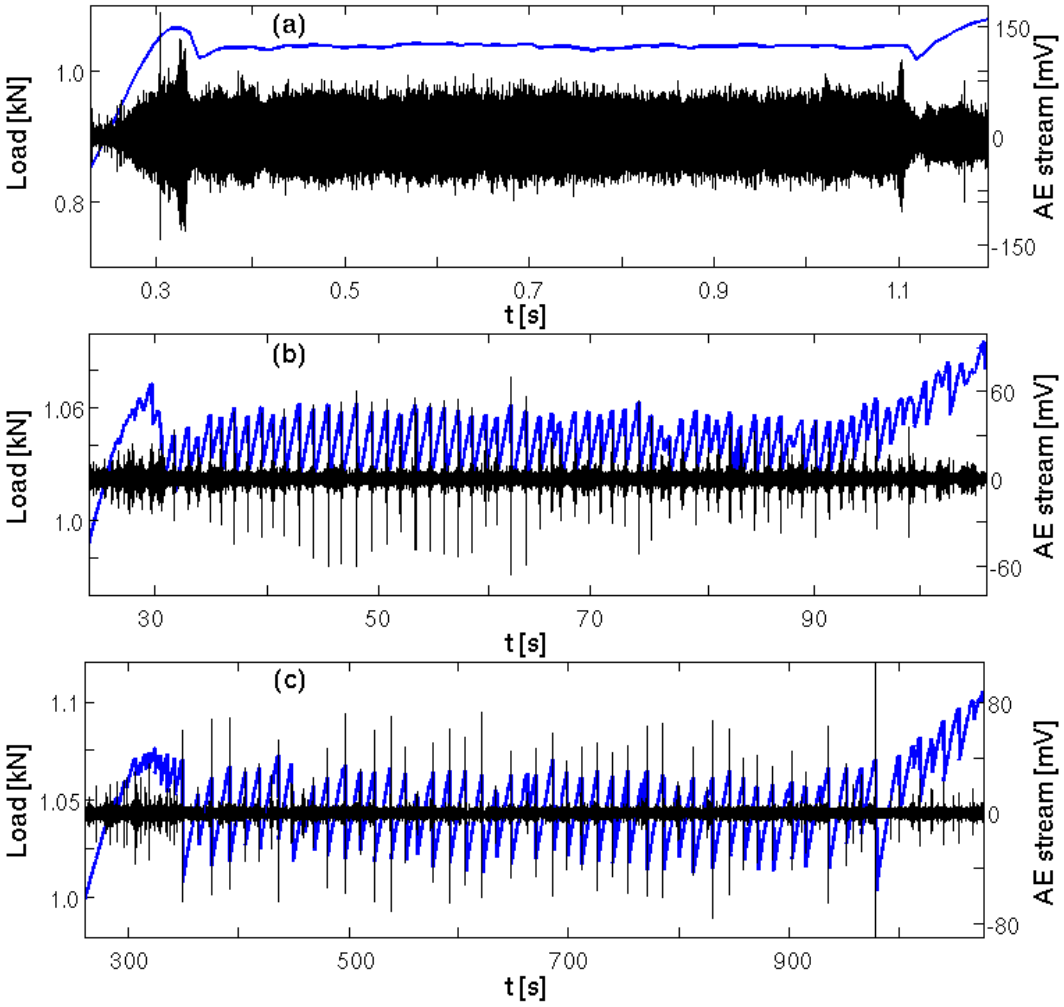

Figure 5.4: Examples of Lüders plateau and the accompanying AE: (a) $\dot{\varepsilon}_a = 2\times10^{-2}s^{-1}$; (b) $\dot{\varepsilon}_a = 2 \times 10^{-4}s^{-1}$; (c) $\dot{\varepsilon}_a = 2 \times 10^{-5}s^{-1}$.

the noise level, superimposed with larger-amplitude bursts.

What attracts attention is that these bursts are not correlated with the deep stress serrations caused by the PLC effect. Indeed, most of them occur during the initial plastic deformation characterized by small stress serrations. Moreover, even the continuous background level decreases during deformation, in spite of the onset of the PLC instability [124]. Important information on this counterintuitive behavior is obtained from consecutive zoom in steps uncovering AE at various scales. Figures 5.6 (b) and 5.6(c) illustrate the AE signal for shorter time intervals selected, respectively, below and above ε_{cr}. In these figures the noise levels appear as black horizontal bands. It can be seen that on the time scale of the figures the signal exceeding the noise level has a persistent

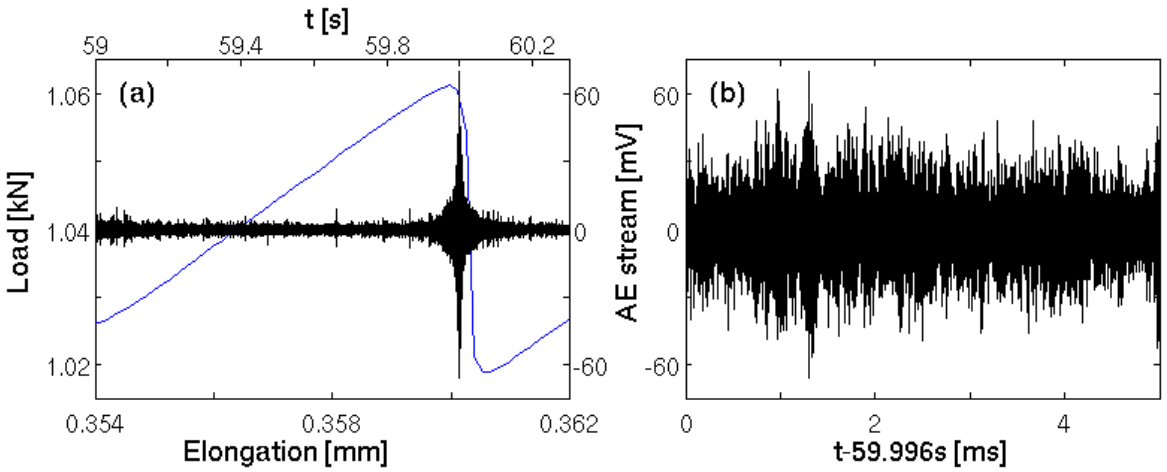

Figure 5.5: Example of an acoustic event accompanying a stress drop during the Lüders plateau. $\dot{\varepsilon}_a = 2 \times 10^{-4} s^{-1}$.

burst-like character. The burst-like events occur across the deformation curve, i.e., not only at the instants of stress drops but also during smooth plastic flow between them. As can be seen in Fig. 5.6(b), the small stress drops observed at the initial deformation stage are characterized by acoustic events with relatively high amplitude. However, the instants of stress drops are not exceptional: AE events with similar amplitudes also occur during smooth plastic flow. Moreover, the correlation between AE and stress drops becomes weaker in the course of deformation. Namely, the difference between the amplitude of the acoustic events accompanying type C serrations and that of neighboring events either becomes less significant, as illustrated by the example of Fig. 5.6(c), or even completely disappears. The latter behavior is similar to the data on Al3Mg alloy studied in[16], where no difference was found between AE events extracted with the help of a standard acoustic equipement during stress drops and during intervals between them.

Further increasing the time resolution allows two principal waveforms of the observed AE events to be distinguished. Figure 5.7 presents a very short isolated burst similar to those shown in Fig. 5.3(c), with the wavefront of several microseconds and duration of several tens of microseconds. Such individual bursts mostly occur during macroscopically smooth plastic flow. Isolated bursts may also be observed during stress drops. More often, however, the stress drops are associated with long events with du-

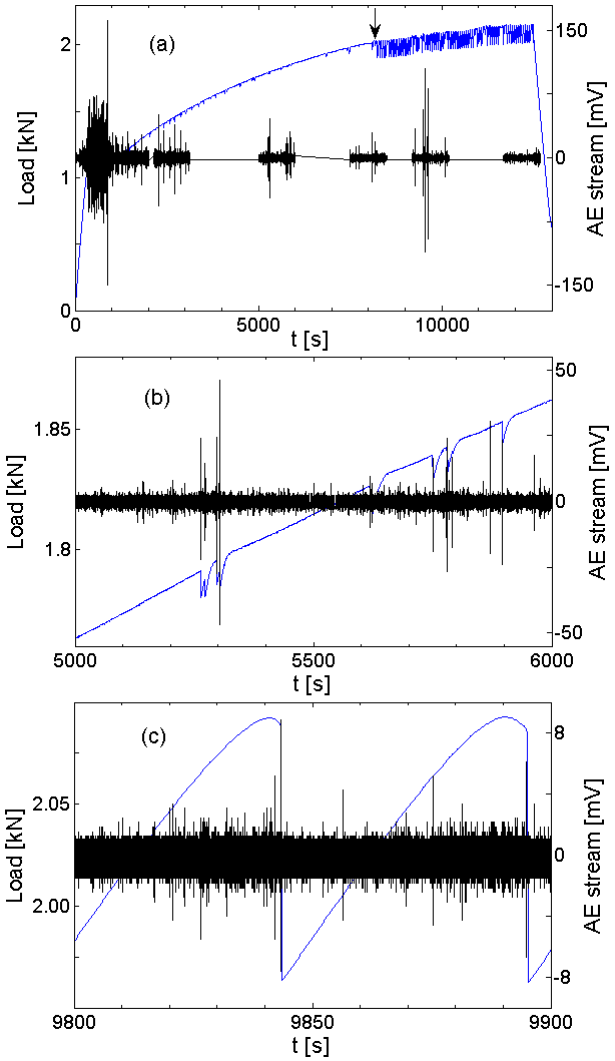

Figure 5.6: Superposition of an entire load-time curve and the accompanying AE signal for an annealed AlMg specimen. The arrow indicates the critical strain ε_{cr} for the onset of the PLC effect; (b) zoom in a time interval corresponding to the deformation stage below ε_{cr} ; (c) zoom in a time interval beyond ε_{cr}. $\dot{\varepsilon}_a = 2 \times 10^{-5} s^{-1}$.

ration varying from hundreds of microseconds to tens or even hundreds of milliseconds, on a background from which some short bursts can be separated, as illustrated in Figs. 5.8(a) and 5.8(b).

Like in the case of the pulses accompanying the Lüders plateau (Fig. 5.5), higher magnification in Figs. 5.8(a) and 5.8(b) shows that the corresponding portions of the signal (see Figs. 5.8(c) and 5.8(d)) appear almost stationary when the time scale is reduced to a millisecond or less. Nevertheless, the totality of observations leads to the suggestion that these events result from merging of the "elementary" bursts closely

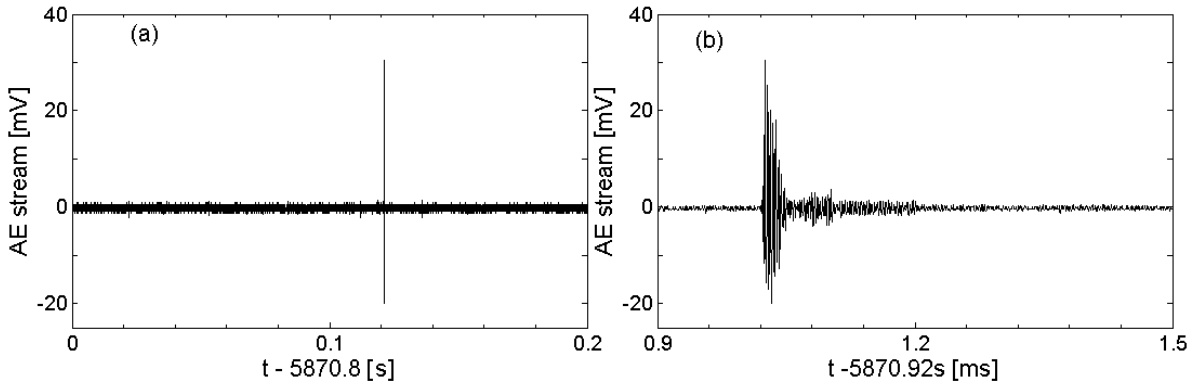

Figure 5.7: Example of a short isolated AE burst at two magnifications. The front of the signal is as short as approximately 2 μs, the main shock lasting about 30 μs. Some aftershocks can also be seen after the main shock.

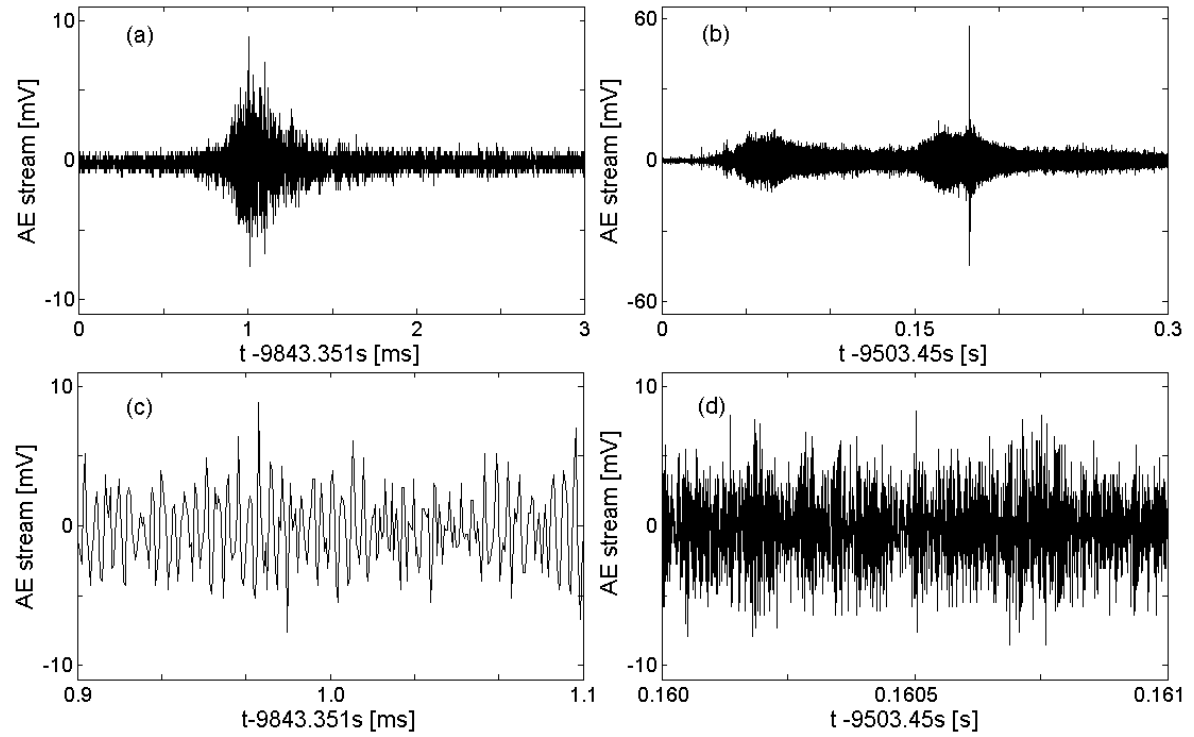

Figure 5.8: (a), (b) Examples of two composed AE events with large duration; (c), (d) respective magnification of these events showing a virtually continuous character of AE at a sufficiently fine time scale.

following each other. In particular, small stress drops are often accompanied by dense sequences of short bursts which can still be isolated from each other. Similarly, their more frequent occurrence often precedes deep stress bursts. The beginning of a very long AE event usually just precedes an abrupt stress drop, thus testifying to a developing deformation process. Another example is given in Fig. 5.8(b), which reveals a short higher-amplitude burst superimposed on a long event. Furthermore, this suggestion is fully consistent with results [28] in which individual long-duration AE events observed during the PLC effect in a AlCu alloy were shown to possess a complex correlated structure revealed by multifractal analysis. A quantitative analysis of such short-time correlations which confirms the complex nature of these signals will be presented in Chapter 6.

The samples not subjected to solution treatment demonstrated the same AE patterns for each scale of observation as those illustrated in Figs. (5.6–5.8). Visual inspection of the overall AE intensity level also did not reveal noticeable difference. However, the maximum amplitude of AE bursts appears to reach values up to twice as high as in the case of annealed specimens. For this reason statistical analyses were performed to reveal possible quantitative changes caused by the thermal treatment of the material.[2] The statistical analysis was performed for one parameter set optimized using tests with the so-called Hsu-Nielsen source (pencil lead break): the amplitude threshold was chosen equal to 27 dB, HDT = 300 μs, HLT = 40μs, and PDT = 40 μs. Power-law probability functions were found for both kinds of samples almost over almost the entire range of AE amplitudes, except for the largest events which showed tendency for an increased probability. An example of a comparison of such dependences is given in Fig. 5.9 for the time interval from 2000 s to 4000 s, which corresponds to the region before onset of the PLC effect. It can be seen that the slope of the power-law function is steeper in the case of the annealed sample. In other words, annealing leads to an increasing probability of smaller events. Consecutive analysis for similar time intervals along the entire deformation curve showed that this tendency does not persist during the test:

[2]A detailed statistical analysis of AE for various strain rates will be presented in the next chapter.

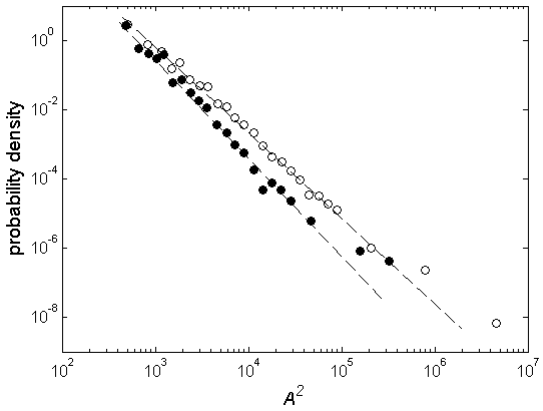

Figure 5.9: Probability density function for the squared amplitude of AE events for an annealed specimen (solid symbols, the slope $\beta \approx -2.9$) and an as-delivered specimen (open symbols, $\beta \approx -2.5$). The events were collected in the time interval [2000 s; 4000 s], corresponding to the strain range $\varepsilon < \varepsilon_{cr}$. $\dot{\varepsilon}_a = 2 \times 10^{-5} s^{-1}$.

the exponent β for the annealed specimens approaches the value for the as-delivered specimens, which changes little with strain hardening (check in Chapter 6), so that the difference between the dependences for annealed and as-delivered samples gradually decreases and finally vanishes beyond ε_{cr}.

The overall behavior of AE on the time scale of the test duration (see Fig. 5.6(a)) is similar in the entire $\dot{\varepsilon}_a$-range. This is illustrated by Figs. 5.10(a) and 5.11(a), which represent AE for annealed specimens deformed at a $\dot{\varepsilon}_a = 2 \times 10^{-4} s^{-1}$ and $\dot{\varepsilon}_a = 2 \times 10^{-2} s^{-1}$, corresponding to type B and type A behavior, respectively. The finer details shown in Figs. 5.10 and 5.11 demonstrate a nonuniform growth of the AE activity with increasing imposed strain rate, similar to the effect discussed above in relation to the AE accompanying microplastic deformation (Fig. 5.3). Nevertheless, all the above conclusions made for type C behavior remain in the case of type B serrations. For example, Fig. 5.10(c) shows that the increased AE activity does not prevent burst-like patterns on a time scale corresponding to several stress drops (cf. Fig. 5.6(c)). Therewith, although the stress drops are often associated with rather intense AE events, events with similar amplitude are also observed in the intervals between stress drops. Finally, at the highest strain rate bursts with not very high amplitude are more difficult to isolate, so that a virtually continuous AE signal on which rare strong bursts are

superimposed is observed at a similar time scale (see Fig. 5.11(b)).

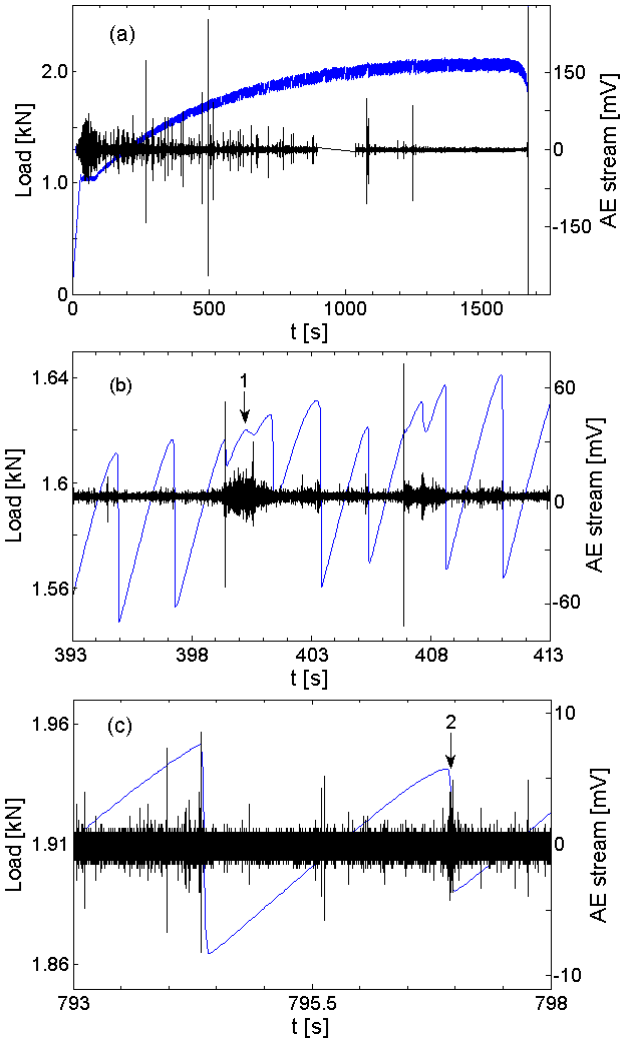

Figure 5.10: Superposition of an entire force-time curve of type B and the accompanying AE signal; (b), (c) consequtive zoom in steps presenting a sequence of serrations and individual stress drops. The arrows (1) and (2) correspond to Figs. 5.12(a) and (b), respectively. $\dot{\varepsilon}_a = 2 \times 10^{-4} s^{-1}$.

An additional feature of the evolution of plastic deformation can be distinguished for intermediate and high strain rates, namely, alternation of the phase of deformation band propagation (quasicontinuous propagation for type *A* or hopping propagation for type *B*) and the phase of nucleation of a new deformation band. It is therefore interesting to compare the corresponding acoustic signals. As can be seen in Figs.5.10(b) and 5.11(b), in both cases the AE is considerably stronger during the nucleation phase, in consistence with the literature data [124, 125, 27]. Subsequent magnification allows distinguishing typical waveforms of AE events during nucleation and propagation of type *B* deformation

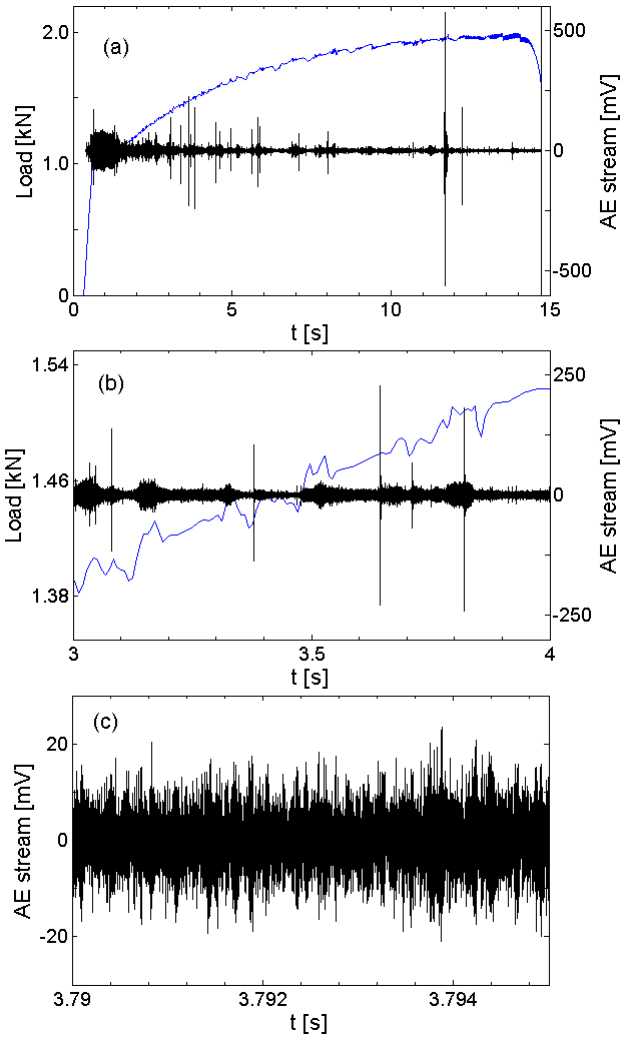

Figure 5.11: Superposition of an entire force-time curve for type A behavior and the accompanying AE signal; (b), (c) consecutive zoom in steps. $\dot{\varepsilon}_a = 2 \times 10^{-2} s^{-1}$

bands, illustrated in Fig. 5.12. It can be seen that discrete burts with amplitudes varying in a wide range accompany the band nucleation (Fig. 5.12(a)). Magnification to the scale of a separate event (Fig. 5.12(c)) shows that they often have a short rise time similar to the pulses presented in Fig. 5.7. The event represented in Fig. 5.12(b) typically occurs at the onset of a "regular" deep stress drop corresponding to the hopping propagation sequence. It is characterized by a large duration but a low amplitude. The magnification in Fig. 5.12(d) shows its close-to-stationary character on a short time scale, similar to Fig. 5.8. It is also worth noting that although the overall shape of the deformation curves recorded for the studied alloy at the lowest strain rate of $\dot{\varepsilon}_a = 2 \times 10^{-5} s^{-1}$ corresponds to usual type C curves, their aspect is similar to type B curves, namely, the presence of

regular clusters of serrations separated by intervals of less regular behavior. It is during the latter periods that the large AE bursts occur in this case too, whereas deep stress serrations are relatively silent. Finally, a substantially continuous signal is observed at the highest strain rate both during nucleation and propagation of deformation bands. This continuous signal displays amplitude rises coincident with the stress humps (Fig. 5.11(b)) associated with nucleation of a new deformation band, similar to modulation of the continuous AE observed in [129] for type A behavior in α-brass.

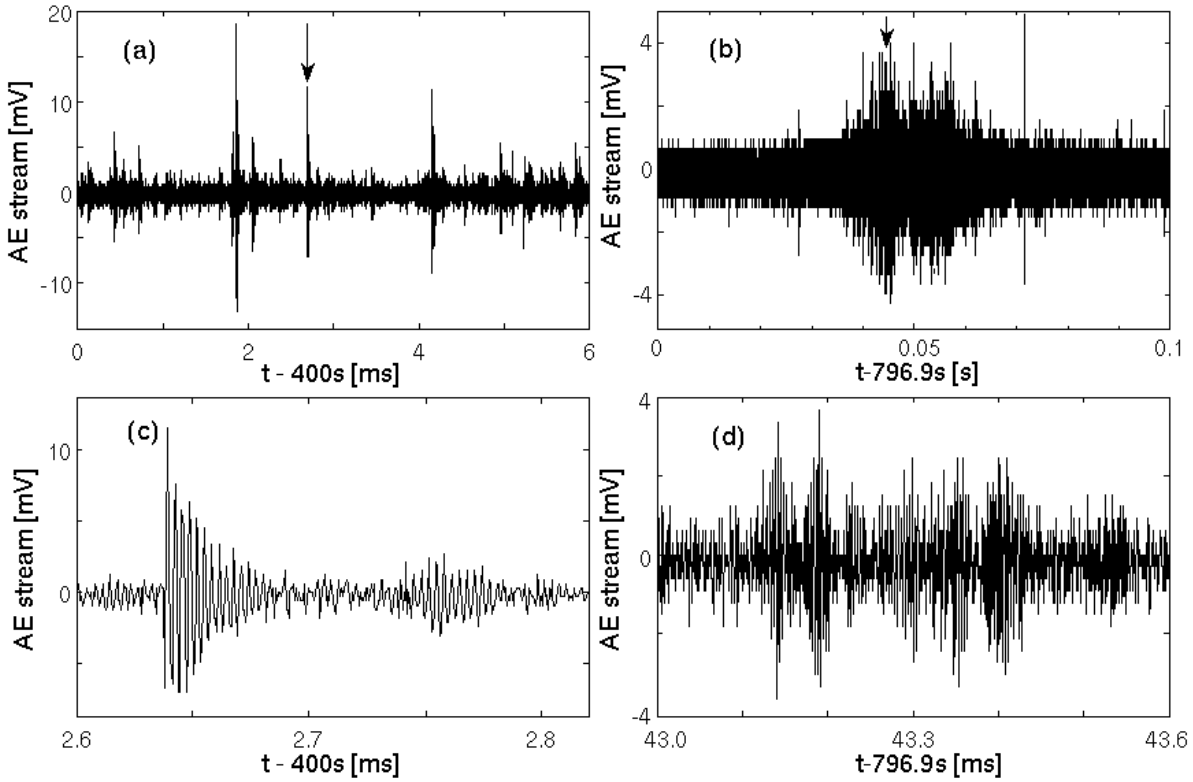

Figure 5.12: Examples of AE waveforms during nucleation (a) and propagation (b) of type B deformation bands; (c), (d) magnification of figures (a) and (b), respectively. Arrows indicate the sites magnified at the bottom figures. $\dot{\varepsilon}_a = 2 \times 10^{-4} s^{-1}$.

5.1.2 Spectral analysis

As described in the previous section, visual examination of AE signals allows distinguishing the main waveforms of acoustic signals accompanying plastic deformation in AlMg. Additional quantitative information can be derived from spectral analysis of both individual waveforms and coarse signals. Figure 5.13 illustrates typical waveforms with

the respective power spectra. Herewith, no significant evolution in spectra of individual events was revealed during deformation. More delicate analysis based on the multifractal formalism and aimed at revealing possible changes will be presented in the next chapter. The portions of the close-to-noise signals selected at different strains give spectral shapes close to the Fourier spectrum of the noise recorded before the loading start, represented in Fig. 5.13(a). The comparison of the power spectra obtained for various types of events (Fig. 5.13(a)-(d)) reveals a persistent peak around 320 kHz, which can therefore be supposed to reflect the properties of the sound propagation in the investigated media for the given specimen geometry. The width and height of this peak, however, depend on the event type. For example, the spectrum of a burst-like event followed by a dozen of regular oscillations with decaying amplitude is mostly determined by this peak, as shown in Fig. 5.13(b). Merging and overlapping of such "elementary" bursts gives rise to complex waveforms and leads to occurrence of new peaks and resultant broadening of spectra (see Fig. 5.13(c),(d)).

Figure 5.13 also indicates that in the case of events with large duration, recorded during deep stress drops, calculation of average characteristics, such as energy E and median frequency f_{med} (see Chapter 3), usually gives higher E value and lower f_{med} value than in the neighboring regions. The correlation between the increasing AE activity and stress drops is confirmed by the graphs of evolution of E and f_{med}, which are presented in Figs. 5.14 and 5.15 for type C and type B behavior, respectively. Indeed, this representation allow detecting discontinuities in AE signal on a coarse scale corresponding to rather continuous appearance of the signal itself. Figures 5.14 and 5.15 illustrate that besides strong discontinuities caused by large AE bursts, practically all stress drops give rise to distinct rises in acoustic energy and simultaneous falls in median frequency. The reduction in f_{med} is usually attributed to an enhanced correlation in dislocation processes and strain localization and therefore, reflects highly cooperative processes (see, e.g., [129, 178]). It should be noted that the changes in E and f_{med} begin well before the stress drop. The closer analysis allows relating this effect to the AE increase prior to the drop, as was specified above. The existence of such predecessors of

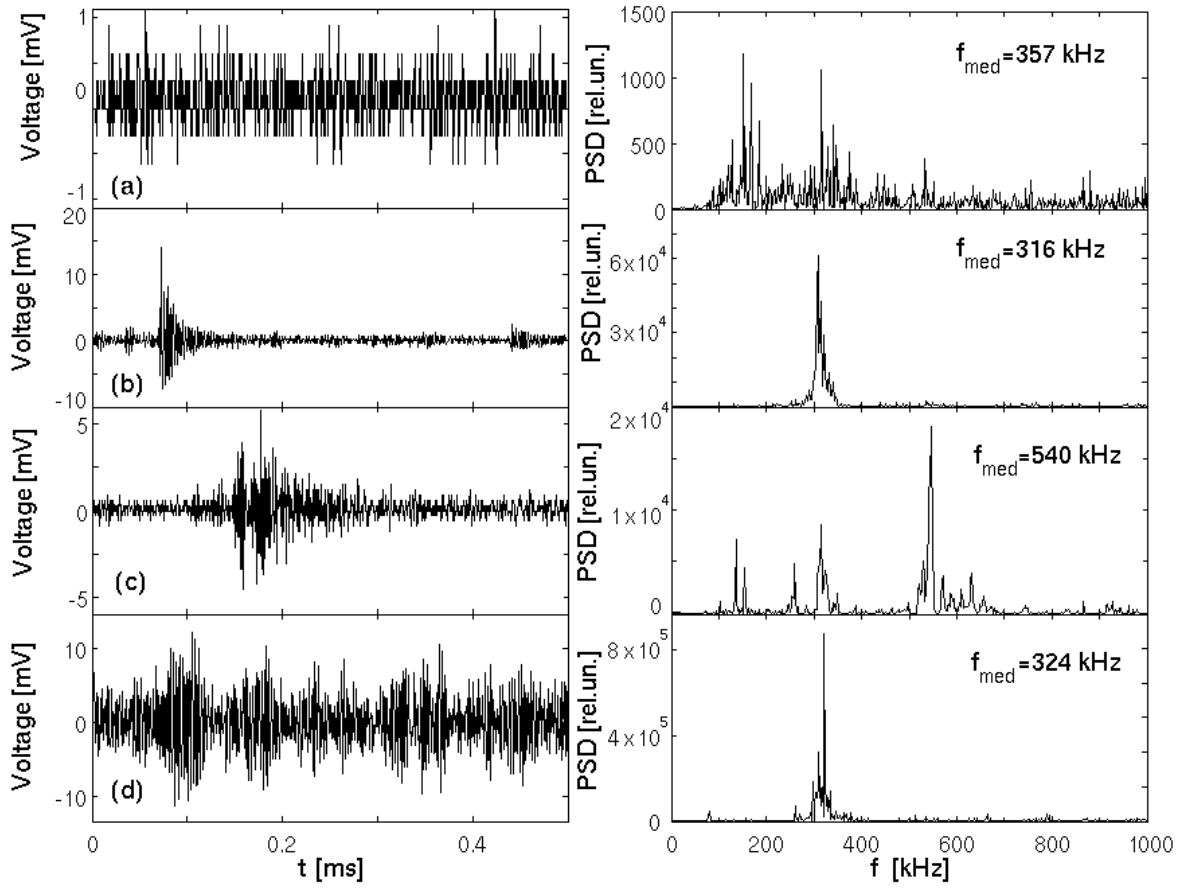

Figure 5.13: Typical patterns of AE and their power spectral density (PSD) function: (a) noise signal during idling of the deformation machine, (b) burst during the period separating two regular series of stress drops, (c) event during reloading between two successive stress drops , (d) portion of a large event recorded during a stress drop. $\dot{\varepsilon}_a = 2 \times 10^{-4} s^{-1}$.

"catastrophes" also agrees with the data of correlation analysis of series of AE events in [18]. Finally, at high strain rates the evolution of E and f_{med} also displays fluctuations on the scale of test duration but, as the almost continuous character of AE complicates distinguishing the individual events, accurate analysis on the scale of one band propagation is difficult (see Fig. 5.16). In this case, local maxima of energy and local minima of the median frequency are found during the stress humps corresponding to nucleation of a new deformation band, but the stress fluctuations accompanying the deformation band propagation do not produce noticeable effects.

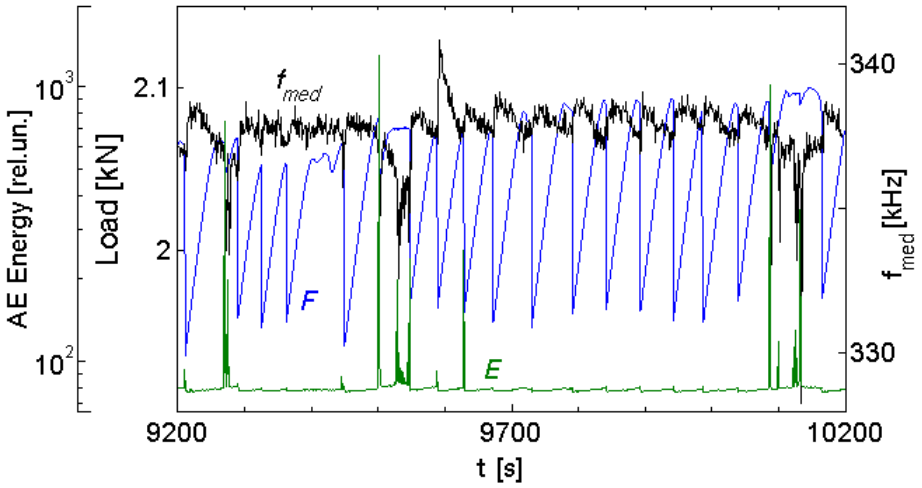

Figure 5.14: Superposition of a portion of the deformation curve with the time evolution of the average AE energy E and the median frequency f_{med}. Annealed specimen; $\dot{\varepsilon}_a = 2 \times 10^{-5} s^{-1}$.

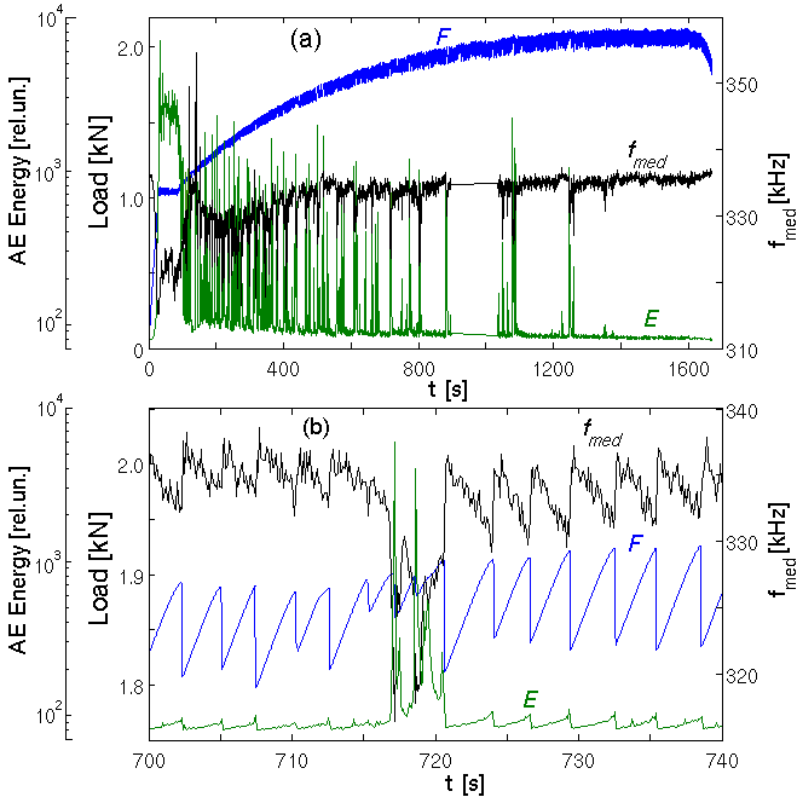

Figure 5.15: (a) Evolution of the PSD function in terms of energy and median frequency; (b) Close up of a portion of the upper figure. Annealed specimen; $\dot{\varepsilon}_a = 2 \times 10^{-4} s^{-1}$.

5.1.3 Discussion

The overall behavior of AE observed in the present work is consistent with the results of earlier studies on the PLC effect interpreted from the viewpoint of generation of AE by

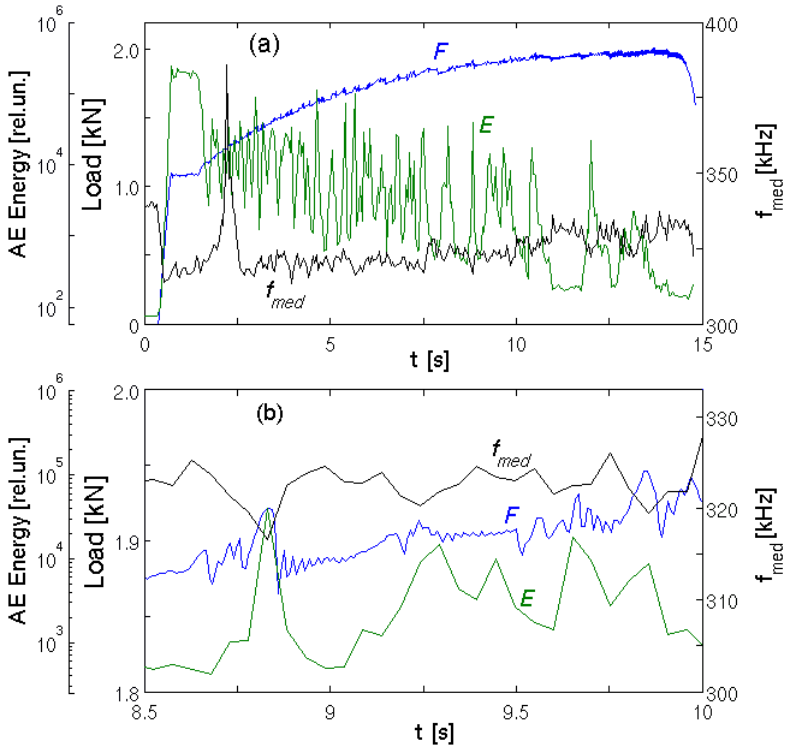

Figure 5.16: Same as Fig. 5.15 for an as-delivered specimen deformed at $\dot{\varepsilon}_a = 2{\times}10^{-2}s^{-1}$.

multiplication and motion of dislocations (e.g., [124, 125, 18]). Further discussion will be developed within the same framework of the dislocation mechanism of AE. However, the possible role of cracking of second-phase particles in the overall AE signal, which is usually disregarded in the literature on AE accompanying the PLC effect, should be mentioned. Indeed, post-mortem electron microscopy of fracture surfaces, although displaying ductile dimpled fracture, revealed some sparse broken inclusions, mainly in the non-annealed specimens (Fig. 5.17). Besides the scarcity of such sites found in the microscopy investigation, some other experimental observations suggest a minor role of cracks. In particular, the exponents of the power-law distributions determined in the present work are close to the data for an AlMg alloy in which no cracks were observed [18], and much higher than the typical values reported for AE caused by cracking (e.g., [179]), which are similar to those found for dislocation glide or twinning in pure materials (e.g.,[21]). However, the role of inclusions as AE sources during plastic deformation of aging alloys remains an open question and would require a special study.

As was underlined in Chapter 1, the conventional vision of AE accompanying the

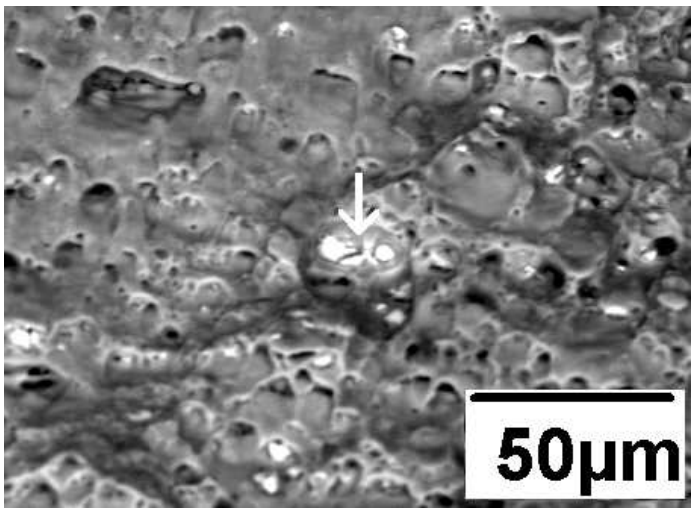

Figure 5.17: SEM image of the fractured surface of a nonannealed AlMg specimen. Arrow shows a broken particle appearing in white color.

PLC effect relates burst-like AE to collective motion of dislocations during stress serrations, while stable plastic flow is considered to produce continuous AE. This intuitive picture agrees with the common understanding of unstable plastic flow as a process involving transient motion of large dislocation ensembles, which stems from investigations of various mechanisms of macroscopic plastic instability. At the same time, it contradicts recent observations of scale-free intermittent behavior of plastic flow in different materials, which led to the hypothesis of the ubiquitous character of the concept of avalanche-like dynamics of dislocations.

The present results show that the interpretation of AE observed during the PLC effect depends on the time scale of observation. At not very high strain rates the component which appears continuous on the global time scale displays an obvious burst-like character at shorter time scales (Figs. 5.6 and 5.10), thus confirming, together with the respective power-law statistics, the hypothesis of intermittency. It is generally considered that the acoustic bursts accompanying dislocation glide are due to breakaway of mobile dislocations pile-ups. This viewpoint is consistent with the above observation of bursts amplitudes decreasing in the course of deformation. Indeed, the dislocation pile-ups may move on large distances in the undeformed material, giving rise to high AE amplitudes (see § 1.3), whereas the increasing density of obstacles in the work hardened material would reduce the free path of mobile dislocations. As argued in [124], the

waveform of such bursts is mainly determined by the properties of sound propagation in the material. More precisely, their leading front time is supposed to arise from different propagation speeds of different (bulk and surface) modes of stress waves, whereas the rear front of these bursts may reflect the developing deformation process and last for a long duration.

On the other hand, the merging of many burst-like events during the development of stress drops leads to a nearly continuous appearance of such composed events when the time scale is further refined (Fig. 5.8). The occurrence of long composed events explains the usually reported observation of drastic count-rate bursts accompanying stress serrations [124, 16], whereas the AE amplitude shows lesser or no bursts. As suggested in [16], the merging of AE events reflects synchronization of the deformation processes which are responsible for large stress serrations. Indeed, at low enough strain rate the internal stress caused by strain incompatibility produced by a deformation band efficiently relaxes during slow reloading following the corresponding stress drop. Therefore, when the threshold of instability is reached at some site in the crystal the neighboring sites are also close to the threshold. In particular, this suggestion is confirmed by the observation of an increasing number of AE bursts preceding the large event (cf. [124, 18]), which is quantitatively confirmed by the results of spectral analysis. Eventually the local dislocation glide may trigger propagation of plastic activity and the formation of a deformation band. The band development is stopped later on by the fall in stress, which moves the system state far from conditions of instability.

When $\dot{\varepsilon}_a$ is increased short AE bursts are still distinguishable on the relevant time scale both during relatively silent intervals corresponding to deformation band propagation and at the background of more intense AE during band nucleation. It can thus be suggested that the "elementary" plasticity events in the investigated material are essentially collective avalanche-like processes, similar at all strain rates, in agreement with the earlier observations of the same AE waveforms for different types of serrations [124]. At the same time growth of the overall plastic activity required to sustain the faster loading results in enhanced merging and superposition of AE events and gives rise to virtually

continuous AE. It can also be suggested that these changes are in fact more profound and reflect changes in the correlations between the elementary processes, which lead to a transition to a different dynamical pattern on the macroscopic scale. Indeed, at high strain rate not only AE but also the (type A) stress serrations are characterized by power-law statistics, whereas peaked distributions are observed for type B and type C serrations [5, 84, 18]. This transition fits in the above-described framework. Namely, when the imposed strain is increased the internal stresses caused by strain heterogeneity do not have enough time to relax so that most dislocation ensembles are constantly close to the threshold of instability. Consequently, an increase in the strain rate leads to a transition from distinct serrations caused by repetitive synchronization of dislocations to a critical-type behavior characterized by stress fluctuations of all sizes.

The other important observation follows from a comparison of AE during smooth and jerky flow for a given strain rate, including the regions before the onset of the PLC effect. It suggests that AE has an essentially intermittent nature over the whole deformation curve, although the AE events show different synergy effects displaying series of individual bursts during smooth plastic flow and a high degree of correlation for jerky flow. This conclusion is consistent with the results of a concurrent multifractal analysis of series of stress serrations and series of AE events in [17], as well as with the observation [27] of the closeness of AE statistics calculated separately for AE events gathered during stress serrations and between them. It can thus be conjectured that the elementary processes of plastic deformation are the same not only for different types of serrations but also for a macroscopically uniform flow. However, it may not be universal for all materials. Specifically, essentially continuous AE at all scales was observed in [129] for the PLC effect in α-brass under type A conditions.

The persistent nature of power-law statistical distributions of AE amplitudes supports the entirety of the above results, leading to the conjecture of an intrinsically intermittent character of the dislocation processes in the investigated material. One feature of the observed distributions is, however, unusual and deserves a special discussion. Namely, the power-law statistics characterizing the dynamics of various real

systems usually manifest a cut-off at the large scale of the analyzed variable. Alongside with various specific mechanisms of cut-off, it is caused by general reasons, such as the limitations imposed on the size of avalanches by the system dimensions, the impossibility of waiting long enough to accumulate sufficient statistics for rare large events, and so on. In contrast, the present data often manifest an enhanced probability of large AE events (see Fig. 5.9). This behavior sheds light on the effect of grain boundaries on the collective dislocation dynamics. Indeed, being effective obstacles to dislocation motion, the grain boundaries may play a dual role. On the one hand, the stress concentration caused by dislocation pile-ups may trigger dislocation sources in the neighboring grains and, therefore, promote large dislocation avalanches. Such a situation seems to be at the origin of the observation in [26] of an increase in the power-law exponent in ice polycrystals, i.e., an increase in the probability of larger AE events, in comparison with single crystals of the same material. On the other hand, the β-values reported in [26] and similar works $\{\beta \approx -(1.3 \div 1.7)\}$ are much higher than those found in the case of the PLC effect $\{\beta \approx -(2 \div 3)\}$. In [16], this difference was ascribed to a more important role of other hardening mechanisms caused by forest dislocations and solutes. The present data provide more arguments confirming this hypothesis. First, although a detailed comparison with the data of [16] is not possible because the Al5Mg alloy investigated in the present chapter has a different Mg content, initial dislocation density, and grain structure, the observation of a similar β-range for two alloys confirms the limitation of avalanche size in such materials. Furthermore, a tendency for an increasing probability of large dislocation avalanches was observed in [16], but this effect is considerably stronger in the present study. Both these observations may be explained within the framework of the discussed hypothesis, taking into account the small grain size in the investigated material, compared with the typical grain size about $30 \div 70$ μm in the alloy studied in [16]. Indeed, the decrease in grain size may reinforce the role of grain boundaries in promoting the transfer of plastic activity to neighboring grains, at least for strong dislocation avalanches. The discussed hypothesis also agrees with both the above-described effect of β decreasing on doubling the grain size by thermal treatment

and its disappearance after work hardening of the material. Finally, it can be suggested that this effect is not specific of AlMg alloys: a similar effect of grain size was reported in Chapter 4 for MgZr alloys.

In summary, among the literature on the intermittency of plastic flow, the phenomenon of jerky flow is usually considered as an exotic case, because of the huge instabilities resulting in macroscopic stress fluctuations. Moreover, these fluctuations show scale-free power-law distributions only at high strain rates, whereas characteristic scales appear for slow deformation. The results of the AE study presented above show that the large stress drops are accompanied with bursts in the duration of acoustic events but, rather counter intuitively, the amplitudes of these events are confined to the same amplitude range as in the absence of macroscopic instabilities. The latter observation indicates some general limitations of the collective dislocation dynamics. In [21], it was argued that the dislocation avalanche size is mainly limited by the sample dimensions in the case of single crystals of ice and pure metals. The present data testify that the grain size and the dislocation microstructure (e.g., forest dislocations) may cause important limiting effects.

Within this limited range, the amplitudes of AE events obey power laws, thus confirming a ubiquitous nature of intermittency and unifying the cases of smooth and jerky flow. At the same time, the power-law exponents are larger than the values found in the case of pure materials, and depend on the material microstructure. As far as the bursts in duration are concerned they may be caused by the synchronization of dislocation avalanches, which is realized as a propagation process, similar to relaxation oscillations [86]. Consequently, although the traditional representation of AE using duration-dependent characteristics displays bursts during stress drops, dense successions of acoustic events may lead to virtually continuous appearance of the AE signal itself, provided that the proper time and voltage resolutions are chosen.

5.2 Twinning and dislocation glide in Mg alloys

As described in § 1.6.1 plastic deformation of *hcp* metals is essentially governed by twinning and dislocation glide. It is known that in some cases twinning manifests itself through macroscopic stress serrations, e.g., at low temperatures or in single crystals. However, deformation curves obtained for polycrystals tested at room temperature are often macroscopically smooth. Up to date, the question on the relative role of twins and dislocations in the total plastic deformation and in the concomitant AE remains a controversy. In several works a high potential of the analysis of the event waveform for separation of AE events was demonstrated [173, 82]. For this reason, application of the data streaming technique seems promising. This paragraph presents the first results of investigation on the AE accompanying deformation of Mg alloys, using the approach described above for the case of the PLC effect.

5.2.1 MgZr alloys

Figure 5.18 presents results of simultaneous recording of a tensile curve and AE signal for a Mg0.04%Zr sample deformed at $\dot{\varepsilon}_a = 3.5 \times 10^{-4} s^{-1}$. Qualitatively similar patterns were observed for alloys with other chemical compositions, although the corresponding difference in the grain size was reflected in their different strength and ductility. The deformation curves of the investigated materials are smooth on the global scale (Fig. 5.18(a)). However, the microstructural analysis of deformed samples reveals a large number of differently oriented twins (Fig. 5.19). That twinning plays a significant role in the plastic flow of this alloys is also confirmed by the character of deformation curves. Indeed, the tensile curve presented in Fig. 5.18(a) demonstrates a substantial strain hardening, which can be attributed to mechanisms related to twins, e.g., by taking into account that twin boundaries are strong obstacles to the motion of dislocations. Further, magnification shown in Fig. 5.18(b) allows discerning irregular stress fluctuations which may be produced by twins.

The data streaming records show that the AE is essentially burst-like in this material.

Indeed, magnification of a signal portion appearing as continuous on a global scale of Fig. 5.18(a) displays a large number of isolated bursts with strongly varying amplitudes, as illustrated in Fig. 5.18(b). The first acoustic events occur during the elasto-plastic transition. The AE sharply increases, reaches a maximum, and gradually decreases to a constant average level which persists up to the specimen failure. However, strong AE bursts are observed during the whole test.

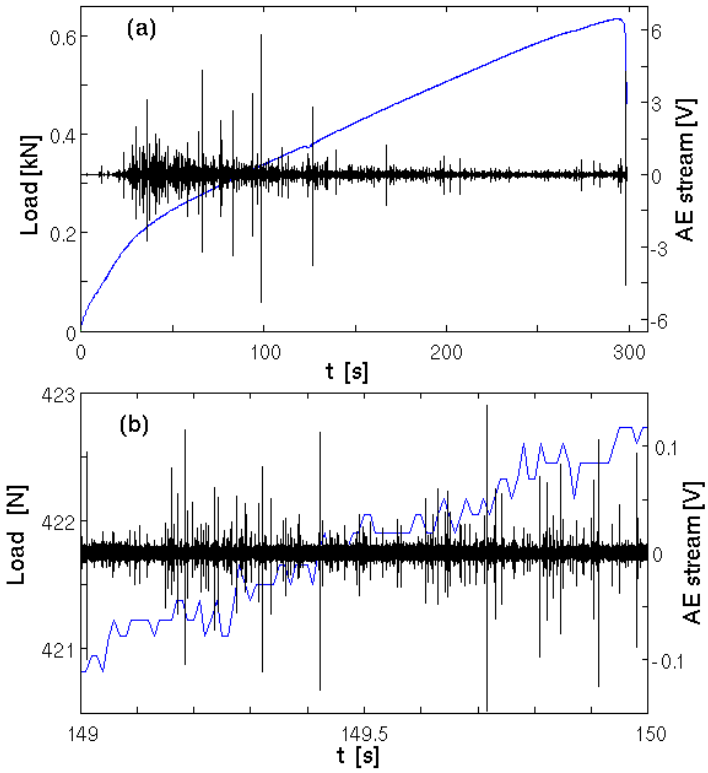

Figure 5.18: Example of load vs. time curve and simultaneously recorded acoustic response for Mg0.04%Zr deformed at $\dot{\varepsilon}_a = 3.5 \times 10^{-4} s^{-1}$.

Figure 5.20 represents typical waveforms observed for the studied materials, and the respective power spectral density functions. The upper pattern presents a noise signal recorded before the test start. The respective Fourier spectrum displays a narrow peak around 120 kHz and another peak at an approximately double frequency. Such a shape of Fourier spectra was found for all noise-like signals extracted during the test in the

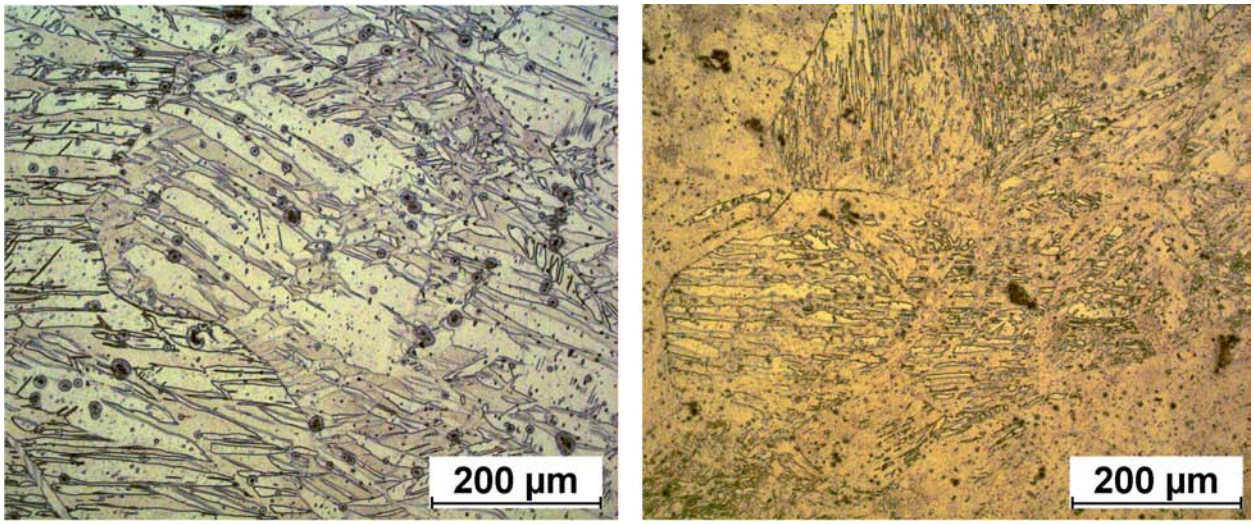

Figure 5.19: Microstructure of polycrystalline Mg samples after deformation. Left: Mg0.35%Zr sample with an average grain size <d>=170μm; right: Mg0.04%Zr sample with an average grain size <d>=550μm.

intervals between acoustic bursts. Figures 5.20(b) and (c) give examples of the most frequently observed waveform. It is characterized by a short rise time of about several microseconds and a rapid decay. It should be noted that the closeness of the wave front duration to the value found for AlMg is accidental, since the specimen geometry is not the same. The comparison of two figures shows that the amplitudes of the bursts described by the similar waveform vary in a remarkably wide range. The shape of the rear front of these events does not show a smooth transient but is rather complex. Consequently, the corresponding spectra are large and strongly vary. Nevertheless, they possess a generic feature, namely an intense peak in the interval 200-300 kHz, which dominates the spectrum. Another waveform, presented in Fig.5.20(d) and, occurs much rarer. It possesses a relatively small amplitude and often a large duration, up to a millisecond. However, in this case too, the signal shows abrupt fluctuations giving rise to a wide spectrum, which often consist of several peaks with similar intensity. Moreover, some of these events follow the short bursts. Taking into account the presence of abrupt fluctuations in the long event, it can be suggested that the deformation processes with different kinetics, giving rise to two different kinds of AE responses, mutually trigger

each other.

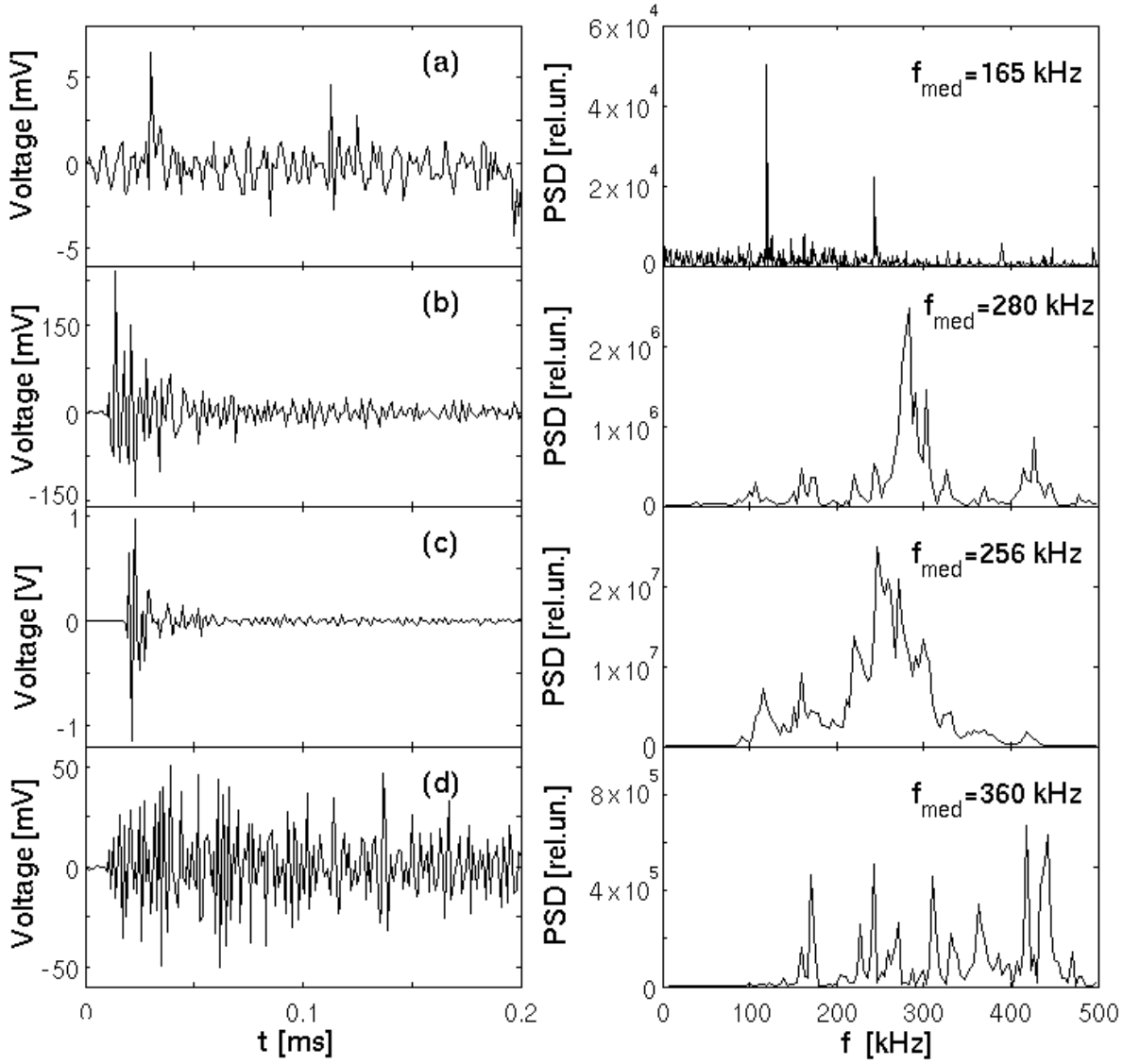

Figure 5.20: Examples of typical waveforms and their power spectral density functions of AE signals in MgZr alloys. (a)- noise-like pattern; (b) and (c) type 1 pattern; (d) - type 2 pattern.

In spite of the fact that the waveforms and their spectra remain qualitatively similar in the course of deformation, inspection of the time evolution of the average energy and median frequency reveals clear quantitative trends, in addition to fluctuation caused by strong AE events. An example of such dependencies is presented in Fig. 5.21. It can be seen that the AE energy rises rapidly from the onset of plastic deformation, passes a maximum, and decreases to an approximately constant level, while the median frequency shifts gradually to higher frequencies. Similar trends were also observed in

the case of the AlMg alloy (see § 5.1.2), although in a less pronounced manner.

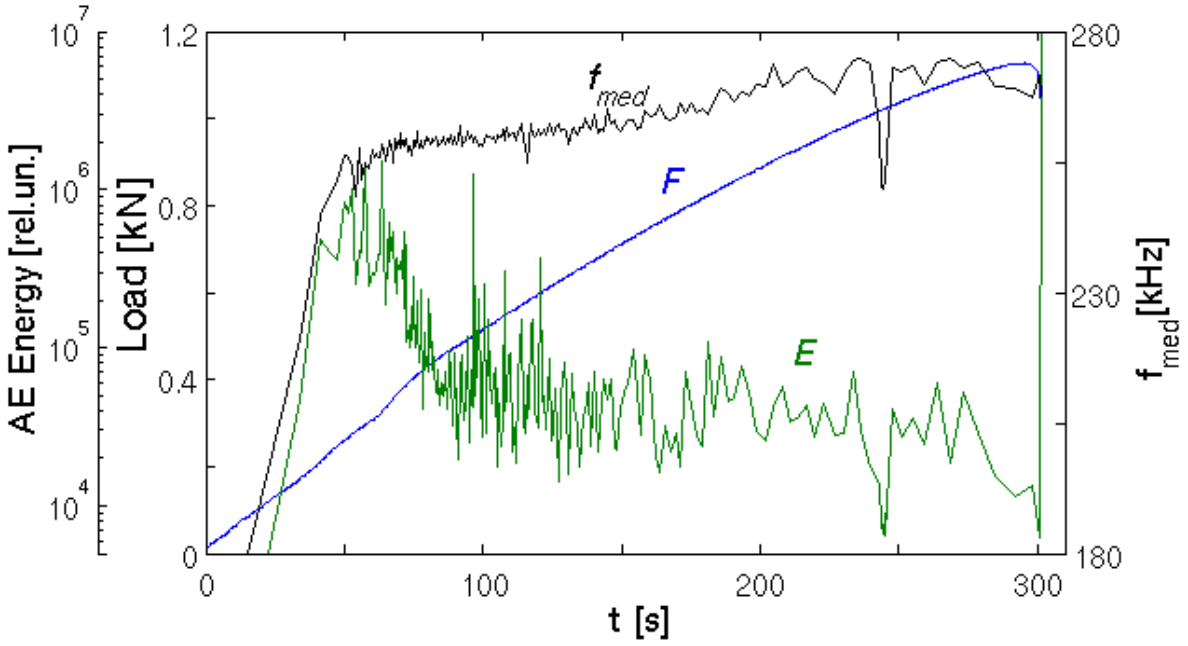

Figure 5.21: Time evolution of AE energy E (top) and median frequency f_{med} (bottom) for Mg0.35%Zr deformed at $\dot{\varepsilon}_a = 3.5 \times 10^{-4} s^{-1}$. The deep drop in both E and f_{med} around 240 s is due to accidental noise pick-up.

5.2.2 AZ31 alloy

As described in Chapter 2, these samples were prepared using different procedures resulting in two different microstructures. Figure 5.22 presents examples of deformation curves and the accompanying AE signals for both kinds of samples deformed at $\dot{\varepsilon}_a = 1 \times 10^{-3} s^{-1}$. It can be seen that the specimen with a heterogeneous grain structure (sample *s1*) is harder than that with a uniform grain structure (sample *s2*). In both cases the acoustic response shows similar patterns in the elastic and elastoplastic regions, characterized by very strong bursts. However, the behaviors becomes completely different after the yield. For sample *s1* the AE almost vanishes and represents rare high-amplitude bursts on a continuous background (Fig. 5.22(a)). In contrast, the response of the sample *s2* gradually decreases with strain and keeps a high burst-like activity up to fracture (Fig. 5.22(b)). The *postmortem* microstructure analysis revealed substantial differences in the nature of plastic deformation of the two kinds of alloys, as shown in

Fig. 5.23. No twins and no significant changes in the grain size have been found in sample *s1* (compare with the initial grain structure in Fig. 2.4). In the second case, many large twins are observed, so that their presence makes impossible the analysis of the grain structure in sample *s2*.

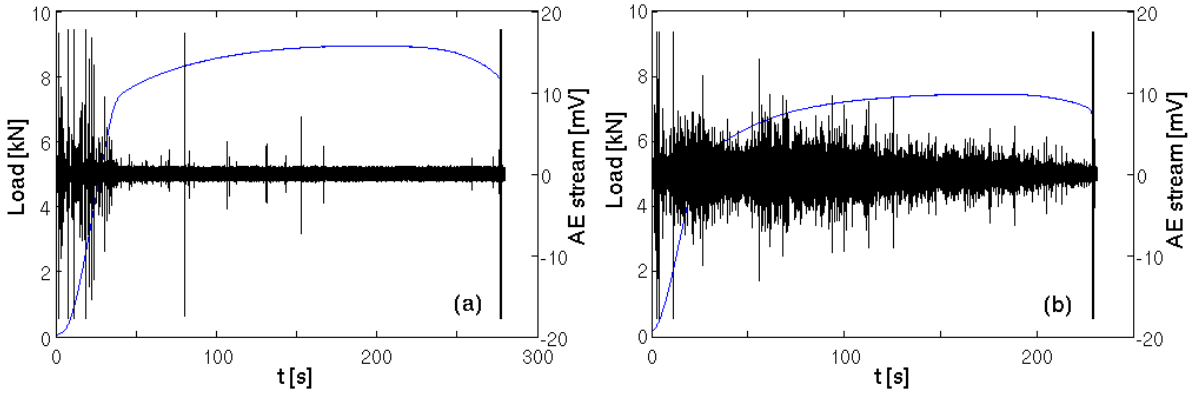

Figure 5.22: Example of deformation curves and AE signals for AZ31 alloy. (a) sample *s1*; (b) sample *s2*.

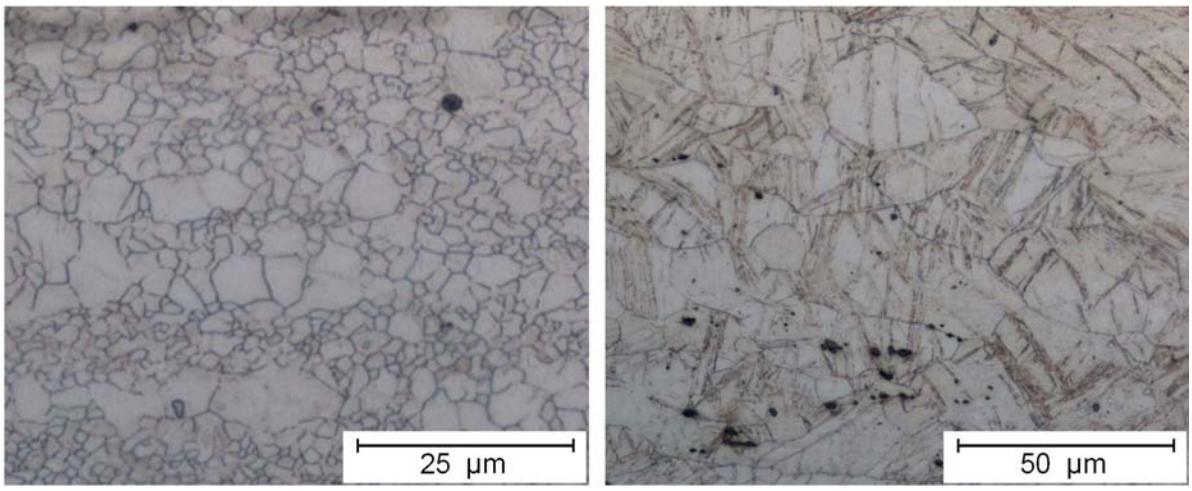

Figure 5.23: Microstructure of AZ31 specimens after tension test. Left: sample *s1*; right: sample *s2*.

The amplitude resolution of the acoustic equipment (12-bit A/D Converter) used in these tests was insufficient for small events to be clearly distinguished in the background noise. The large events reveal two kinds of waveforms, represented in Figs. 5.24(a) and (b). Relatively short bursts were usually observed for sample *s2*, as illustrated in Figs. 5.24(a),(c). The powerful AE events observed in the case *s1,* which seem on the scale of Fig. 5.22 as short as those in the sample *s2*, appear quite different on a finer time scale

(see Fig. 5.24(b),(d)). It can be seen that they are characterized by very long durations reaching ten milliseconds. It should be noted that such long pulses were sometimes observed during deformation of sample *s2* and, *vice versa*, the short bursts occurred during deformation of sample *s1.* However, each kind of material was characterized by one dominating waveform.

The spectral shapes present similarities with the results for MgZr alloys. So, the spectra of short pulses are characterized by the presence of one main component (Fig.5.24(e)), although, in contrast to Figs. 5.18(b) and (c), it completely dominates the spectrum, almost reducing it to one narrow peak. The spectra of long events are more complex. Besides peaks located in approximately the same frequency range (350-400 kHz), they also present rather high peaks at different frequencies. However, in comparison with the spectra obtained for long events in MgZr samples (Fig. 5.18(d)), these components are shifted to the low-frequency part of the spectrum (Fig.5.24(f)), thus indicating the absence of abrupt fluctuations in the corresponding waveforms. The PSD analysis of the entire AE signals was complicated in these tests because of the low resolution of the equipment. Nevertheless, its results confirm the same qualitative trends as discussed above.

5.2.3 Discussion

The observed overall evolution of AE is similar to the literature data reported for magnesium alloys of different chemical composition (e.g., [152, 174]). *Mathis et al.* [152] distinguished three stages of AE evolution corresponding to distinct mechanisms of deformation:

- At the beginning of deformation, basal slip (easy glide system in Mg) and primary $\{10\bar{1}2\} < 10\bar{1}\bar{1} >$twins in the grains unfavorably oriented for slip are found. Both this processes are considered to be effective sources of sound waves, contributing to the initial strong AE.

- The maximum of AE corresponds to twining activation in other slip systems.

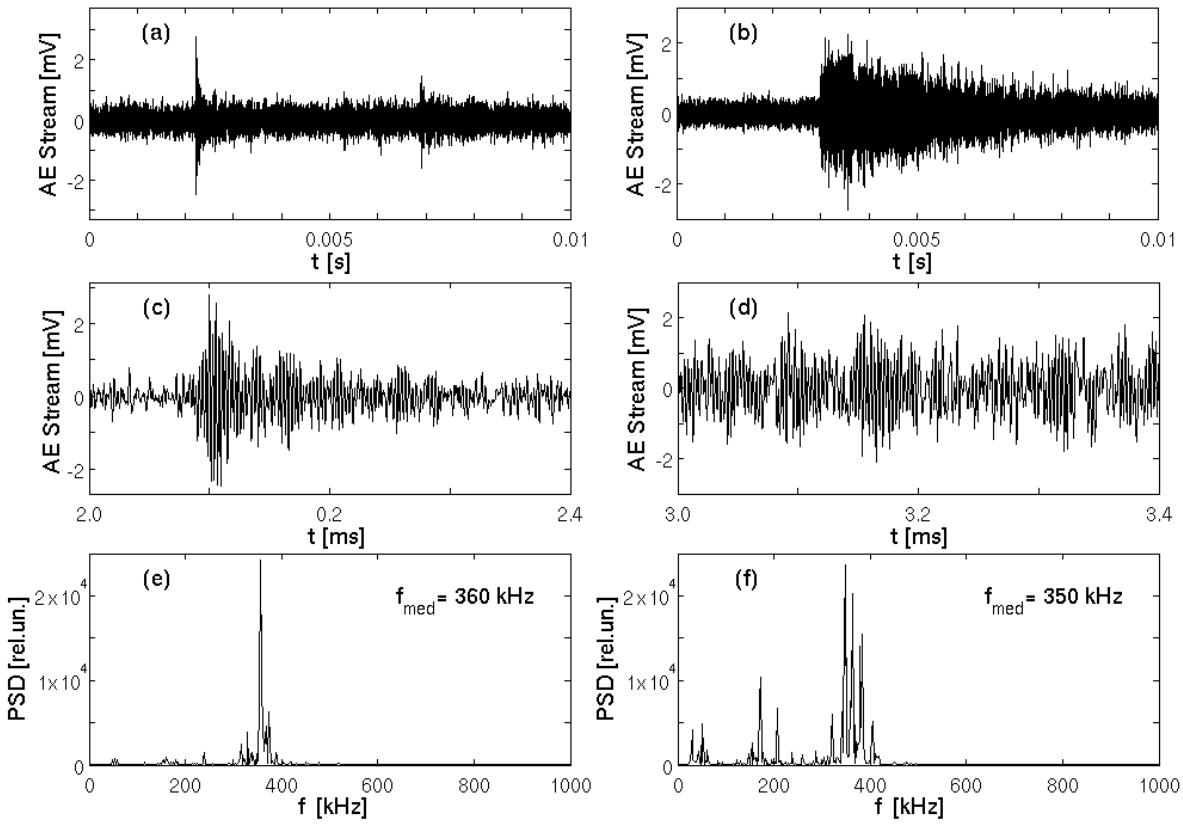

Figure 5.24: (a), (b) Examples of two AE events in AZ31 alloy; (c), (d) magnification of the same events; (e), (f) the corresponding Fourier spectra.

- The following deformation leads to a decreasing AE. *Mathis et al.* [152] observed formation of dislocation walls on this stage in a material with Al and Mn as main alloying elements. This suggests that the decrease in AE is caused by the increasing pinning of mobile defects, leading to reduction of their free mean path. As the dislocation walls are strong obstacles to the motion of dislocations, this observation bears witness to an important production of AE by dislocations. At the same time, it is usually considered that twinning generates a stronger AE activity than dislocation glide and is mostly responsible for high-amplitude acoustic bursts. It is also possible to explain the decreasing AE within the assumption of the dominant role of twins, e.g., by taking into account that the twin boundaries themselves are effective obstacles to propagation of twins in other crystallographic planes.

Another point of discussion in the literature concerns the characteristic waveforms generated due to twinning and dislocation glide. *Richeton et al.* [82] studied AE in Cd and

Zn single crystals and observed two kinds of acoustic events: transient-like waveforms similar to those shown in Fig.5.20(b, c), with duration of several tens of microseconds, and long signals with duration of several hundreds of microseconds, in which the initial sharp transient is followed by a sustained activity. Qualitatively similar patterns, although with considerably shorter durations (10-20 μs for short transients and 20-50 μs for long events) were found in *Tymiak et al.* [156] for sapphire single crystals. In this work the long events were only observed in crystals displaying twinning. Therefore, these data provided an explicit proof that such events are generated by twins. The authors suggested that the sharp transient is due to twin nucleation and the slowly decaying part is controlled by its growth, whereas the events displaying only sharp transients may be due to dislocation avalanches. Based on the similarity of the observed waveforms, a similar hypothesis was adopted in [82] to interpret the results obtained for single crystals of hexagonal metals. An opposite conclusion was drawn in *Vinogradov et al.* [173] for Cu alloys containing various percentage of Ge. It was shown that twinning occurs only in the material with a high Ge content. These aloys present sharp AE bursts with duration about 100 μs, while the samples with a low Ge content deform by dislocation glide and are characterized by essentially continuous emission, in which individual bursts can hardly be isolated. However, the authors admit that some of the short bursts can be due to dislocation avalanches. The existence of diverse hypotheses on the waveforms generated by dislocation avalanches is not surprising, in view of the above results of investigation on Al5Mg alloy, which prove that both sharp transients and almost continuous signals can occur during dislocation glide. It can be suggested that the kinematics of deformation processes may considerably vary even in the same test and under conditions of one mechanism of plasticity, because of the variation of local conditions controlling spatial correlations. Obviously, the characteristic waveforms may also strongly depend on the studied material. It is also noteworthy that analysis of the correlation between different kinds of AE events, reported by *Richeton et al.* [82], indicated that twinning and dislocation glide may mutually trigger each other.

The results obtained in the present study are consistent with the hypothesis that twins are responsible for essentially burst-like behavior displaying short transients and amplitudes reaching very high values. This conclusion directly follows from the comparison of two types of AZ31 samples, one deformed by dislocation glide (Fig. 5.22(a)) and the other showing intense twinning (Fig. 5.22(b)). It is also confirmed by the observation of burst-like behavior in MgZr alloys characterized by twinning. The occurrence of strong bursts at the beginning of deformation in Fig. 5.22(a) proves that dislocation avalanches can also produce very intense events, at least at small strains, when the dislocation can move over long distances. However, these events usually last much longer than those associated with twinning. The short duration and the distinct isolation of AE events from each other in the case of twinning bears witness that the deformation processes involving twinning provide more efficient relaxation of the constrained microstructure, and lead to an abrupt interruption of the localized fast deformation.

Another feature that could be marked out is that Fourier spectra of the waveforms observed for Mg alloys are usually remarkably wider than those found for AlMg (cf. Figs. 5.13, 5.20, and 5.24). This difference reflects a more complex shape of the waveforms for Mg alloys and may be due to the conditions for plastic flow being more constraining in *hcp* than in *fcc* metals. This view is consistent with the conjecture of a complex nature of the processes determining the shape of an individual burst in a Mg alloy, which includes mutually triggering twinning and dislocation glide. Such coupling may be due to various mechanisms. For example, the elastic wave generated because of formation of a twin may trigger other twins, even in remote regions, whereas the concomitant reorientation of the crystal lattice facilitates the motion of dislocations within the twin region.

Finally, it is noteworthy that the PSD analysis revealed a persistent feature of plastic deformation consisting in gradual increasing of the median frequency f_{med} during deformation and observed both for Mg and Al alloys. Such changes are usually attributed to a decrease in the dislocation mean free path because of the increasing density of obstacles to their motion. Indeed, the respective reduction of the mean free flight time of dislocations would result in an increase in f_{med}. The same reasoning can also be applied

to twinning. Another aspect of this behavior which was discussed in § 5.1.2 should also be noted. Namely, the higher f_{med} means a weaker correlation of the processes giving rise to AE. Therefore, the observed increase in the average median frequency suggests progressive stochastization of deformation processes on the global time scale. This question, concerning the changes in the correlations between deformation processes in the course of work hardening, will be addressed in the next chapter using statistical and multifractal analyses of AE on different time scales.

Chapter 6

Statistical and multifractal analysis

This chapter presents the results of the statistical and multifractal analysis of AE accompanying plastic deformation of the materials used in the study. The investigation is performed at various strain rates, various stages of deformation, and on various time scales. Until recently, only statistical analysis of AE was used to reveal information about the collective dislocation dynamics [20, 82, 18, 16]. In the case of the PLC effect [16, 18] our attention was attracted by the observation of considerable changes in the indices of power-law statistical distributions during deformation of an Al3%Mg alloy. The increase in the slope of the dependencies indicates a tendency to a transition from scale invariance to a behavior characterized by an intrinsic scale. To verify this hypothesis we performed a similar analysis for a Al5%Mg alloy as well as for MgZr alloys. The investigation is corroborated by the multifractal analysis. It should be noted in this relation that the statistical distributions only characterize the probability of plastic activity with a given intensity during the test duration, but they do not provide information on the relative arrangement of plastic events. The multifractal analysis has the advantage of uncovering the presence of correlations and characterizing their scaling properties.

6.1 Statistical analysis

6.1.1 AlMg alloy

The analysis was performed for Al5%Mg samples in both as-delivered and annealed state. As shown in Chapter 4, the choice of the event individualization parameters only weakly affects the apparent AE statistics. Thanks to this observation the statistical analysis in the present work was performed for one parameter set for both kinds of material: U_0 =2.2 mV (27 dB), HDT=HLT=300 μs. Except for the initial stage of deformation with the highest strain rate of $2 \times 10^{-2} s^{-1}$, where the analysis was impeded by a very strong events overlapping, power-law probability functions were found for all deformation conditions and almost over the entire range of AE amplitudes, as illustrated in Fig. 6.1. It can also be seen that the largest events show a tendency to an increased probability. The possible nature of this unusual deviation was discussed in § 5.1.3 and attributed to overstresses generated by dislocation pile-ups stopped at grain boundaries, which can trigger dislocation sources in neighboring grains.

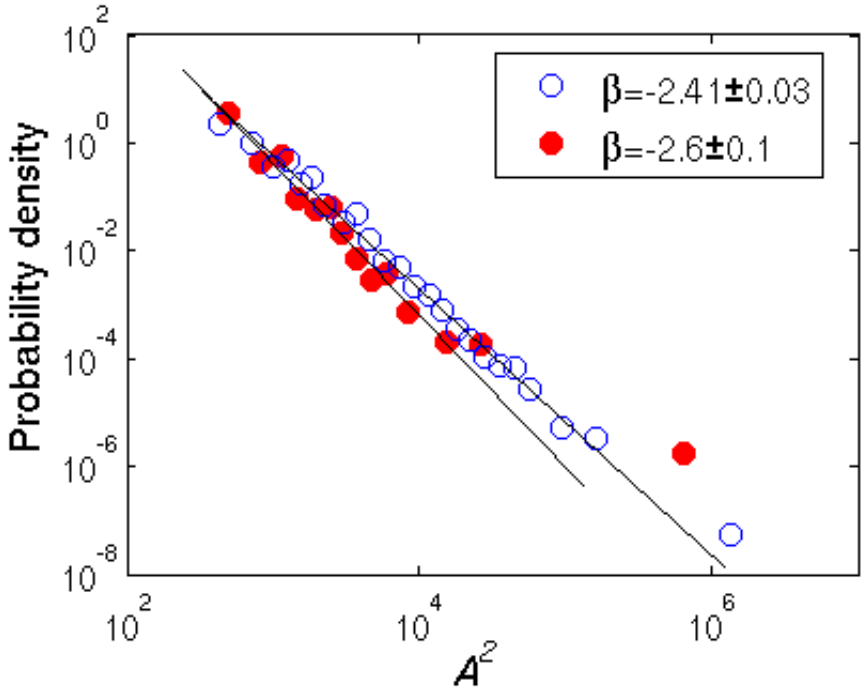

Figure 6.1: Probability density functions for squared amplitude of AE events, for an annealed Al5%Mg specimen deformed at $\dot{\varepsilon}_a = 2 \times 10^{-4} s^{-1}$. Open circles: events extracted in the time interval T=[100s; 400s]; solid circles: T=[1000s; 1500s].

Figure 6.2 demonstrates the evolution of the slope of power-law distributions with strain, for four strain-rate values. As said above, at the highest strain rate the AE initially displays virtually continuous signals with superimposed large discrete bursts, so that only a few events are extracted by the applied numerical procedure. However, the AE signal acquires a more discrete character after some work hardening, providing enough data for statistical analysis. The results shown in Fig. 6.2(a) were obtained on statistical samples containing about 1000 events, which allowed for reliable detection of the power law. At least ten times larger statistical samples were typically obtained for lower strain rates, except for the quasi-elastic region before the Lüders plateau and the late intervals preceding the specimen rupture. The data for lower strain rates, represented in Fig. 6.2(b-d), testify that for a given $\dot{\varepsilon}_a$ the exponent β evolves during deformation. Both the overall behavior and the β-range are similar to the data for the Al3%Mg alloy [16]. Depending on $\dot{\varepsilon}_a$ the value of β varies between -1.8 and -2.4 at the onset of plastic deformation. Then it decreases and varies from -2 to less than -3. Finally, an inverse trend (an increase in β) occurs after some deformation at $\dot{\varepsilon}_a = 2 \times 10^{-5} s^{-1}$.

The comparison of the data obtained in similar strain intervals for different strain rates reveals a tendency to a decrease in β with decreasing $\dot{\varepsilon}_a$, in the strain-rate range corresponding to type A and type B behavior (Fig. 6.2(a-c)). At this stage of investigation it is difficult to say whether such a trend is meaningful. It qualitatively agrees with the influence of the rate of change of the magnetizing field on the power-law statistics of the Barkhausen effect, as well as with theoretical predictions of the role of overlapping [93] (see § 1.4.3). Importantly, this trend does not show up when $\dot{\varepsilon}_a$ is further reduced (cf. Figs. 6.2(c) and (d)). It can thus be conjectured that correct values of β, unaffected by the overlapping, are obtained for $\dot{\varepsilon}_a \leq 2 \times 10^{-4} s^{-1}$. This observation explains the remarkable robustness of β with regard to the events individualization parameters, which was reported in [16] for a similar $\dot{\varepsilon}_a$-range.

The data of Fig. 6.2 make more exact the observation noticed in Chap. 5 in regard to the difference between β-values for as-delivered and solution treated samples. Namely, the slope of the power-law dependence is generally steeper for annealed samples, i.e.,

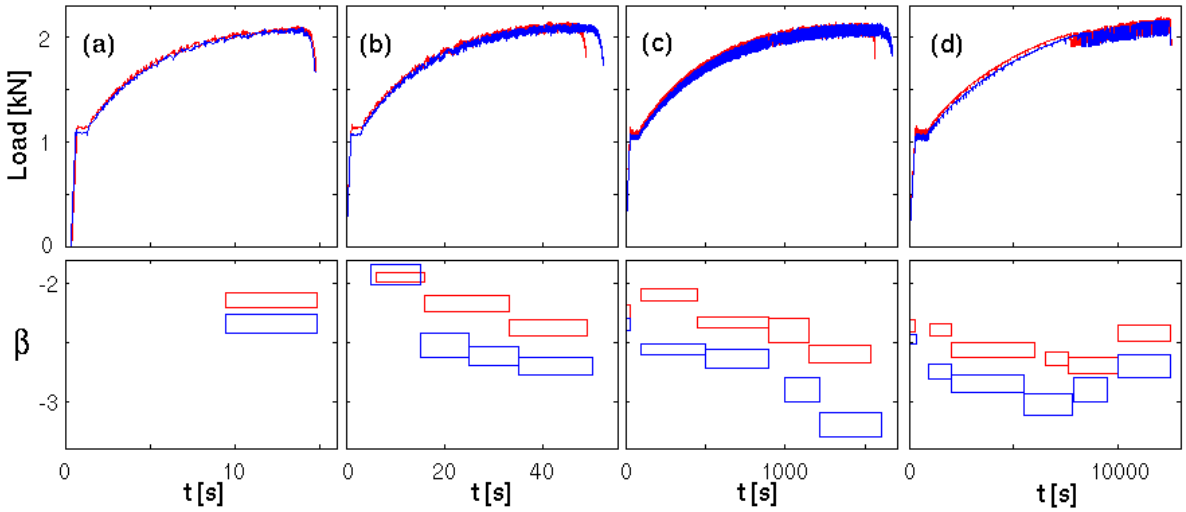

Figure 6.2: Example of collation of deformation curves with the evolution of power-law indexes β for the AE energy distribution. The rectangles designate the time intervals corresponding to statistically stationary series of AE events; their heights give the error of β determination, as defined by the least square method. Data for two samples are displayed for each strain rate: blue - annealed specimens, red - as delivered specimens. (a) $\dot{\varepsilon}_a = 2 \times 10^{-2} s^{-1}$; (b) $\dot{\varepsilon}_a = 6 \times 10^{-3} s^{-1}$; (c) $\dot{\varepsilon}_a = 2 \times 10^{-4} s^{-1}$; (d) $\dot{\varepsilon}_a = 2 \times 10^{-5} s^{-1}$.

annealing leads to increasing the probability of smaller events, although in the case of type C instability this difference decreases during the test or even vanishes. The difference between β-values for as-delivered and annealed samples is conform with the conjecture that the grain boundaries may promote powerful avalanches due to triggering new dislocation sources in the neighboring grains. Indeed, the thermal treatment leads to growth of grain size and reduction of stress concentration on grain boundaries, which would reduce the triggering effect. The observation of a decrease in this difference after some deformation in the tests at $\dot{\varepsilon}_a = 2 \times 10^{-5} s^{-1}$ does not seem to contradict this conjecture, because the low strain rate provides more time for relaxation of local overstresses on the grain boundaries. Consequently, the accumulation of the dislocation density would put in the forefront the forest dislocations as obstacles to slip, and reduce the role of grain boundaries.

6.1.2 MgZr alloys

As reported in Chapter 4, power-law statistical distributions of AE were observed for all Mg alloys studied in the dissertation. Figure 6.3 summarizes the data of statistical

analysis for MgZr with different Zr content, the latter being the principal factor determining the grain size. The following event individualization parameters were used to extract AE events: HDT=50 μs, HLT=100 μs and U_0 =9.1 mV (≈39 dB). It can be recognized that in spite of the different mechanisms of deformation and different character of AE in Al and Mg alloys (cf. Chap. 5), the principal trends found in the previous paragraph for AlMg are also valid for MgZr. The main conclusions which can be drawn from this figure are as follows: (1) the power-law index β is higher than in the case of AlMg and varies in a range close to the values reported previously for single crystals of hexagonal metals [82, 23]; (2) despite this difference with the DSA materials, the effect of the grain size and strain is the same, i.e., β decreases in the course of deformation, and the material with a smaller grain size shows a trend to an enhanced probability of large avalanches (flatter slope of the power-law function). This observation presents an essential difference with the case of single crystals, for which no strain dependence of β was reported.

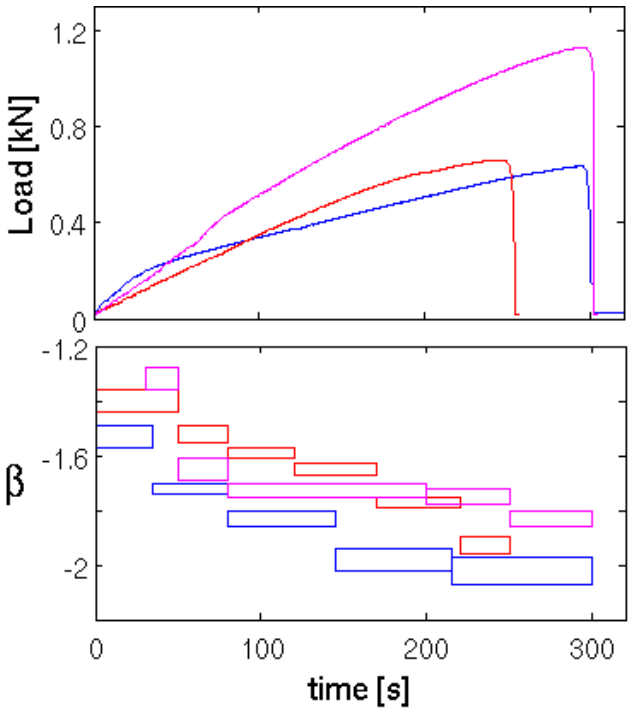

Figure 6.3: Load vs. time curves and variation of the power-law index β for the AE energy distribution. Blue - Mg0.04%Zr (grain size about 550 μm); red - Mg0.15%Zr (360 μm); magenta - Mg0.35%Zr (170 μm).

6.2 Multifractal analysis

6.2.1 General approach

Two kinds of time series were used to reveal the multifractal properties of AE signals. One approach was based on the analysis of series of peak amplitudes of the events extracted from a signal (cf. [17, 16]). This method allows analyzing large time intervals. It also provides a way to filter the events that do not belong to the detected multifractal set. For this purpose, the calculation of the partition functions $Z_q(\delta t)$ (see § 3.3) is repeated several times, for different choices of the threshold which serves for cutting off events with either the lowest or the highest amplitudes. In the second approach, the time series is represented by the AE signal itself. Such time series are usually limited by short time intervals (< 5 s) to provide a reasonable computation time, but this limit can be considerably widened through removal of a noise component below a threshold. This approach is particularly useful for the analysis of individual waveforms, and also in the case of high strain-rate data for which the extraction of individual events is impeded because of their merging.

Figure 6.4(a) presents examples of partition functions for two q-values for a noise signal recorded during idling of the deformation machine. All dependencies follow very closely the trivial unity slope, which qualifies the numerical procedure for the MF analysis. This figure also shows the effect of the finite size of the analyzed set, which manifests itself in the form of steps occurring when δt approaches the length of the total time interval. Figure 6.4(b) displays the result of truncation of a part of the same signal below a threshold. It leads to gradual deviation of the dependencies in the limit of small δt, because of addition of voids to the initially continuous signal.

Figures 6.5(a) and (b) illustrate the masking effect of noise on a multifractal set and the result of truncation of the noise component. It is seen that the presence of noise may completely mask the multifractality (Fig. 6.5(a)). It is not a rule, though. Opposite examples may be found in [120]. The removal of noise allows detecting the multifractality in an interval of large enough δt, from 30 ms to about 1 s (Fig. 6.5(b)). As this

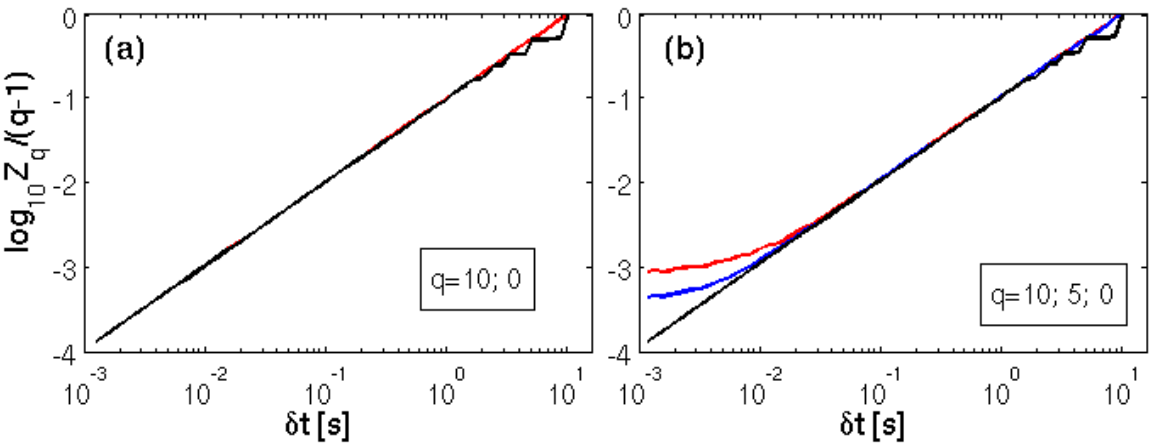

Figure 6.4: Examples of partition functions for experimental noise: (a) total signal; (б) after removal of a part of the signal below 1 mV. The red, blue, and black color correspond to q =10, 5, and 0.

procedure leads to the above-described degradation of the partition functions, nothing can be said about the extension of multifractality on shorter time scales. Obviously, truncation removes both the noise and the possibly present low-amplitude component of the signal. For this reason wavelet analysis was also applied to denoise the signals and avoid thresholding. The first attempts of such treatment have not allowed improving the results. The MF analysis of wavelet-denoised signals yielded similar intervals of linear behavior on $\log(Z_q)/(q-1)$ *vs.* $\log \delta t$ dependencies. Consequently, truncation was mostly used in the present dissertation, due to its simplicity. The research with the aid of wavelet analysis will be continued in the future.

6.2.2 AlMg alloy

Analysis in large time intervals As reported in Chapter 1, application of the MF analysis to series of stress serrations revealed multifractality of deformation curves at all strain rates [84, 106, 103, 17]. In [17], multifractal behavior was also found for the corresponding series of amplitudes of AE events, except for the highest strain rate, $\dot{\varepsilon}_a = 6 \times 10^{-3} s^{-1}$. In this last case the failure of the MF analysis was explained by a strong overlapping of AE events, which made it difficult to resolve individual bursts. For this reason we mostly used direct processing of AE signals when it was possible, in order to avoid errors associated with events individualization.

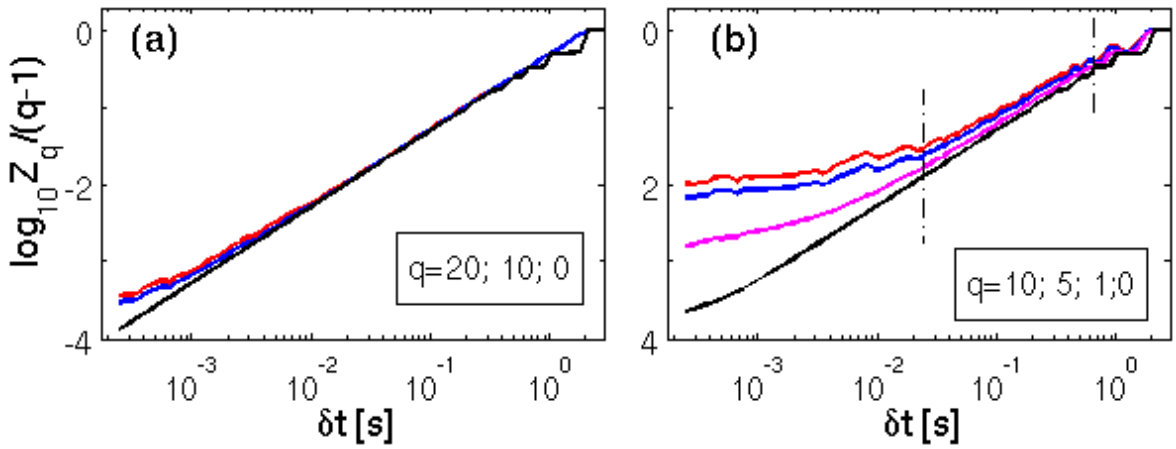

Figure 6.5: Example of the effect of noise on the partition functions for a signal recorded during deformation of an AlMg sample and displaying multifractal features: (a) total signal; (b) after truncation of a part of the signal below 1 mV (the noise level in the tests on AlMg samples was about 1.5 mV).

Similar to the calculation of statistical distributions, the MF analysis was performed in time intervals corresponding to statistically stationary AE. Figures 6.6(a) and 6.6(b) represent examples of partition functions for two AE signals. The fans of approximately linear $\log(Z_q)/(q-1)$ *vs.* $\log \delta t$ dependencies are found over intervals covering noticeably more than an order of magnitude of δt. The dependencies deviate from straight lines when δt is decreased to a scale corresponding to separate events. The upper scaling limit is related to the finite length of the analyzed time series. Using families of such dependencies, spectra of generalized dimensions, $D(q)$, and singularity spectra, $f(\alpha)$, were calculated for different $\dot{\varepsilon}_a$. Smooth MF spectra were found for all applied strain rates. It should be noted, however, that at low and intermediate strain rates, there exist time windows during which multifractality was not detected.

Figure 6.7 shows MF spectra for AE signals recorded at different stages of deformation in a test conducted at $\dot{\varepsilon}_a = 2 \times 10^{-5} s^{-1}$. The first interval is selected before ε_{cr} in a range of macroscopically uniform plastic flow between two low-amplitude stress drops (see Fig.6.8(a)). It yields smooth MF spectra, thus testifying that the correlations of the dynamics of dislocations, which lead to the emergence of multifractral patterns, exist before the occurrence of strong self-organization effects associated with the macroscopic plastic instability. Figure 6.7 also presents MF spectra for two subsequent intervals, one

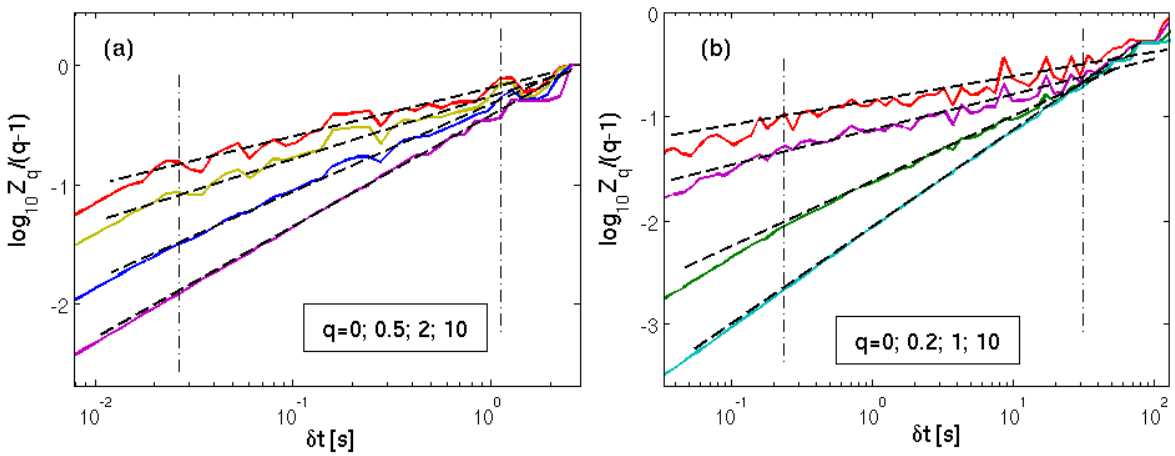

Figure 6.6: Examples of partition functions $Z_q(\delta t)$ for AE time series. (a)$\dot{\varepsilon}_a = 6 \times 10^{-3}s^{-1}$, T=[17.5s; 20s]; (b)$\dot{\varepsilon}_a = 2 \times 10^{-4}s^{-1}$, T=[500s; 700s]. The vertical dash-and-dotted lines indicate the upper and lower scaling limits.

of which, selected beyond ε_{cr}, is shown in Fig. 6.8(b)). It can be seen that the spectra gradually expand and deteriorate in the course of deformation. Furthermore, the multifractality is usually not detected for the latest portions of deformation curves. That the branches corresponding to negative q-values (right-hand parts of singularity spectra) are particularly sensitive to any deviation from fractal behavior and are difficult to obtain in a reliable way, is a general problem for the treatment of real signals because the negative qs correspond to the subsets with the poorest statistics (see, e.g., [122, 106]). Nevertheless, the increase in the spectra width in the range of $q > 0$ indicates an increasing heterogeneity of the signal.

In order to verify the conclusions on the evolution of MF spectra, the calculations were also made for series of amplitudes of AE events. Figure 6.9 presents the resulting singularity spectra for time intervals including those processed in Fig. 6.7 (larger intervals are taken to provide statistically significant numbers of extracted AE events). As could be expected, the spectra do not coincide with those in Fig. 6.7. However, they fall into a similar range of singularity strength α. Importantly, the qualitative effect of the work hardening is the same for the two kinds of time series.

Despite the increase in AE activity with increasing $\dot{\varepsilon}_a$, the overlapping of AE events at intermediate strain rates seems insignificant during the macroscopically smooth parts of the deformation curves. Taking into account that the test duration diminishes accord-

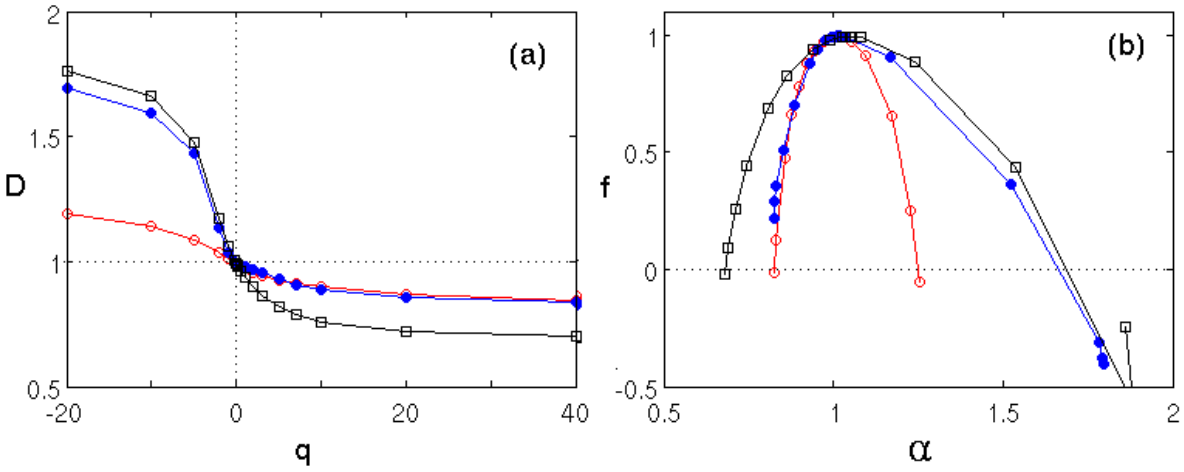

Figure 6.7: Examples of MF spectra for three portions of an AE signal recorded at $\dot{\varepsilon}_a = 2 \times 10^{-5} s^{-1}$: open circles - T=[2700s; 2900s], before ε_{cr}, U>1.7 mV; solid circles - T=[5300; 5600], before ε_{cr}, U>1.7 mV; open squares - T=[9650s; 10050s], beyond ε_{cr}, U>1.5 mV. The deformation curve and the AE signal are illustrated in Fig. 6.8 for the first and the third intervals.

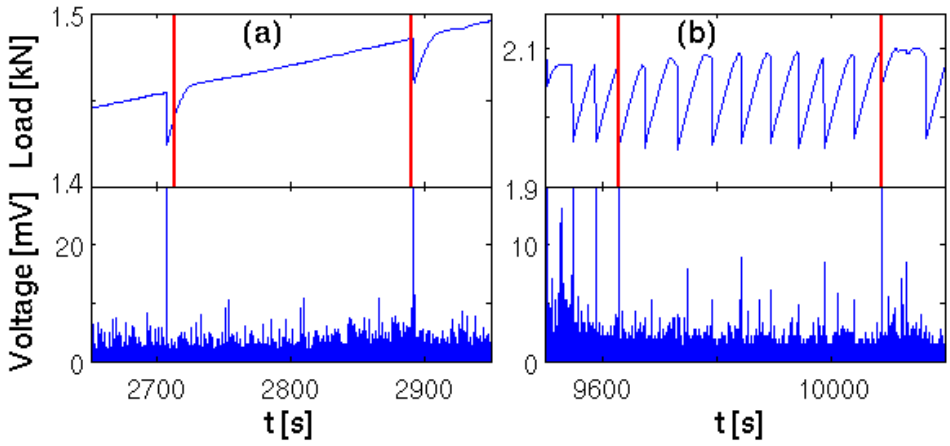

Figure 6.8: Examples of portions of the deformation curve and the accompanying acoustic signal (only the positive half-waves of oscillations are shown) from an annealed Al5Mg specimen deformed at $\dot{\varepsilon}_a = 2 \times 10^{-5} s^{-1}$: (a) and (b) correspond to the regions before and beyond ε_{cr}, respectively. Red lines mark the analyzed time intervals. U_{tr}=1.52 mV.

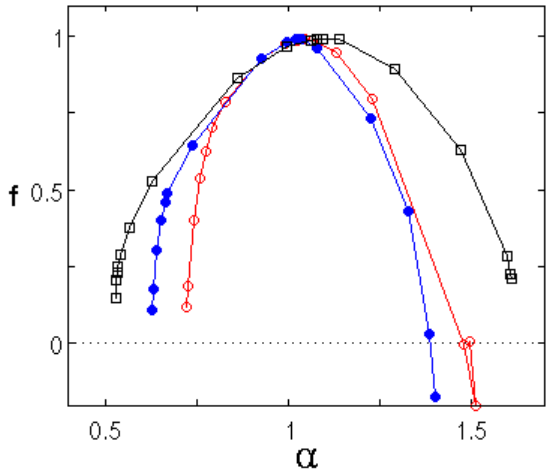

Figure 6.9: Examples of singularity spectra for series of events amplitudes: open circles - T=[2100s, 3100s]; solid circles - T=[5000s, 6000s]; open squares - T=[9200s;10200s]. The event selection settings were as follows: U_0=6 mV; HDT=HLT=300 μs.

ingly to $\dot{\varepsilon}_a$, both approaches to MF analysis of AE can be applied comfortably. Moreover, in these conditions the numerical procedure allows for processing time intervals covering several sequences of stress serrations, associated with the relay-race propagation of type B deformation bands. Examples of MF spectra for $\dot{\varepsilon}_a = 2 \times 10^{-4} s^{-1}$ are given in Fig. 6.10. For one segment, T=[520s; 700s], results obtained using both kinds of time series are presented. It can be seen that the entire AE signal yields in this case an apparently distorted spectrum (open circles), thus questioning the suggestion, based on the visual examination of the signal, that the events are weakly overlapped. In contrast, the series of amplitudes in the same time interval produces a smooth spectrum (solid circles). In any case, the comparison of MF spectra obtained for different time segments using the same approach proves that their evolution with deformation is similar to that found for type C behavior. In particular, the AE is depressed on the latest stages of deformation, so that many stress serrations do not show an acoustic response, and the multifractality completely disappears. For illustration purposes, the dependencies marked by open squares show the results of formal calculation of MF spectra in this last case. It can be recognized that no smooth curve is found.

Besides the treatment of large time intervals, the relatively high AE activity observed at intermediate strain rates allows for scaling examination on a scale of one "period" of

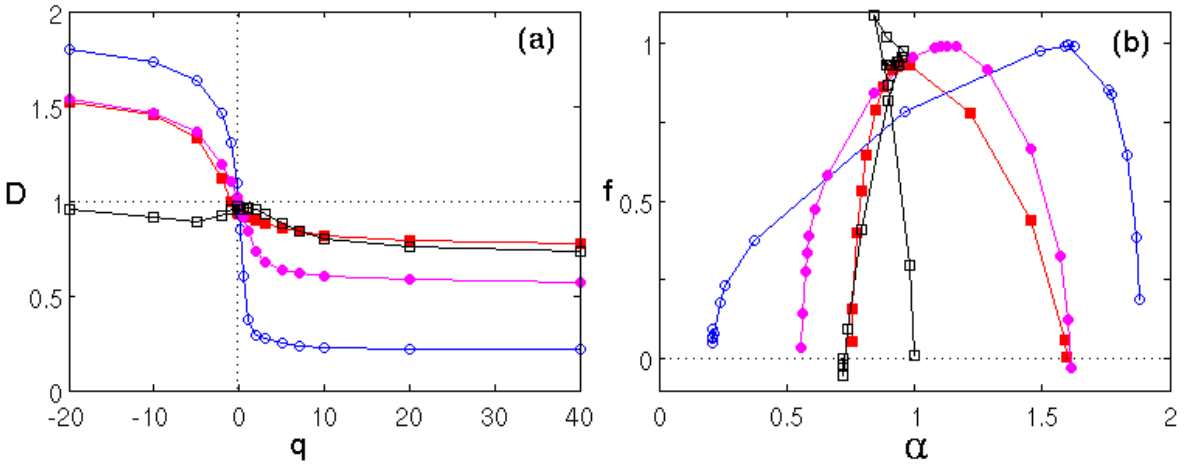

Figure 6.10: Examples spectra of (a) generalized dimension $D(q)$ and (b) singularity spectra $f(\alpha)$ for portions of AE signal from an annealed Al5%Mg specimen deformed under type B conditions; $\dot{\varepsilon}_a = 2 \times 10^{-4} s^{-1}$. Solid squares - T=[100s; 260s], before ε_{cr}; open circles - T=[520s; 700s], beyond ε_{cr}; open square: T=[1300s; 1600s]. The solid circles illustrate MF spectra for series of amplitudes in the interval T=[520s; 700s]. U_{tr}=1.8 mV.

relaxation oscillations, i.e., during one reloading/serration sequence. Figure 6.11(a) presents details of a portion of the AE signal considered in Fig. 6.10. The segment is selected within the time interval corresponding to the spectra denoted by red color and solid squares. Figure 6.11(b) displays the corresponding singularity spectrum for this short segment, found for a δt-range from about 40 ms to 0.6 s. It is noteworthy that the spectrum has a similar shape and width as its counterpart in Fig. 6.10, determined for $\delta t \approx$[10 s; 100 s]. Although there is a gap between these two δt-ranges, it is likely to be artifact of the truncation procedure, which imposes the small-range limit of scaling. Indeed, it was verified by repeating the analysis using intervals with intermediate lengths. Thus, the observed similarity testifies to the same mechanism of correlations operating in a rather wide time range, from milliseconds to tens of seconds, although further verification of this conjecture is needed. Unfortunately, the number of AE events occurring during reloadings decreases with deformation, which makes difficult a systematic analysis.

The further increase in $\dot{\varepsilon}_a$ leads to strong overlapping of acoustic events. Nevertheless, multifractal scaling is found for type A instability, too. Although the evolution of spectra with strain makes difficult evaluation of the effect of $\dot{\varepsilon}_a$, the comparison of

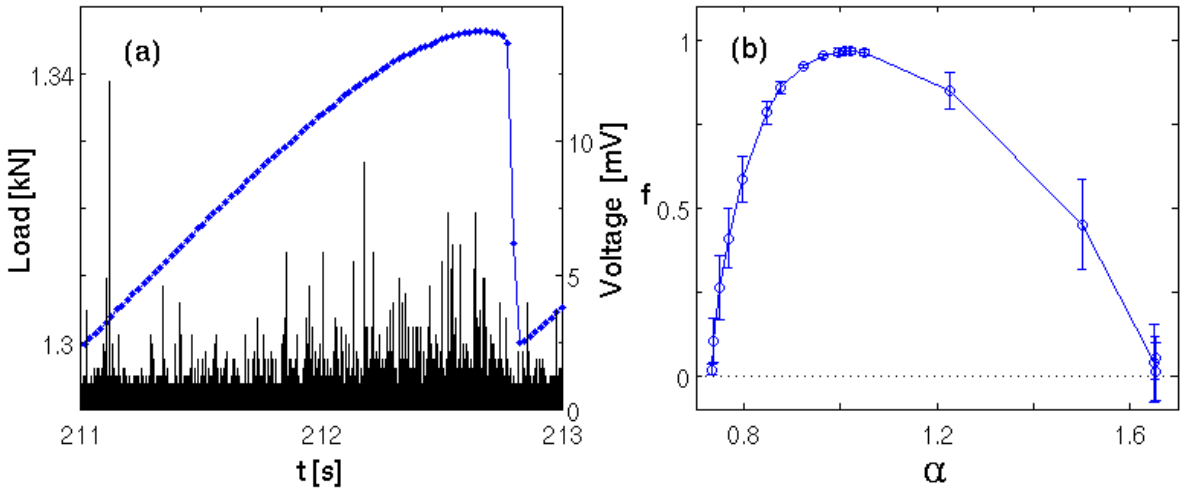

Figure 6.11: (a) Example of AE burst-like signal accompanying reloading between two stress serrations (the same test as in Fig. 6.10); (b) - the corresponding singularity spectrum obtained after cutting off the background noise below U_{tr} = 1.5 mV. δt=[40ms; 0.6s].

MF spectra obtained in similar strain intervals for different $\dot{\varepsilon}_a$ shows a trend to more heterogeneous behavior (wider spectra) at higher strain rates. This observation agrees with the results of analysis of stress serrations in the literature [84, 8, 122]. It can be illustrated using the example of a test at $6 \times 10^{-3} s^{-1}$, which displays type A serrations at the beginning of the test and a progressive transition to type B serrations. Figure 6.12 shows the shapes of the analyzed AE signals and the results of the MF analysis. The AE initially appears to be essentially continuous on the scale of the figure (signal 1). The transition to type B instability is also reflected in AE, as a transition to more discrete behavior (signals 2 and 3). The comparison of MF spectra for the signals 1 and 2 shows a higher spectrum width for type A behavior, although it corresponds to an earlier deformation stage. Finally, the signal 3 selected on a late deformation stage does not possess a MF spectrum, in consistence with the above results for type B instability.

Interestingly, the deterioration of correlations illustrated by the case of signal 3 concerns the coarse time scale (T = 3 s) of Fig. 6.12, but the correlations persist on a finer time scale. Indeed, figure 6.13 presents results of analysis in a much shorter interval (T = 0.1 s) corresponding to reloading between two stress serrations. The approach is similar to that used in Fig. 6.11, with the only difference that the latter corresponds to a much lower driving velocity, for which the reloading time is about 2 s. Figure 6.13(b)

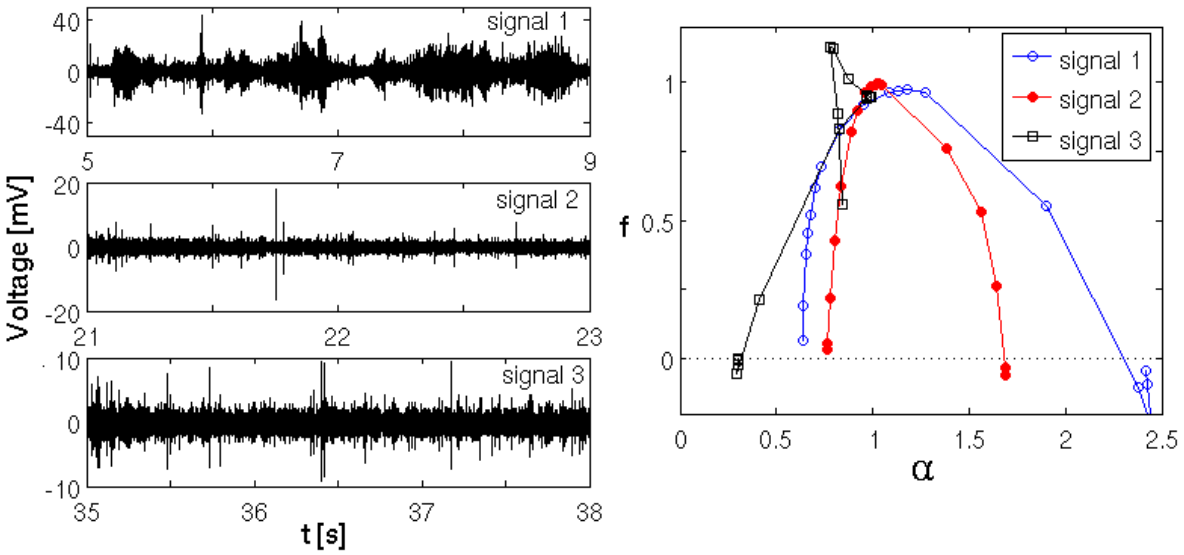

Figure 6.12: Examples of AE signals and their singularity spectra for a specimen deformed at $\dot{\varepsilon}_a = 6 \times 10^{-3} s^{-1}$.

displays a smooth MF spectrum found for δt=[1 ms; 20 ms]. This result indicates that although work hardening leads to a progressive lost of correlations between deformation processes on a long-range time scale, shorter-time memory can still be present.

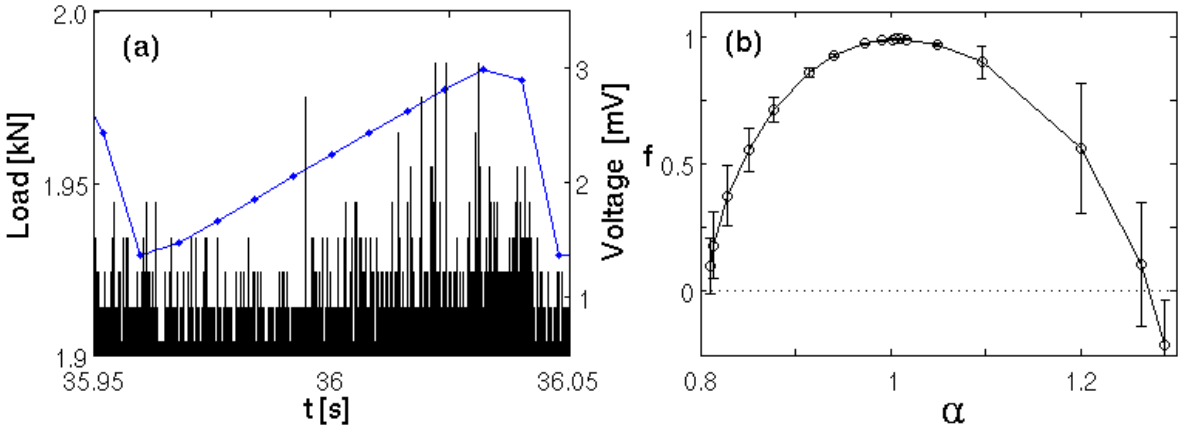

Figure 6.13: Example of (a) AE signal accompanying a sequence of reloading followed by a type B serration at $\dot{\varepsilon}_a = 6 \times 10^{-3} s^{-1}$; (b) the corresponding singularity spectrum, revealed after truncation of the background below $U_{tr} = 0.8$ mV.

Analysis of separate AE events So far in this Chapter the analysis was devoted to long time segments, from 0.1 s to several hundreds of seconds, the shortest of which correspond to a serration/reloading sequence. The above-discussed results testify to the existence of correlations in the ensemble of dislocations on time scales above 1 ms. At

the same time, they do not allow judging about memory effects on finer time scales, most probably because of the hiding effect of noise. Such short time scales are globally inaccessible for the traditional AE technique, which at most provides an opportunity of capturing short continuous records triggered by strong enough acoustic events. The analysis of separate waveforms in a millisecond range, described below, was motivated by the work [28] reporting MF spectra for such records of acoustic events that are usually considered as "elementary". This work only examined the events occurring at the instants of type C serrations in one kind of alloy, namely, in AlCu. Besides, without the data streaming technique, doubts remained on the accuracy of collation of the observed signals to the stress serrations. The aim of the present study was to provide a more detailed analysis of separate waveforms. The challenges are the understanding whether the observed short-range time correlations (i) are governed by the same mechanism (or mechanisms) as the long-range time correlations and (ii) are due to spatially long-range internal stresses or short-range interactions governed by dislocation mechanisms.

The characteristic waveforms observed at the lowest strain rate are presented in Fig. 6.14 (see also Chap. 5). The small stress fluctuations below ε_{cr} are accompanied by merging sequences of closely following events (Fig. 6.14(a)). The deep PLC serrations generate long waveforms with a millisecond duration (Fig. 6.14(b)), which apparently present a finer structure but are usually extracted as single events by the standard AE methods. The macroscopically smooth regions of the deformation curve between two successive stress drops usually display separate short events. However, sequences of events are also observed and present interest for the analysis. The corresponding pattern is shown in Fig. 6.14(c).

Figure 6.15 shows the MF spectra which testify to the presence of multifractal scaling in all signals presented in Fig. 6.14. Scaling behavior was found over δt intervals between a few microseconds and 0.1 ms for the first two waveforms and between 60μs and 1 ms for the last signal. It seems important that the AE activity is weak at the low strain rate and the above-described events are followed by periods without activity, when only noise is present. Consequently, increasing the analyzed time interval leads to disappearance

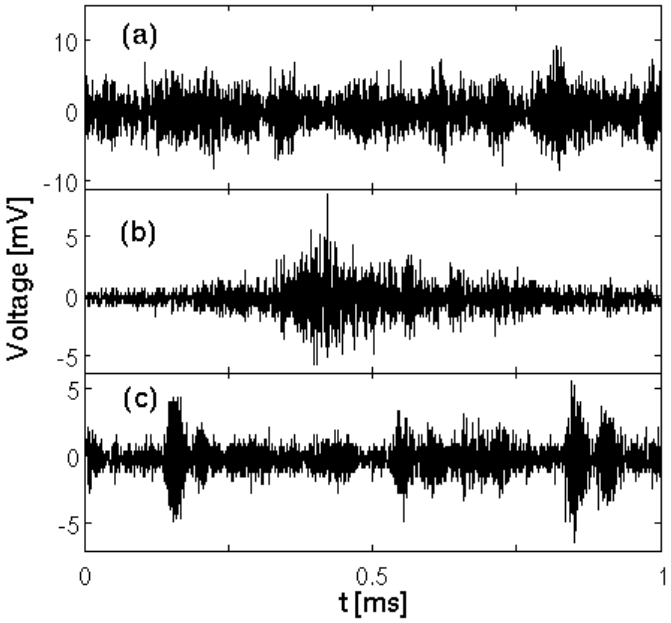

Figure 6.14: Examples of long AE events observed during deformation with $\dot{\varepsilon}_a = 2 \times 10^{-5} s^{-1}$.

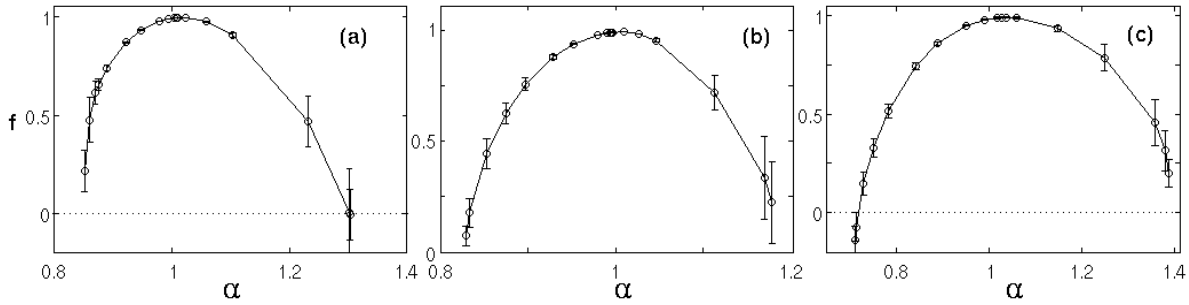

Figure 6.15: Singularity spectra of acoustic events exhibiting a complex temporal structure at $\dot{\varepsilon}_a = 2 \times 10^{-5} s^{-1}$. The notations (a), (b) and (c) correspond to Fig. 6.14.

of scaling. Scaling occurs again for long enough time intervals containing several stress serrations, as described in the previous paragraph. Thus, at this strain rate the AE is not globally multifractal: the detected correlations correspond to either a separate event (or cluster of events) or to rather long series of events.

Figure 6.16 shows some typical examples of acoustic signals observed in an AlMg sample deformed at the $\dot{\varepsilon}_a = 2 \times 10^{-4} s^{-1}$. Individual bursts with a short rising time, like the one displayed in Fig. 6.16(a), are usually observed during reloading parts of deformation curves. Such type of signals was studied in detail in [28]. Its structure is obviously not multifractal because it involves two distinct scales corresponding to the burst itself and the background signal. It was shown that some deviations from the

trivial scaling occur, seemingly because of the presence of some fine structure during the burst decay. However, no smooth MF spectra were found.

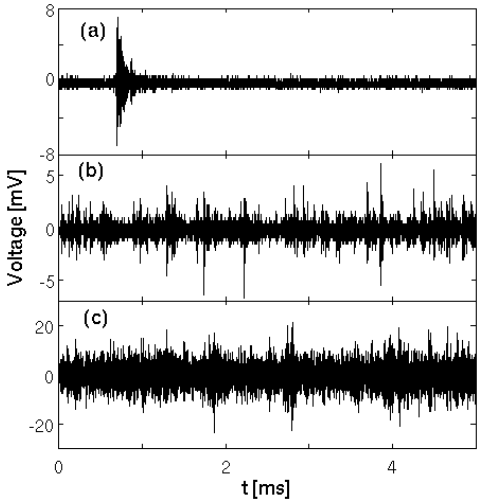

Figure 6.16: Examples of acoustic emission events observed during jerky flow of an annealed specimen deformed at $\dot{\varepsilon}_a = 2 \times 10^{-4} s^{-1}$.

The signal in Fig. 6.16(b), displaying a sequence of short consecutive bursts, often accompanies the phase of nucleation of a new relay race of type B deformation bands (see § 1.5.1, 1.5.3). The partition functions computed for the entire signal (without truncation) are shown in Fig. 6.17(a)). They exhibit approximately straight segments at small time scales and gradually converge to unity slope for δt above several hundreds of microseconds. The corresponding singularity spectrum presented in Fig.6.18 (open circles) testifies to multifractality of the considered signal, but reveals strong imperfections even for $q > 0$. By selecting several values of threshold U_{tr} and truncating the signal below the threshold, it was possible to uncover approximate scaling at larger scales, as illustrated in Fig. 6.17(b), at the same time causing degradation of the small-scale scaling. Linear segments were found in a similar δt-range for all trial values U_{tr}=0.5 mV, 0.75 mV, and 1 mv, but the corresponding spectra vary considerably, depending on U_{tr} (Fig. 6.18). Thus, a good approximation of the true MF spectrum was not found. Nevertheless, the obtained results testify with certainty to the presence of correlations in the treated signal.

Figure 6.16(c) shows a part of an AE event with large duration. Such events occur during stress drops and seemingly consist of overlapping consecutive bursts. In these

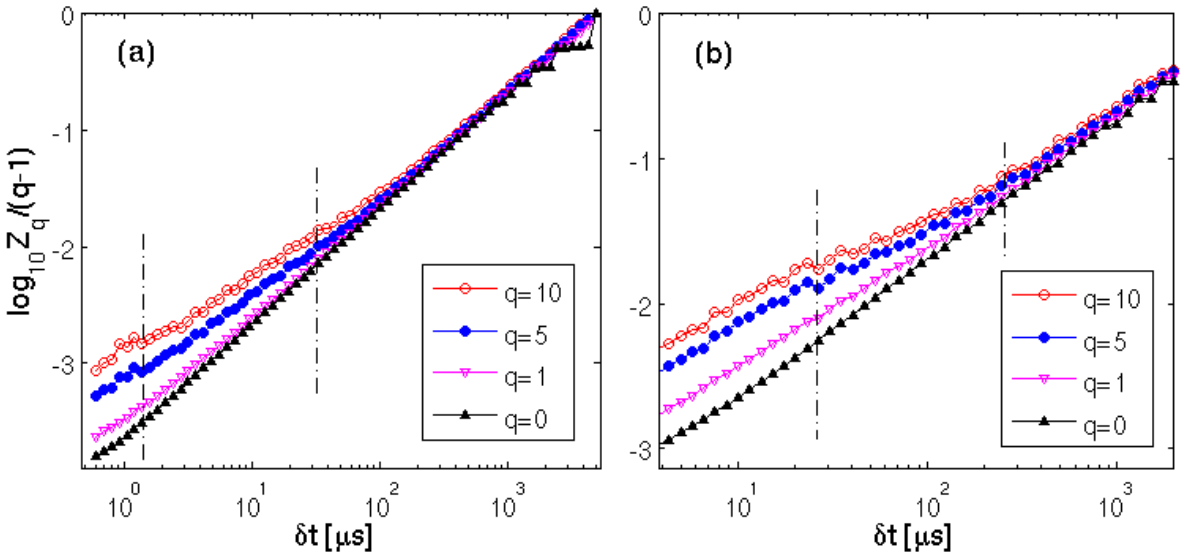

Figure 6.17: Partition functions for the AE signal in Fig.6.16(b): (a) entire signal; (b) after truncation of the part of the signal below $U_{tr} = 0.5$ mV.

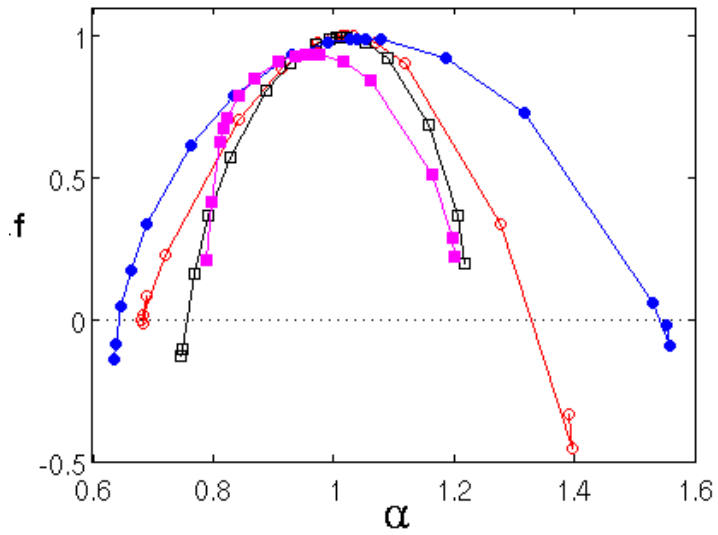

Figure 6.18: Singularity spectra $f(\alpha)$ for the AE signal in Fig.6.16(b): open circles - entire signal; open squares - after truncation of the signal below $U_{tr} = 0.5$ mV; solid circles - $U_{tr} = 0.75$ mV; solid squares - $U_{tr} = 1$ mV.

cases, MF spectra are usually comfortably determined. The signal presented in the figure ilustrates one more interesting feature. The partition functions presented in Fig. 6.19(a) seem to display scaling behavior over more than two orders of magnitude of δt. However, the resulting MF spectra (not shown) present some sharp bends. More careful examination of the partition functions reveals a crossover between two slopes. The calculation separately for two time domains yields good spectra for the small scale

range (Fig. 6.19, open circles), proving the existence of short-range correlations in the signal structure. Multifractal behavior for positive $q-$values is found for the next time interval as well (solid circles), but the negative q branches of the spectra are strongly distorted. The latter behavior suggests two hypotheses: (1) taking into account that the slopes only slightly differ for $q > 0$, the second linear segment may be due to a slow deviation from the scaling law established for the first segment, thus reflecting a decay of correlations on larger time scales; (2) there is a crossover between two scaling domains. The latter situation might reflect a change in the physical mechanism of correlation.

It is also noteworthy that similar to the low strain-rate case and in spite of the higher overall AE activity, the analysis in time intervals intermediate between the scale of the individual waveforms and that of the series of events often did not reveal scaling behavior.

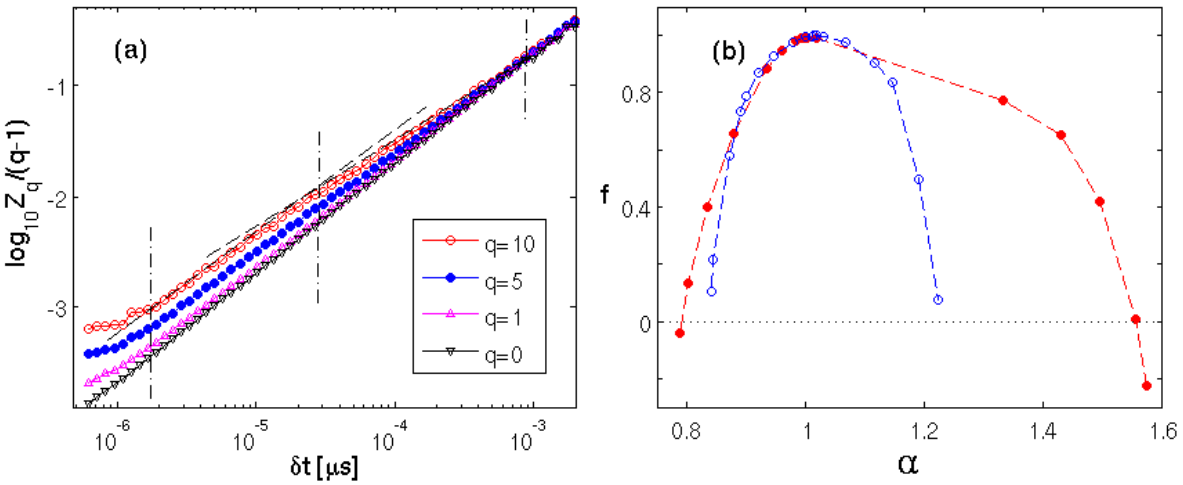

Figure 6.19: (a) Partition functions and (b) singularity spectra for the AE signal from Fig.6.16(c). Open circles represent the spectrum for small time scales ($3\mu s \leq \delta t < 30\mu s$); solid circles denote that for larger time scales ($30\mu s \leq \delta t < 1ms$).

Finally, under conditions of type A behavior at $\dot{\varepsilon}_a \geqslant 6 \times 10^{-3} s^{-1}$, the signals are essentially continuous, similar to that presented in Fig.6.16(c), and yield similar MF spectra. Some of the treated signals also showed a crossover between two scaling laws but this was rather exception than a rule. In contrast to the cases of lower strain rates, multifractality was found for all time scales. This universality may indicate formation of a globally correlated behavior, in consistence with the conjecture of self-organization to

a critical state. However, this hypothesis needs a very accurate verification because, as follows from above, whereas the detection of multifractality is relatively simple, reliable quantitative determination of spectra and their comparison could only be made in rare cases. Further investigation, perhaps, using different methods of analysis is needed.

6.2.3 Mg alloys

The behavior of the AE accompanying deformation of MgZr alloys differs from that for AlMg but it is also characterized by multifractal correlations. The salient features observed are similar for all samples. Figure 6.20 presents examples of AE signals and MF spectra for different stages of deformation of a Mg35%Zr specimen. The upper example is taken from the initial part of deformation, which is usually interpreted as due to basal slip of dislocations, perhaps, accompanied by some twinning [152]. It displays strong discrete AE bursts separated by long periods with close to noise emission. After truncation of the latter background (U_{tr} equal to 3 mV was used), calculations yield smooth spectra for the entire q-range (Fig. 6.20, open symbols), indicating that the main signal is characterized by a unique physical mechanism of correlation. At the same time, the relatively large span of α-values qualifies the signal as a complex heterogeneous structure. This initial AE activity is followed by a period of very intense non-stationary emission ascribed to the occurrence of primary twins. In this case the analysis was only performed during short time intervals, as described below, because of the non-stationary character of the AE signal. This stage is succeeded by a stage of dominant secondary twinning, giving rise to a stationary pattern of incessant burst-like AE, as shown on bottom of Fig. 6.20. This dense pattern gives a narrower MF spectrum in the range of positive qs, which testifies to a more uniform AE activity (Fig. 6.20, solid symbols). However, the spectrum is obtained after truncation of a significant low-amplitude part of the signal, using a threshold of 50 mV, which leads to deterioration of the negative q-branch. Finally, similar to experiments on AlMg, scaling fails at late stages of deformation.

As discussed in concern with Fig. 6.16(a), the MF method cannot be applied to

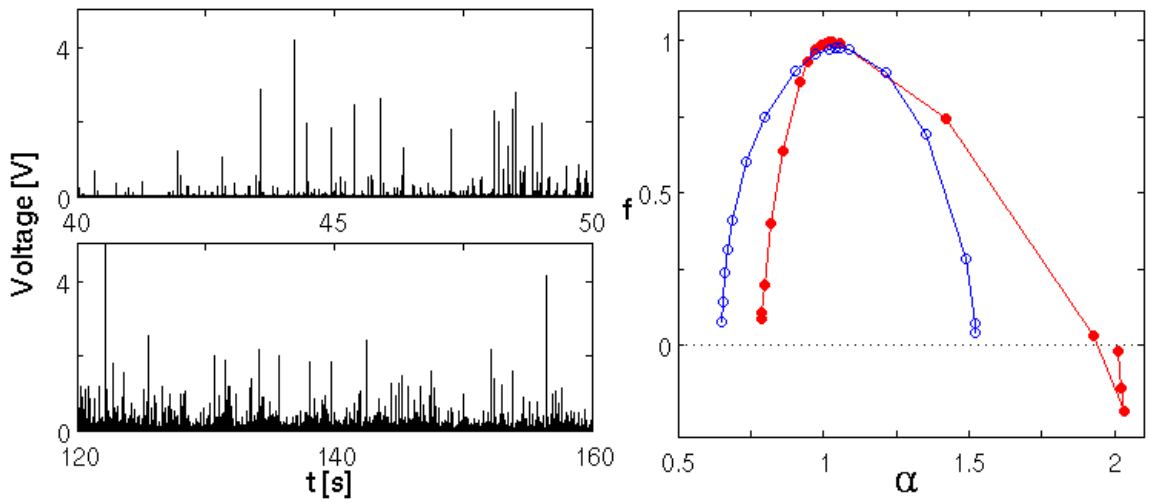

Figure 6.20: Examples of AE signals (left panel) and corresponding singularity spectra $f(\alpha)$(right panel) for Mg35%Zr specimen. Open symbols: T=[40s; 50s], U_{tr}=3 mV; solid symbols: T=[120s; 160s], U_{tr}=50 mV. The scaling dependences were found for δt ∈[0.3s; 4s] and δt ∈[2s; 16s], respectively.

study a separate short burst because its fine structure is masked by a rapid decay function. To uncover correlations on short time scales the analysis was performed over segments of 10-20 ms. Such analysis was not possible on the stage of basal glide because of large distances between events. The results for the next two stages of deformation are illustrated in Fig. 6.21. Since the short intervals contain only several high-amplitude bursts (which largely determine the spectra of Fig. 6.20) the truncation of the lower part would leave insufficient amount of data for the analysis. Therefore, no thresholding was applied. The upper signal corresponding to primary twinning yields a smooth singularity spectrum (solid symbols) for a δt-range extending beyond the average distance ($\sim$ 1 ms) between separate bursts, δt =[0.1 ms, 2 ms]. It is characterized by a rather big width ($\alpha_{min} < 0.5$), in consistence with a strongly clustered AE pattern. The bottom signal, representing a magnification of its counterpart in Fig. 6.20, also shows nontrivial partition functions but does not provide a smooth spectrum (open symbols). Taking into account that the spectrum in Fig. 6.20 was obtained after truncation of a large background, it is clear that the low-amplitude and high-amplitude parts of this signal do not belong to the same set of events. However, it does not mean that the low-amplitude component is uncorrelated. Indeed, the treatment of short segments (about

1 ms) between intense bursts proved that the background signal also gives multifractal spectra with relatively small width ($\alpha_{min} \approx 0.8$). Moreover, a similar check in the range of basal glide showed that the background, having in this case a much lower level, cannot be attributed to random noise either. It reveals scaling of partition functions, resulting in a narrow MF spectrum ($\alpha_{min} \approx 0.9$). It can be concluded on the whole that the deformation processes are essentially correlated, but these correlations cannot be described by unique scaling dependencies and may be due to various mechanisms.

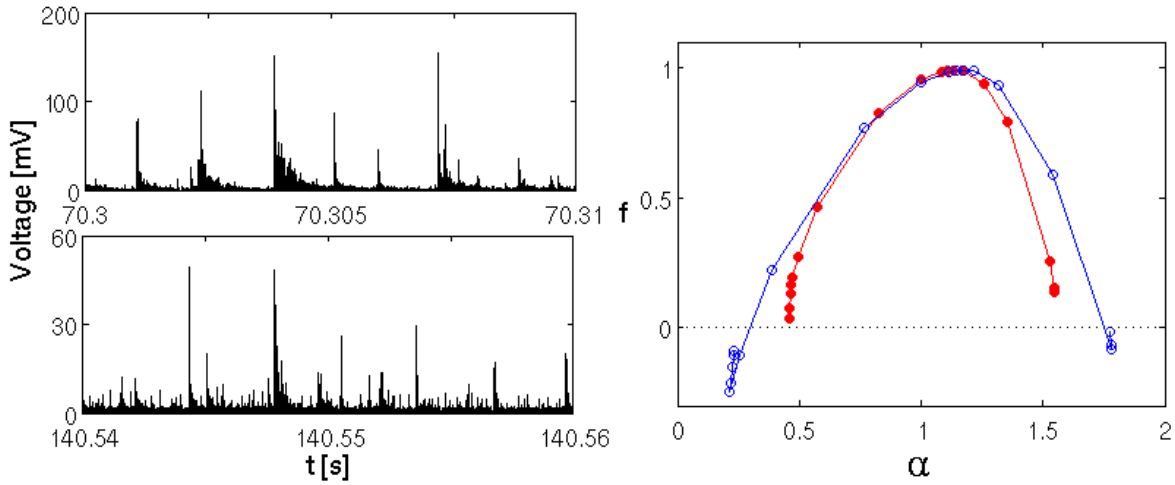

Figure 6.21: AE signals (left) and the corresponding MF spectra (right) in shorter time intervals for the same Mg35%Zr specimen. Solid symbols - T=[70.3s; 70.31s], δt ∈[0.1ms, 2ms]; open symbols - T=[140.54s; 140.56s], δt ∈[0.24ms, 4ms]. U_{tr}= 0 mV.

6.3 Discussion and conclusions

6.3.1 AlMg alloy

Mechanisms of correlation of deformation processes The MF analysis of continuous AE records confirms the correlated nature of the avalanche deformation processes and provides new information on both the extension of such correlations and the relevant physical mechanisms. Taking into account the results of the analysis of AE in the present Chapter and the data of the previous studies of stress serrations (see Chap. 1), it can be suggested that time correlations in a very wide range, from about a hundred of milliseconds to hundreds of seconds, are due to internal stresses and are

governed by two competing processes: that of the generation of microstructural heterogeneities because of the intermittent localized deformation and that of plastic relaxation of the resulting incompatibility stresses (which is also realized through motion of dislocations). It is likely that this picture should also apply to mesoscopic-scale processes during macroscopically smooth plastic flow of pure materials. It would be of interest to realize a similar investigation in this case, too, whereas only the statistical method was applied to such data so far. The case studied in the dissertation is peculiar in the sense that the deformation of DSA alloys is unstable. One consequence of the macroscopic instability is that it may give rise to characteristic scales, associated with the ideal case of cyclic relaxation oscillations, according to the N-shaped SRS function (see § 1.5.2), or, in other words, with the tendency to synchronization of dislocations. This is a possible reason why scaling is not found all over the test duration for type C and type B behaviors but there exist time windows of non-fractal behavior. Second, the plastic instability leads to emergence of correlations in a range of short time scales (from microseconds to milliseconds), associated with the development of catastrophic processes of plastic instability. In this case it is natural to suggest that the correlations may be governed not only by the (fast) changes in the internal stress field but also by a direct impact of elastic waves, involving dislocations to a chain process. Actually, such a pattern corresponds well to the general statement that multifractal time sequences may be generated by cascade processes [162]. It is more surprising that the language of cascade processes also applies to long-range time scales. It can also be conjectured that there is no principal difference between these two cases, although at low and intermediate strain rates there is a "gap" in the observation of scaling between the short and long ranges. Indeed, this gap disappears when the strain rate is increased.

Another interesting observation for small scale behavior concerns the crossover between two slopes illustrated in Fig. 6.19. It implies that an additional mechanism of correlations may act on small scales, for example, the mechanism of double cross-slip of dislocations, as was recently justified theoretically [137]. It is noteworthy that investigation of heterogeneous distributions of dislocation densities in ice single crystals

[180] led to a similar conjecture on a possible effect of this mechanism on short-range spatial correlations in dislocation arrangements. This analogy raises a question of a relationship between self-organized dynamics dislocations and the resulting dislocation microstructure.

Effect of work hardening Two competing factors seem to determine the evolution of the statistics and multifractal scaling of AE during deformation. On the one hand, work hardening creates obstacles to the motion of mobile dislocations and must cause deterioration of correlations between deformation processes. On the other hand, it leads to homogenization of the internal stress field and, therefore, will promote synchronization of dislocation avalanches. The increase in the probability of low-amplitude AE events which is reflected in the decrease in the exponent β of power-law statistical distributions (Fig. 6.2), suggests stochastization of the dislocation dynamics. The stochastization might also be responsible for the failure of multifractal scaling at late stages of deformation. However, the conjecture of stochastization cannot allow for the totality of observations. First, it would lead to collapse of multifractal behavior into the trivial scaling with unity fractal dimension, whereas experiment shows an increase in the width of MF spectra with deformation. A possible explanation of this observation evokes the tendency to synchronization of dislocations under conditions of the PLC effect. Indeed, it may lead to emergence of distinct scales which would enhance the heterogeneity. Moreover, it may eventually cause the failure of scaling and, therefore, provides an alternative interpretation of the final non-fractal behavior. Second, attention should be drawn to the inverse trend observed for β at large strains in the tests at $\dot{\varepsilon}_a = 2 \times 10^{-5} s^{-1}$. A similar change was reported in [16] for a region close to fracture and attributed to localization of the PLC bands because of the developing necking. Indeed, the localization enhances simultaneity of slip, which results in the superposition of AE events and a higher probability of large amplitude bursts. In the present case this change was observed to take place before the beginning of necking. To explain this effect, it should be taken into account that as far as the slow loading provides conditions

for efficient plastic relaxation of internal stresses, the resulting homogenization would promote the effect of synchronization. Finally, it is noteworthy that synchronization may also contribute to the tendency to an increased probability of the largest events, observed for type B and type C behavior (Fig. 6.1).

6.3.2 Magnesium based alloys

The results obtained for MgZr alloys are qualitatively similar to those for AlMg. First, the slope of the power-law statistical distributions of AE amplitudes increases (β decreases) with deformation. Second, the multifractal scaling fails at large strains. At the same time, the width of MF spectra does not increase during deformation, in contrast to the above-described behavior of the PLC effect. Actually, the data obtained for MgZr may be interpreted using the conjecture of stochastization of deformation processes. This also concerns the behavior on short time scales, namely, the observation of a gradually increasing contribution of low-amplitude events which are characterized by narrow MF spectra.

In the case of AlMg the stochastization was explained by a decaying correlation between dislocations, because of the increasing density of obstacles to slip. It is not obvious whether the same logic can be applied to twinning. However, as far as the twinning may be considered from the viewpoint of the motion of twinning dislocations, it can be suggested that work hardening results in reduction of the width of the twin nuclei, which are supposed to be the main AE sources during twin formation, while the further twin growth may not generate acoustic waves. This conjecture is indirectly confirmed by the observation of thinner twins in secondary twinning systems which start operating after some deformation [154]. However, the *post-mortem* microscopy can only provide indirect proofs because it reveals the ultimate size of twins. *In situ* investigations will perhaps be able to verify the discussed hypothesis. Besides, the growing density of twins may cause an increase in the contribution of the dislocation glide which would lead to efficient relaxation of internal stresses and to a decrease in the correlation of the deformation processes.

General conclusions and perspectives for future research

Since the 1980th the application of the concepts of nonlinear dynamical systems to plasticity problems revealed a variety of complex behaviors which cannot be predicted by the traditional theory of dislocations. In particular, using the AE technique evidence was found for an intermittent collective motion of dislocations on a mesoscopic scale, which obeys power-law statistics, characteristic of avalanche-like dynamics. Furthermore, the values of the power-law exponents were observed not to vary considerably for single crystals of various pure materials and to be similar to critical exponents describing avalanche processes in other fields of physics, e.g., the motion of domain walls in magnetic materials or the martensitic transformations. The observed universality of dynamics allows generalizing some of the findings obtained in the study of the collective motion of dislocations to other dynamical systems. At the same time, recent investigations on polycrystals and alloyed materials showed limitations of the concept of universality. In the present dissertation, the effect of the experimental conditions and microstructure on the statistical and fractal properties of AE was studied using alloys characterized by different mechanisms of deformation. Alongside with the statistical investigation, the evolution of the acoustic signal during deformation was examined and the possible mechanisms of the observed changes were discussed. The main results of this research are shortly summarized below.

Power-law amplitude distributions of AE accompanying plastic flow in AlMg and MgZr alloys were obtained in different experimental conditions. An important result of

statistical analysis is that the criteria used to extract individual AE events have little effect on the apparent statistics. A very weak effect was found for MgZr, in consistence with the literature data showing that the materials deforming by twinning generate well separated abrupt AE hits. A less favorable situation for the statistical analysis of AE appears under conditions of the PLC effect. The entirety of the results obtained in the dissertation show that this difficulty is caused by the plastic instability being related to the tendency to synchronization of the dynamics of dislocations, which leads to localization of deformation on the macroscopic scale and merging of acoustic events on a mesoscopic scale. Nevertheless, even in this case the effect of the criteria used to identify AE events is not crucial and does not prevent from detecting the changes in the power-law exponents when the experimental conditions are modified. It should be noted that this result is of general importance for the study of avalanche processes in various fields of science.

Statistical analysis of the amplitudes of AE events showed that the slope of the power-law distributions depends on the microstructure, particularly, the grain size and the microstructural changes induced by deformation and related to accumulation of dislocations and twins. More specifically, these results provided a direct proof of an important role of local stress concentrations on grain boundaries. Indeed, reduction of the grain size in both kinds of materials led to an increase in the probability of higher-amplitude AE events. This effect can be explained by an efficient transfer of plastic activity to neighboring grains, promoting formation of powerful avalanches. On the contrary, the forest hardening results in an increase in the probability of lower-amplitude AE events, which indicates gradual weakening of correlations between dislocations, i.e., stochastization of plastic deformation processes. The conjecture of stochastization is also confirmed by the observation of a progressive increase in the median frequency of the acoustic signal during deformation, usually associated with a decrease in the mean free path of the defects generating the AE, which was also observed for both kinds of alloys.

The data streaming technique allowed investigating the jerky flow of an AlMg al-

loy on different timescales and provided various evidences to support the hypothesis of a relation between type C and type B PLC instability and the phenomenon of synchronization in dynamical systems. In particular, it allowed clarifying a contradiction existing in the literature on the PLC effect, with regard to discrete and continuous attributes of the accompanying AE. Namely, the observation of huge AE count rate bursts at the instants of type B or type C stress serrations has led to contraposition between discrete AE associated with the PLC instability and continuous AE during stable flow. Among other, this contraposition contradicts the experimental fact that the amplitudes of AE events do not show peculiarities during stress serrations. The analysis of continuously recorded AE signals in the present work proved that AE has a burst-like character during both stress serrations and smooth flow, with amplitudes of bursts varying in the same range. At the same time, the apparent behavior, discrete or continuous, of the AE accompanying stress serrations is found to depend on the scale of observation. When viewed on a traditionally used time scale, which does not resolve the structure of individual AE bursts, their amplitudes are indistinguishable during the periods of smooth plastic flow and at the instants of stress drops. However, the synchronization of the dynamics of dislocations at the moments of stress drops leads to generation of AE events with millisecond durations, which exceed by more than an order of value the durations of the hits observed during smooth flow.

The application of the multifractal analysis to continuous AE records permitted us to quantitatively characterize the correlations between deformation processes in various time scale ranges. Under conditions of the PLC effect, the time correlations observed in a very wide range, from about a hundred of milliseconds to hundreds of seconds, are most probably governed by internal stresses. Importantly, evidence was found that synchronization of dislocations leads to emergence of a distinct time scale associated with abrupt stress drops (types B and C of behavior) and corresponding to a microsecond range. Observation of a crossover in the multifractal scaling suggests that in this case, besides the changes in the internal stress field (and perhaps a direct impact of elastic waves), another mechanism of correlations may be present, e.g., the transfer of plastic

activity due to double cross-slip of dislocations.

Finally, in the case of MgZr alloys, the MF analysis revealed the existence of two scale ranges of amplitudes of AE events, which correspond to different correlations as revealed by MF spectra. High-amplitude bursts are generally attributed to mechanical twinning and are usually considered in AE studies of plastic deformation of such materials. However, we found that the low-amplitude events are by no means random noise, because they also show correlations leading to emergence of MF spectra. The nature of the two different sets of AE events is not clear yet. However, as the dislocation pile-ups are believed to yield lower-amplitude AE bursts than the twins, we hope that such a quantitative analysis would help distinguishing the AE related to twins and dislocations.

Perspectives for further research

The present dissertation is one of the first works aiming at multiscale quantitative analysis of plastic deformation with the help of continuously recorded AE signals. The results obtained testify to the occurrence of complex temporal patterns during plastic deformation of *fcc* and *hcp* metals and raise various questions related to the description of the collective dynamics of dislocations. Some of the possible directions of future research are listed below:

- A detailed investigation of the role of cracking of second phase particles, using both the analysis of microstructure at different stages of deformation and the comparison of statistical properties of AE with the results obtained for cracking in brittle materials;

- Investigation of the spatial aspect of collective processes with the aid of localization of AE sources not only in time but also in space, using two acoustic sensors. Reconstruction of spatio-temporal patterns of deformation processes in various materials. For this purpose, it would be of interest to combine the AE technique with high-resolution local extensometry methods;

- Investigation of the initial stage of plastic deformation during elastoplastic transition. This transition is almost unstudied experimentally from the viewpoint of collective phenomena. It can be expected that the AE technique would be able to judge not only about the collective motion of dislocations but also about the processes of their multi-

plication;

- Statistical analysis of durations of AE events, which remained beyond of this dissertation;

- Multifractal analysis of AE signal in pure single crystals, for which only data on the amplitude distributions are available in the literature. It should be underlined that the observation of power-law amplitude distributions does not provide sufficient criteria to verify or falsify the hypothesis of SOC, which is most often applied to interpret these data;

- Investigation of AE accompanying deformation by compression. It might be especially interesting in the case of *hcp* materials which present a strong asymmetry of plastic flow, e.g., different twinning systems operate in tension and compression.

Appendix A

Multifractal analysis

A.1 Fractals, fractal dimension

An accurate mathematical description of the (multi)fractal analysis can be found in a number of books and reviews, e.g. [162]. The aim of this section is to provide a brief qualitative consideration highlighting the physical meaning of the concept of fractals and its usefulness for characterization of complex structures and signals.

The name "fractals" was proposed by Benoît Manelbrot [181] to describe specific non-Euclidean geometrical constructions which present self-similar, or scale-invariant, patterns. Soon afterwards, it has been understood that various natural objects manifesting complex spatial structures or evolution patterns possess the property of self-similarity in some range of scales and may be described using concepts of fractal geometry. Self-similar objects are abundant in nature and are found in everyday life as well as in various fields of science, starting from the obvious self-similarity of the hierarchic structure of snowflakes (see Fig. A.1) or leaves of trees and ending with statistical self-similarity found for a broken-up coastline [162] or human heart rate [182].

Mandelbrot defined a "fractal" as a complex geometric figure, self-similar at all scales. The rigorous mathematic definition of a fractal is based on the so-called Hausdorff–Besicovitch dimension [162], which is equal to the topological dimension for a Euclidean object but exceeds it in the case of fractals. The correct definition of the

Figure A.1: Example of a self-similar object: snowflake under microscope.

Hausdorff–Besicovitch dimension is sophisticated and goes beyond the scope of the thesis. A simpler consideration is provided by a practically equivalent capacity dimension D_0. Its determination picks up the procedure used in the traditional geometry to measure the length of a line segment, the area of a surface, the volume of a body, and so on. In the general case of a n-dimensional object, it consists in counting the minimum number N of n-dimensional hypercubes of linear size l, needed to cover the object. In Euclidean geometry, this number obeys an obvious scaling law

$$N(l) \sim l^{-D_0} \tag{A.1}$$

in the limit $l \to 0$, where D_0 coincides with the (integer) topological dimension: $D_0 = 1$ for a line, $D_0 = 2$ for a surface, and $D_0 = 3$ for a body. As illustrated below, the same scaling law is valid for fractals but the corresponding dimension may take on non-integer values.

As the signals to be studied are represented by events distributed over a time interval, fractal structures constructed in 1D-space are of great interest for the following discussion. Let us consider a well-known example of a Cantor set. It is created by applying a simple recursion rule to a line segment: starting by removing the middle third from the initial segment [0,1], the middle thirds are further removed at each step from all segments remaining after the previous step. After n iterations, the set consists of 2^n segments with the same length $l = (1/3)^n$ (see Fig. A.2). The continuation of this process *ad infinitum* results in a structure with a zero topological dimension, which

contains voids everywhere so that the total length of the segments, $L = 2^n(1/3)^n$, tends to zero when $l \to 0$ (i.e., n tends to infinity) [162].

Figure A.2: Example of a first six steps of the creation of Cantor set.

However, the application of the equation (A.1) results in a fractional positive D_0 value, which is called fractal dimension and is usually denoted D_f. Indeed, choosing segments of length $l = (1/3)^n$ to cover the Cantor set readily gives $N(l) = 2^n$ and therefore, $D_f = -lnN(l)/lnl = ln2/ln3$. This value is greater than the (zero) topological dimension of the Cantor set and smaller than that of the embedding space - the initial 1D segment. This property leads to various peculiar features of fractals. In particular, it follows that $L \sim l^{1-D_f}$, i.e., measuring the length of the Cantor set gives results depending on the scale of observation.

The modification of the recursion rule will lead to generation of a set with a different value of D_f. Thus, the fractal dimension allows not only checking whether the set is self-similar, but also characterizing it quantitatively. At the same time, the fractal dimension is a global characteristic of the occupancy of the space (a hypercube is either occupied or not), which disregards local properties, such as the events amplitudes or clustering of the events, the latter leading to inhomogeneous filling of the space and various occupancy of the hypercubes at a given scale of observation. This problem is attacked with the aid of the multifractal formalism described in the following section.

A.2 Multifractals

The description of natural objects usually requires more than one scaling index. The reason for this is that besides the underlying fractal geometry, characterized by the fractal dimension, they may carry a locally fluctuating physical property. In addition to

the examples in the previous paragraph, frequent examples concern magnetic or electric moments, masses of structural elements, and so on. To describe such heterogeneous systems, the multifractal analysis must handle both the underlying fractal geometry and the variations of the physical property distributed on the fractal support.

The way to do it can be illustrated by adding complexity to the recurrent procedure of generation of the Cantor set. Let us begin with assigning a uniform weight distribution to the segments of the Cantor set. The modified procedure starts from a unit segment with a weight $\mu = 1$ and includes an additional rule: the weight of each segment obtained at the current generation step is shared equally between the two segments created from it at the next step. After m iterations, the set consists of 2^m segments with the same length $l_i = (1/3)^m$ and weight $\mu_i = (1/2)^m$. Thus, the following power-law relationship holds:

$$\mu_i \sim l_i^{\alpha}. \tag{A.2}$$

The Lipschitz-Hölder index α is often called singularity strength because when $\alpha < 1$, the local density diverges in the limit $l \to 0$: $\mu_i/l_i \sim l_i^{\alpha-1}$. The weight μ is an example of a probability measure which makes it possible to describe the distribution of a physical quantity on a fractal support. In the considered case, two indices, D_f and α, provide such a description (for Cantor set, $\alpha = ln2/ln3 = D_f$).

This simple case can be further generalized to allow for description of real heterogeneous self-similar objects. As demonstrated, e.g., in Ref. [162], the modification of the recurrent rules so that the segments are divided into unequal parts and the weights are assigned with unequal probabilities results in heterogeneous fractal sets, for which α takes on a continuous range of (non-negative) values corresponding to different regions of the set. The heterogeneous set may then be described by calculating fractal dimensions $f(\alpha)$ of the subsets corresponding to close values of the singularity exponent between α and $\alpha + d\alpha$:

$$N(\alpha) \sim l^{-f(\alpha)}, \tag{A.3}$$

where $N(\alpha)$ is the number of segments in the given subset. In the general case, the

dependence $f(\alpha)$, often called singularity spectrum, is a continuous function. Obviously, f varies in a range between 0 and 1 for a $1D$ signal. The spectrum $f(\alpha)$ degrades to a single point in the case of a uniform fractal.

The singularity spectrum makes clear the physical meaning of the multifractal formalism but the above definitions do not provide a method to calculate it. A convenient numerical procedure was proposed in [183]. Using a normalized measure $\tilde{\mu}_i(l,q) = \frac{\mu_i^q}{\sum_j \mu_j^q}$, where $q \in Z$, the values of $f(\alpha)$ can be found from the following scaling relationships

$$\begin{cases} \sum_\alpha(l,q) &= \sum_i \tilde{\mu}_i(l,q) ln \mu_i(l) \sim \alpha(q) lnl \\ \sum_f(l,q) &= \sum_i \tilde{\mu}_i(l,q) ln \tilde{\mu}_i(l,q) \sim f(q) lnl \end{cases} \tag{A.4}$$

As presented in Section 1.3, there also exists an alternative description in terms of generalized dimensions $D(q)$ which are found from the scaling laws

$$\begin{cases} Z_q(l) &= l^{(q-1)D(q)} \\ Z_1(l) &= D(1) lnl \end{cases} \tag{A.5}$$

where the partition functions $Z_q(l)$ are defined by the relationships

$$\begin{cases} Z_q(l) &= \sum_i \mu_i^q, q \neq 1 \\ Z_1(l) &= \sum_i \mu_i ln \mu_i, q = 1 \end{cases} \tag{A.6}$$

$D(q)$ is constant for simple fractals, while the decreasing $D(q)$ is a signature of a multifractal object. The two kinds of multifractal spectra, $D(q)$ and $f(\alpha)$, are related with each other by the Legendre transform: $f(\alpha) = q\alpha - \tau(q)$ and $\alpha = d\tau(q)/dq$, where $\tau(q) = (q-1)D(q)$.

Bibliography

[1] G. Nicolis and I. Prigogine, *Self-organization in nonequilibrium systems : from dissipative structures to order through fluctuations* (Wiley, New York, 1977)

[2] H. Haken, *Synergetik* (Springer-Verlag, Berlin Heidelberg New York, 1982)

[3] A. Portevin and F . Le Chatelier, *Comptes Rendus Acad Sci Paris*, **167**(1923):507

[4] L.P. Kubin, C. Fressengeas and G. Ananthakrishna, *Dislocations in Solids*, volume 11, pp. 101 – 192 (Elsevier, 2002)

[5] M.A. Lebyodkin, Y. Brechet, Y. Estrin and L.P. Kubin, *Phys Rev Lett*, **74**(1995)(23):4758

[6] M. Lebyodkin, L. Dunin-Barkowskii, Y. Bréchet, Y. Estrin *et al.*, *Acta Mater*, **48**(2000)(10):2529

[7] G. Ananthakrishna, S.J. Noronha, C. Fressengeas and L.P. Kubin, *Phys Rev E*, **60**(1999):5455

[8] M.S. Bharathi, M. Lebyodkin, G. Ananthakrishna, C. Fressengeas *et al.*, *Acta Mater*, **50**(2002)(11):2813

[9] D. Kugiumtzis, A. Kehagias, E.C. Aifantis and H. Neuhäuser, *Phys Rev E*, **70**(2004):036110

[10] K. Darowicki, J. Orlikowski, A. Zieliński and W. Jurczak, *Comp Mater Sci*, **39**(2007)(4):880

[11] A. Sarkar, L. Charles, Jr. Webber, P. Barat *et al.*, *Phys Lett A*, **372**(2008):1101

[12] G. Ananthakrishna, C. Fressengeas, M. Grosbras, J. Vergnol *et al.*, *Scripta Metall Mater*, **32**(1995):1731

[13] H.D.I. Abarbanel, R. Brown, J.J. Sidorowich and L.Sh. Tsimring, *Rev Mod Phys*, **65**(1993):1331

[14] P. Bak, C. Tang and K. Wiesenfeld, *Phys Rev A*, **38**(1988):364

[15] L.P. Kadanoff, *J Stat Phys*, **43**(1986):395

[16] Y. Bougherira, *Etude des phénomènes d'auto-organisation des ensembles de dislocations dans un alliage au vieillissement dynamique*, Phd thesis, Université Paul Verlaine - Metz (2011)

[17] M.A. Lebyodkin, N.P. Kobelev, Y. Bougherira, D. Entemeyer *et al.*, *Acta Mater*, **60**(2012):844

[18] M.A. Lebyodkin, N.P. Kobelev, Y. Bougherira, D. Entemeyer *et al.*, *Acta Mater*, **60**(2012):3729

[19] J. Weiss and J.R. Grasso, *J Phys Chem B*, **101**(1997):6113

[20] J. Weiss, J.-R. Grasso, M.-C. Miguel, A. Vespignani *et al.*, *Mater Sci and Eng A*, **309**(2001):360

[21] J. Weiss, T. Richeton, F. Louchet, F. Chmelik *et al.*, *Phys Rev B*, **76**(2007):224110

[22] C. Fressengeas, A.J. Beaudoin, D. Entemeyer, T. Lebedkina *et al.*, *Phys Rev B*, **79**(2009):014108

[23] T. Richeton, J. Weiss, F. Louchet, P. Dobron *et al.*, *Kovove Materialy*, **45**(2007):149

[24] D.M. Dimiduk, C. Woodward, R. Lesar and M.D. Uchic, *Science*, **312**(2006):1188

[25] M. Zaiser, *Advances in Physics*, **55**(2006):185

[26] T. Richeton, J. Weiss and F. Louchet, *Nat Mater*, **4**(2005):465

[27] Y. Bougherira, D. Entemeyer, C. Fressengeas, N.P. Kobelev *et al.*, *J Phys*, **Conf. Series 240**(2010):012009

[28] M.A. Lebyodkin, T.A. Lebedkina, F. Chmelik, T.T. Lamark *et al.*, *Phys Rev B*, **79**(2009):174114

[29] N.A. Koneva, E.V. Kozlov and L.I. Trishkina, *Metallophysica (in russian)*, **10**(1991):49

[30] L.P. Kubin, *Materials Science and Technology*, volume 6 (VCH, Weinheim, 1993) p. 139

[31] R. Madec, B. Devincre and L.P. Kubin, *Scripta Mat*, **47**(2002)(10):689

[32] B. Devincre, L. Kubin and T. Hoc, *Scripta Mat*, **54**(2006)(5):741

[33] P.D. Ispanovity, I. Groma, G. Györgyi, F.F. Csikor *et al.*, *Phys Rev Lett*, **105**(2010):085503

[34] E.N. da C. Andrade, *Proc R Soc Lond A*, **84**(1910):1

[35] E. Orowan, *Z Phys*, **89**(1934):634

[36] A.H. Cottrell, *Dislocations and plastic flow in crystals*, p. 147 (University Press, Oxford, 1953)

[37] Y. Estrin and L.P. Kubin, *J Mech Behavior Mater*, **2**(1989):255

[38] L.P. Kubin and Yu. Estrin, *CrystRes and Technol*, **19**(1984):853

[39] G.A. Malygin, *Phys Stat Sol b*, **61**(1974):K45

[40] V.V. Demirski and S.N. Komnik, *Acta Metall*, **30**(1982)(12):2227

[41] S.V. Lubenets, V.I. Startsev and L.S. Fomenko, *PhysStatSolA*, **92**(1985):11

[42] T. Ogata, T. Yuri and Y. Ono, *AIP Conference Proceedings*, **824**(2006)(1):122

[43] L. Zhang, B. An, T. Iijima, S. Fukuyama *et al.*, *J Appl Phys*, **110**(2011)(3):033540

[44] P. Bak, C. Tang and K. Wiesenfeld, *Phys Rev Lett*, **59**(1987):381

[45] M.B. Weissman, *Rev Mod Phys*, **60**(1988):537

[46] P. Bergé, Y. Pomeau and C. Vidal, *Order within chaos, towards a deterministic approach to turbulence* (New York: Wiley, 1984)

[47] V.S. Bobrov, S.I. Zaitsev and M.A. Lebedkin, *Fizika Tverdogo Tela*, **32**(1990):3060

[48] V.S. Bobrov, V.Ya. Kravchenko and M.A. Lebyodkin, *Mater Sci and Eng A*, **164**(1993)(1–2):252

[49] M.-C. Miguel, A. Vespignani, S. Zapperi, J. Weiss *et al.*, *Nature*, **410**(2001):667

[50] D.M. Dimiduk, M.D. Uchic and T.A. Parthasarathy, *Acta Materialia*, **53**(2005)(15):4065

[51] D.M. Dimiduk, E.M. Nadgorny, C. Woodward, M.D. Uchic *et al.*, *Phil Mag*, **90**(2010)(27-28):3621

[52] Rebecca N. Mudrock, Mikhail A. Lebyodkin, Peter Kurath, Armand J. Beaudoin *et al.*, *Scripta Mater*, **65**(2011)(12):1093

[53] A. Roth, T.A. Lebedkina and M.A. Lebyodkin, *Mater Sci and Eng A*, **539**(2012)(0):280

[54] P.J. Cote and L.V. Meisel, *Phys Rev Lett*, **67**(1991):1334

[55] S. Field, J. Witt, F. Nori and X. Ling, *Phys Rev Lett*, **74**(1995):1206

[56] P.A. Lee and T.M. Rice, *Phys Rev B*, **19**(1979):3970

[57] J. Aué and J.T.M. de Hosson, *J Mater Sci*, **33**(1998):5455

[58] G. Cannelli, R. Cantelli and F. Cordero, *Phys Rev Lett*, **70**(1993):3923

[59] E. Vives, J. Ortin, L. Manosa, I. Rafols *et al.*, *Phys Rev Lett*, **72**(1994):1694

[60] J.M. Carlson, J.S. Langer and B.E. Shaw, *Rev of Mod Phys*, **66**(1994)(2):657

[61] B. Gutenberg and C.F. Richter, *Ann Geofis*, **9**(1956):1

[62] H. Barkhausen, *Phys Z*, **20**(1919):401

[63] D.-H. Kim, S.-B. Choe and S.-C. Shin, *Phys Rev Lett*, **90**(2003):087203

[64] G. Bertotti, *Hysteresis in magnetism* (Academic Press, 1998)

[65] P.G. McCormick, R. Street and Y. Estrin, *J Phys: Condens Matter*, **2**(1990):3681

[66] P. Gaunt, *Phil Mag B*, **48**(1983):261

[67] R. Prozorov and D. Giller, *Phys Rev B*, **59**(1999):14687

[68] E.V. Matizen, S.M. Ishikaev and V.A. Oboznov, *J Exp Theor Phys*, **99**(2004):1065

[69] S.M. Ishikaev and E.V. Matizen, *New Developments in Josephson Junctions Research* (Transworld Research Network, 2010)

[70] L.D. Landau and E.M. Lifshitz, *The Classical Theory of Fields*, volume 2 (Butterworth–Heinemann, 1975), 4th edition

[71] J. Friedel, *Dislocations* (Pergamon Press, Oxford, 1964)

[72] M.A. Lebyodkin, Y. Brechet, Y. Estrin and L.P. Kubin, *Solid State Phenomena*, **42-43**(1995):313

[73] J. Kaiser, *Archiv Eisenhüttenwesen*, **24**(1953):43

[74] J. Kaiser, *Untersuchung über das Auftreten von Geräuschen beim Zugversuch*, Phd thesis, Technische Universität München München. (1950)

[75] K. Mathis and F. Chmelik, *Acoustic Emission*, chapter Exploring Plastic Deformation of Metallic Materials by the Acoustic Emission Technique, p. 23 (InTech, 2012)

[76] C.R. Heiple and S.H. Carpenter, *J Acoust Em*, **6**(1987):177

[77] P.P. Gillis and M.A. Hamstad, *Mater Sci Eng A*, **14**(1974):103

[78] D. Rouby, P. Fleischmann and C. Duvergier, *Philos Mag A*, **47**(1983a):671

[79] T. Richeton, J. Weiss and F. Louchet, *Acta Materialia*, **53**(2005):4463

[80] E. Orowan, *Proc Phys Soc*, **52**(1940):8

[81] D.A. Lockner, J.D. Byerlee, V. Kuksenko, A. Ponomarev *et al.*, *Nature*, **350**(1991):39

[82] T. Richeton, P. Dobroň, F. Chmelík, J. Weiss *et al.*, *Mater Sci Eng A*, **424**(2006):190

[83] J.D. Eshelby, *Proc R Soc Lond A*, **266**(1962):222

[84] M.S. Bharathi, M. Lebyodkin, G. Ananthakrishna, C. Fressengeas *et al.*, *Phys Rev Lett*, **87**(2001):165508

[85] S.H. Strogatz, *Physica D: Nonlinear Phenomena*, **143**(2000)(1-4):1

[86] C.J. Pérez, A. Corral, A. Diaz-Guilera, K. Christensen *et al.*, *J Mod Phys*, **B 10**(1996):1111

[87] A.A. Andronov, A.A. Vitt and S.E. Khaikin, *Theory of Oscillators* (Pergamon, Oxford, 1966)

[88] K. Chen, P. Bak and S.P. Obukhov, *Phys Rev A*, **43**(1991):625

[89] Z. Olami, H.J.S. Feder and K. Christensen, *Phys Rev Lett*, **68**(1992):1244

[90] J.P. Sethna, K. Dahmen, S. Kartha, J.A. Krumhansl *et al.*, *Phys Rev Lett*, **70**(1993):3347

[91] D. Sornette, *Phys Rev Lett*, **72**(1994):2306

[92] G. Durin and S. Zapperi, *Phys Rev Lett*, **84**(2000):4705

[93] R.A. White and K.A. Dahmen, *Phys Rev Lett*, **91**(2003)(8):085702

[94] F. Heslot, B. Castaing and A. Libchaber, *Phys Rev A*, **36**(1987):5870

[95] F. Le Châtelier, *Rev de Métalurgie*, **6**(1909):914

[96] A. Portevin and F. Le Châtelier, *Trans of Amer Soc for Steels Treating*, **5**(1924):457

[97] Y. Estrin and L.P. Kubin, in *Continuum Models for Materials with Microstructure*, edited by H.B. Muhlhaus, p. 395 (Wiley, New York, 1995)

[98] R.B. Schwarz and L.L. Funk, *Acta Metall*, **33**(1985)(2):295

[99] K. Chihab, Y. Estrin, L.P. Kubin and J. Vergnol, *Scripta Metall*, **21**(1987)(2):203

[100] F. Savart, *Ann Chim Phys*, **65**(1837):337

[101] A. M. Masson, *Ann Chim Phys*, **3**(1841):451

[102] J. Balík, *Mater Sci Eng A*, **316**(2001):102

[103] T.A. Lebedkina and M.A. Lebyodkin, *Acta Mater*, **56**(2008):5567

[104] J. Balik, P. Lukac and L.P. Kubin, *Scripta Mater*, **42**(2000):465

[105] P. Rodriguez and S. Venkadesan, *Solid State Phenomena*, **42-43**(1995):257

[106] M.A. Lebyodkin and T.A. Lebedkina, *Phys Rev E*, **77**(2008):026111

[107] A.V.D. Beukel, *Phys Stat Sol A*, **30**(1975):197

[108] P.G. McCormick, *Acta Metall*, **20**(1972):351

[109] P. Penning, *Acta Metallurgica*, **20**(1972)(10):1169

[110] P.N. Butcher, *Rep Prog Phys*, **30**(1967):97

[111] N. Louat, *Scripta Metall*, **15**(1981)(11):1167

[112] L.P. Kubin and Y. Estrin, *Acta metall mater*, **38**(1990):697

[113] A.H. Cottrell and B.A. Bilby, *Proc Phys Soc London*, **A62**(1949):49

[114] A. Kalk and Ch. Schwink, *Phys Stat Sol (b)*, **172**(1992)(1):133

[115] A. Van Den Beukel and U.F. Kocks, *Acta Metall*, **30**(1982)(5):1027

[116] T. Böhlke, G. Bondár, Y. Estrin and M.A. Lebyodkin, *Comp Mater Sci*, **44**(2009)(4):1076

[117] S. Zhang, P.G. McCormick and Y. Estrin, *Acta Mater*, **49**(2001)(6):1087

[118] M. Mazière and H. Dierke, *Comp Mater Sci*, **52**(2012)(1):68

[119] A. Konstantinidis and E.C. Aifantis, *J Eng Mater Tech*, **124**(2002):358

[120] M. A. Lebyodkin, T. A. Lebedkina and A. Jacques, *Multifractal analysis of unstable plastic flow* (Nova Science Publishers, NY, 2009)

[121] G. Ananthakrishna G. and M.S. Bharathi, *Phys Rev E*, **70**(2004):026111

[122] M.A. Lebyodkin and Y. Estrin, *Acta Mater*, **53**(2005)(12):3403

[123] M. Abbadi, P. Hähner and A. Zeghloul, *Mater Sci and Eng A*, **337**(2002)(1–2):194

[124] F. Chmelík, A. Ziegenbein, H. Neuhäuser and P. Lukáč, *Mater Sci Eng A*, **324**(2002):200

[125] J.M. Reed and M.E. Walter, *Mater Sci and Eng A*, **359**(2003)(1–2):1

[126] F. Chmelík, F.B. Klose, H. Dierke, J. Šachl *et al.*, *Mater Sci and Eng A*, **462**(2007)(1–2):53

[127] Z. Jiang, Q. Zhang, H. Jiang, Z. Chen *et al.*, *Mater Sci and Eng A*, **403**(2005)(1–2):154

[128] A.A. Shibkov and A.E. Zolotov, *JETP Lett*, **90**(2009):370

[129] A. Vinogradov and A. Lazarev, *Scripta Mater*, **66**(2012)(10):745

[130] H.M. Zbib and E.C. Aifantis, *Scrip Metall*, **22**(1988)(8):1331

[131] V. Jeanclaude and C. Fressengeas, *Scrip Metall et Mater*, **29**(1993)(9):1177

[132] J.D. Eshelby, in *Progress in Solid Mechanics 2*, edited by I.N. Sneddon and R. Hill, p. 89 (North-Holland, Amsterdam, 1961)

[133] G. Canova, L.P. Kubin and Y. Brechet, in *Large Plastic Deformations*, edited by C. Teodosiu and et al, p. 27 (A.A. Balkema, Rotterdam, 1993)

[134] P. Hähner, *Scripta Metall et Mat*, **29**(1993)(9):1171

[135] P.W. Bridgman, *Studies in large plastic flow and fracture* (McGraw-Hill, NY, 1952)

[136] M. Lebyodkin, Y. Brechet, Y. Estrin and L. Kubin, *Acta Mater*, **44**(1996)(11):4531

[137] S. Varadhan, A.J. Beaudoin and C. Fressengeas, *J MechPhysSolids*, **57**(2009)(10):1733

[138] P.G. McCormick and C.P. Ling, *Acta Metall et Mater*, **43**(1995)(5):1969

[139] G. Ananthakrishna, *Physics Reports*, **440**(2007):113

[140] S. Kok, A.J. Beaudoin, D.A. Tortorelli and M. Lebyodkin, *Model Sim Mater Sci and Eng*, **10**(2002)(6):745

[141] E. Rizzi and P. Hähner, *Inter J Plasticity*, **20**(2004)(1):121

[142] G. Lasko, P. Hähner and S. Schmauder, *Model Sim Mater Sci and Eng*, **13**(2005):645

[143] J. Hirth and J. Lothe, *Theory of dislocations* (McGraw-Hill, NY, 1968)

[144] N. Thompson and D.J. Millard, *Philos Mag*, **43**(1952)(339):422

[145] B.J. Shaw, *Metall and Mater Trans B*, **4**(1973):1003, 10.1007/BF02645602

[146] V.I. Bashmakov and M.M. Brodsky, *Crystallography*, **17**(1972):833

[147] V.S Boiko, L.G. Ivanchenko and L.F. Krivenko, *Fizika Tverdogo Tela*, **26**(1984):2207

[148] R. von Mises, *Z Angew Math Mech*, **8**(1928):161

[149] K. Máthis, K. Nyilas, A. Axt, I. Dragomir-Cernatescu *et al.*, *Acta Mater*, **52**(2004)(10):2889

[150] B. Reh and G. Hötzsch, *physica status solidi (a)*, **8**(1971)(2):423

[151] Mark Friesel and Steve H. Carpenter, *J Acoust Em*, **3**(1984)(1):11

[152] K. Máthis, F. Chmelík, M. Janeček, B. Hadzima *et al.*, *Acta Mater*, **54**(2006)(20):5361

[153] P. Dobroň, J. Bohlen, F. Chmelík, P. Lukáč *et al.*, *Mater Sci Eng A*, **462**(2007):307

[154] K. Mathis, J. Capek, Z. Zdrazilova and Z. Trojanova, *Mater Sci and Eng A*, **528**(2011)(18):5904

[155] I.V. Shashkov, T.A. Lebedkina, M.A. Lebyodkin, P. Dobron *et al.*, *Acta Phys Pol A*, **122**(2012)(3):430

[156] N.I. Tymiak, A. Daugela, T.J. Wyrobek and O.L. Warren, *Acta Mater*, **52**(2004)(3):553

[157] J. Gauthier, P.R. Louchez and F.H. Samuel, *Inter J Cast Metals Research*, **8**(1995)(2):106

[158] A. Clauset, C. Shalizi and M. Newman, *SIAM Review*, **51**(2009)(4):661

[159] J.W. Cooley and J.W. Tukey, *Mathematics of Computation*, **19**(1965):297

[160] A. Vinogradov, *Acoustic Emission*, **16**(1998):S158

[161] Y. Hayakawa, S. Sato and M. Matsushita, *Phys Rev A*, **36**(1987):1963

[162] J. Feder, *Fractals* (Plenum Press, New York and London, 1988)

[163] L. Niemeyer, L. Pietronero and H.J. Wiesmann, *Phys Rev Lett*, **52**(1984):1033

[164] C. Godano and L. Civetta, *Geophys Res Lett*, **23**(1996):1167

[165] D. Schertzer and S. Lovejoy, *J Geophys Res*, **92**(1987):9693

[166] X. Li and P. Shang, *Chaos, Solitons & Fractals*, **31**(2007)(5):1089

[167] K.J. Falconer, *Fractal Geometry, Mathematical Foundations and Applications* (Wiley, Chichester, 1990)

[168] T.A. Lebedkina and M.A. Lebyodkin, *Acta Mater*, **56**(2008)(19):5567

[169] T.C. Halsey, M.H. Jensen, L.P. Kadanoff, I. Procaccia *et al.*, *Phys Rev A*, **33**(1986):1141

[170] B. Lashermes, P. Abry and P. Chainais, *Inter J Wavelets, Multires and Inform Proces*, **02**(2004)(04):497

[171] I. Daubechies, *Ten Lectures on Wavelets* (Philadelpha, Pa.: Society for Industrial and Applied Mathematics, 1992)

[172] D.B. Percival and A.T. Walden, *Wavelet Methods for Time Series Analysis* (Cambridge University Press, 2000)

[173] A. Vinogradov, D.L. Merson, V. Patlan and S. Hashimoto, *Mater Sci and Eng A*, **341**(2003)(1-2):57

[174] J. Bohlen, F. Chmelik, P. Dobron, F. Kaiser *et al.*, *Journal of Alloys and Compounds*, **378**(2004)(1–2):207

[175] I.V. Shashkov, M.A. Lebyodkin and T.A. Lebedkina, *Acta Mat*, **60**(2012)(19):6842

[176] R.T. Sedgwick, *Journal of Applied Physics*, **39**(1968)(3):1728

[177] J. Bohlen, P. Dobron, J. Swiostek, D. Letzig *et al.*, *Mater Sci and Eng A*, **462**(2007):302

[178] M.M. Krishtal, A.K. Khrustalev, A.A. Razuvaev and I.S. Demin, *Deformation Fract Mater (in Russian)*, **1**(2008):28

[179] A. Petri, G. Paparo, A. Vespignani, A. Alippi *et al.*, *Phys Rev Lett*, **73**(1994):3423

[180] J. Chevy, C. Fressengeas, M. Lebyodkin, V. Taupin *et al.*, *Acta Materialia*, **58**(2010)(5):1837

[181] B. Mandelbrot, *The Fractal Geometry of Nature* (W.H. Freeman, 1983)

[182] P.C. Ivanov, L.A. Amaral, A.L. Goldberger, S. Havlin *et al.*, *Nature*, **399**(1999):461

[183] A. Chhabra and R.V. Jensen, *Phys Rev Lett*, **62**(1989):1327